

Total Measurement Uncertainty in Neutron Coincidence Multiplicity Analysis



Robert D. McElroy, Jr.

November 2020

Approved for public release.
Distribution is unlimited.

DOCUMENT AVAILABILITY

Reports produced after January 1, 1996, are generally available free via US Department of Energy (DOE) SciTech Connect.

Website www.osti.gov

Reports produced before January 1, 1996, may be purchased by members of the public from the following source:

National Technical Information Service
5285 Port Royal Road
Springfield, VA 22161
Telephone 703-605-6000 (1-800-553-6847)
TDD 703-487-4639
Fax 703-605-6900
E-mail info@ntis.gov
Website <http://classic.ntis.gov/>

Reports are available to DOE employees, DOE contractors, Energy Technology Data Exchange representatives, and International Nuclear Information System representatives from the following source:

Office of Scientific and Technical Information
PO Box 62
Oak Ridge, TN 37831
Telephone 865-576-8401
Fax 865-576-5728
E-mail reports@osti.gov
Website <http://www.osti.gov/contact.html>

This report was prepared as an account of work sponsored by an agency of the United States Government. Neither the United States Government nor any agency thereof, nor any of their employees, makes any warranty, express or implied, or assumes any legal liability or responsibility for the accuracy, completeness, or usefulness of any information, apparatus, product, or process disclosed, or represents that its use would not infringe privately owned rights. Reference herein to any specific commercial product, process, or service by trade name, trademark, manufacturer, or otherwise, does not necessarily constitute or imply its endorsement, recommendation, or favoring by the United States Government or any agency thereof. The views and opinions of authors expressed herein do not necessarily state or reflect those of the United States Government or any agency thereof.

Nuclear Nonproliferation Division

**TOTAL MEASUREMENT UNCERTAINTY IN NEUTRON COINCIDENCE
MULTIPLICITY ANALYSIS**

Robert D. McElroy, Jr.

Date Published: November 2020

Prepared by
OAK RIDGE NATIONAL LABORATORY
Oak Ridge, TN 37831-6283
managed by
UT-BATTELLE, LLC
for the
US DEPARTMENT OF ENERGY
under contract DE-AC05-00OR22725

CONTENTS

LIST OF FIGURES	v
LIST OF TABLES	viii
ABBREVIATED TERMS	ix
ACKNOWLEDGMENTS	xi
1. INTRODUCTION	1
2. THE POINT MODEL EQUATIONS	1
2.1 LIMITATIONS OF THE POINT MODEL	2
2.1.1 Extensions to the Point Model	3
2.2 CALIBRATIONS	3
2.2.1 Die-Away Time	5
2.2.2 Dead-Time Parameters.....	6
2.2.3 Axial and Radial Response Profiles.....	7
2.2.4 Efficiency Determination Using a ²⁵² Cf Point Source	10
2.2.5 Efficiency Determination Using Plutonium Button Sources	10
2.2.6 Calibration with Representative Standards	11
3. UNCERTAINTY CONTRIBUTIONS	11
3.1 COUNTING STATISTICS.....	12
3.1.1 Impact of the Counting Statistics on the Mass Result.....	13
3.1.2 Predicted Measurement Precision	17
3.2 DETECTOR PARAMETERS	18
3.2.1 Dead-time Parameters.....	18
3.2.2 Efficiency and Gate Fractions.....	20
3.3 ²⁴⁰ Pu-EFFECTIVE SCALING FACTOR	23
3.3.1 Isotopics Decay Correction and Uncertainty	23
3.3.2 ²⁴⁰ Pu _{effective} Uncertainty due to the Isotopics Declaration and Decay Correction	25
3.3.3 ²⁴⁰ Pu _{effective} Conversion Constants Contribution	25
3.4 FISSION PARAMETERS	26
3.5 FILL HEIGHT	32
3.6 RADIAL OFFSET	34
3.7 DENSITY EFFECTS.....	35
3.7.1 Multiplication Bias Correction Factor	42
3.7.2 Estimation of Bias Using the Ring Ratio	44
3.8 U _{Pu} RATIO	45
3.9 (ALPHA, n) UNCERTAINTY CONTRIBUTION	49
3.9.1 Impact of (α,n) due to Low-Z Impurities	52
3.9.2 Estimation of the Bias due to (α, n) Events	55
3.10 BURNUP UNCERTAINTY CONTRIBUTION	56
3.11 MODERATOR UNCERTAINTY CONTRIBUTION	57
4. TOTAL MEASUREMENT UNCERTAINTY.....	61
5. CONCLUSIONS	64
5.1 FUTURE WORK.....	65
6. REFERENCES	65
APPENDIX A. MULTIPLICITY TMU ESTIMATOR	A-1

LIST OF FIGURES

Figure 1. Example doubles gate fraction curve from a high-efficiency multiplicity counter [18].	5
Figure 2. Plot of the non-dead-time-corrected triples/doubles rate ratios as a function of the singles count rate for a standard PSMC.	6
Figure 3. Measured axial response profiles for a PSMC compared with the estimates from Eq. (1).	7
Figure 4. Comparison of predicted and measured radial response profiles for the Large Epithermal Multiplicity Counter (LEMC).	8
Figure 5. MCNP simulated average neutron detection efficiency as a function of fill height for a non-multiplying MOX container in the PSMC relative to a point ^{240}Pu point source in the center of the assay cavity.	9
Figure 6. Doubles and Triples gate fractions as a function of fill height for non-multiplying MOX items, illustrating the lack of dependence on fill height.	9
Figure 7. Doubles gate fraction as a function of position within the LEMC for a ^{252}Cf point source.	10
Figure 8. MCNP-simulated multiplication as a function of Pu mass for a 2.5 g/cc \times 10 cm ID container.	17
Figure 9. Expected measurement precision as a function of Pu mass for high-burnup MOX ($^{240}\text{Pu}_{\text{eff}} = 0.33$ g/g) in the PSMC (600 s count time).	18
Figure 10. Bias in the mass assay result as a function of singles rate introduced by a 1% change in the characteristic dead-time parameter.	19
Figure 11. Bias introduced in the reported assay mass value for the measurement of high-burnup MOX materials in the PSMC where the efficiency has been biased high by 1%.	21
Figure 12. Bias introduced in the reported assay mass value for the measurement of high-burnup MOX materials in the PSMC if the doubles gate fraction is biased low by 0.25%.	22
Figure 13. Bias introduced in the reported assay mass value for the measurement of high-burnup MOX materials in the PSMC if the triples gate fraction is biased low by 0.5%.	22
Figure 14. Impact of a 1% positive bias in the value of $\mathbf{vs2}$ on the mass assay result.	28
Figure 15. Impact of a 1% positive bias in the value of $\mathbf{vs3}$ on the mass assay result.	28
Figure 16. The m_{240} uncertainty contribution due to the spontaneous fission data.	29
Figure 17. Impact of a 1% positive bias in the value of $\mathbf{vi1}$ on the mass assay result.	30
Figure 18. Impact of a 1% positive bias in the value of $\mathbf{vi2}$ on the mass assay result.	31
Figure 19. Impact of a 1% positive bias in the value of $\mathbf{vi3}$ on the mass assay result.	31
Figure 20. Uncertainty contribution from the induced fission moments assuming the values of $\mathbf{vi1}$, $\mathbf{vi2}$, and $\mathbf{vi3}$ are uncorrelated (left) and fully correlated (right).	32
Figure 21. Calculated fill height impact on the average neutron detection efficiency for a typical multiplicity measurement.	33
Figure 22. Expected bias in the mass assay result due to the container fill height for a 10 cm ID container located 5 cm above the assay cavity floor of a PSMC.	33
Figure 23. Estimated m_{240} assay result probability distribution due to fill height variation based on a random distribution of fill heights (based on 20,000 random fill heights) for measurements with a PSMC.	34
Figure 24. Estimated m_{240} assay result probability distribution due to fill height variation based on a random distribution of fill heights for a PSMC with a 80 cm tall assay cavity.	34
Figure 25. Change in volume average efficiency with radial offset (for a 10 cm OD can with 5 cm fill height).	35
Figure 26. Probability distribution of reported assay results for a 10 cm OD container with a 1 cm typical radial offset and 1 cm deviation about that offset.	35
Figure 27. Mass assay bias resulting from the use of point source calibration parameters for volumetric items (PuO_2 at 2.5 g/cc).	37

Figure 28. Mass assay bias using the PSMC following calibration based on the 2.5 g/cc PuO ₂ containers.	38
Figure 29. Mass assay bias using the ENMC following calibration based on the 2.5 g/cc PuO ₂ containers.	38
Figure 30. Mass assay bias as a function of Pu mass for several PuO ₂ densities using the PSMC when calibrated using representative standards of a single density (2.5 g/cc).....	39
Figure 31. Mass assay bias as a function of Pu mass for several PuO ₂ densities using the PSMC when calibrated using representative standards covering a broad range of PuO ₂ densities.	40
Figure 32. Mass assay bias as a function of Pu mass for several PuO ₂ densities using fill height and density-dependent efficiency.....	41
Figure 33. Simulated neutron detection efficiency as a function of neutron energy for the ENMC and PSMC systems.....	42
Figure 34. Simulated neutron detection efficiency as a function of increasing oxygen content for various fill heights in the PSMC. The 10 cm diameter canister contained 1 g Pu/cm fill height (0.0062 g/cc) while the oxygen content was increased incrementally from 0.06 to 0.6 g/cc.....	42
Figure 35. Mass assay bias as a function of Pu mass for several PuO ₂ densities using fill height and density-dependent efficiency.....	43
Figure 36. Mass assay bias as a function of Pu mass for several PuO ₂ densities using fill height and density-dependent efficiency after application of the multiplication correction.	44
Figure 37. Mass assay bias as a function of ring ratio for several PuO ₂ densities using fill height and density-dependent efficiency.....	45
Figure 38. Simulated mass assay bias as a function of Pu mass and UPu ratio based on a traditional multiplicity counter mass calibration ($\rho=3.0$ g/cc, $^{240}\text{Pu}_{\text{eff}}/\text{g}=0.3144$) using the PSMC.....	46
Figure 39. Simulated mass assay bias as a function of Pu mass and UPu ratio based on a traditional multiplicity counter mass calibration ($\rho=3.0$ g/cc, $^{240}\text{Pu}_{\text{eff}}/\text{g}=0.3144$, $\alpha=0.76$) over all masses and UPu ratios in the collection.	46
Figure 40. Simulated mass assay bias as a function of Pu mass and UPu ratio using fill height and density-dependent efficiency ($\rho=3.0$ g/cc, $^{240}\text{Pu}_{\text{eff}}/\text{g}=0.3144$) using the PSMC.....	47
Figure 41. Simulated mass assay bias as a function of Pu mass and UPu ratio using fill height and density-dependent efficiency ($\rho=3.0$ g/cc, $^{240}\text{Pu}_{\text{eff}}/\text{g}=0.3144$) using the ENMC.....	47
Figure 42. Simulated mass assay bias as a function of fill height and UPu ratio using fill height and density-dependent efficiency ($\rho=3.0$ g/cc, $^{240}\text{Pu}_{\text{eff}}/\text{g}=0.3144$) using the ENMC.	48
Figure 43. Comparison of the simulated and empirical bias estimates for assay of MOX material of varying fill height and UPu ratio efficiency ($\rho=3.0$ g/cc, $^{240}\text{Pu}_{\text{eff}}/\text{g}=0.3144$) using a PSMC.....	49
Figure 44. Mass assay bias as a function of Pu mass for increasing alpha value ($\rho=3.0$ g/cc, $^{240}\text{Pu}_{\text{eff}}/\text{g}=0.3141$), using the point source calibration.	50
Figure 45. Mass assay bias as a function of Pu mass for increasing alpha value ($\rho=3.0$ g/cc, $^{240}\text{Pu}_{\text{eff}}/\text{g}=0.3141$), using the volumetric calibration for containers of similar density and $^{240}\text{Pu}_{\text{eff}}/\text{g}$	51
Figure 46. Mass assay bias as a function of Pu mass for increasing alpha value ($\rho=2.0$ g/cc, $^{240}\text{Pu}_{\text{eff}}/\text{g}=0.2569$), using the volumetric calibration for containers of $\rho=3.0$ g/cc, $^{240}\text{Pu}_{\text{eff}}/\text{g}=0.3141$	51
Figure 47. Simulated mass assay bias as a function of Pu mass for increasing alpha value ($\rho=3.0$ g/cc, $^{240}\text{Pu}_{\text{eff}}/\text{g}=0.3141$), using the volumetric calibration optimized for this material type.	52
Figure 48. Mass assay bias as a function of Pu mass for constant alpha value ($\alpha=1.52$, $\rho=2.5$ g/cc, $^{240}\text{Pu}_{\text{eff}}/\text{g}=0.2479$) from various impurities.....	53
Figure 49. Mass assay bias as a function of ring ratio for constant alpha value ($\alpha=1.52$, $\rho=2.5$ g/cc, $^{240}\text{Pu}_{\text{eff}}/\text{g}=0.2479$) from various impurities.....	53

Figure 50. Assay bias as a function of mass for PuO ₂ ($\rho=3.0$ g/cc, $^{240}\text{Pu}_{\text{eff}}/\text{g}=0.3144$) containing fluorine impurities (ranging from 800 to 8000 ppm).	54
Figure 51. Assay bias as a function of mass for PuO ₂ ($\rho=3.0$ g/cc, $^{240}\text{Pu}_{\text{eff}}/\text{g}=0.3144$) containing boron impurities (ranging from 400 to 4000 ppm).	54
Figure 52. Assay bias as a function of mass for PuO ₂ ($\rho=3.0$ g/cc, $^{240}\text{Pu}_{\text{eff}}/\text{g}=0.3144$) containing carbon as an impurity (ranging from ~5 to 50% by weight).	55
Figure 53. Comparison of the simulated and estimated biases for assay of PuO ₂ containing significant boron impurities.	56
Figure 54. Bias as a function of Pu mass for several $^{240}\text{Pu}_{\text{effective}}$ values (PuO ₂ , $\rho=2.5$ g/cc, $\alpha=0.76$).	57
Figure 55. Simulated bias resulting from the assay of “damp” PuO ₂ using the ENMC for increasing content of H ₂ O.	58
Figure 56. Simulated bias resulting from the assay of “damp” MOX using the ENMC for increasing content of H ₂ O.	58
Figure 57. Volume average detection efficiency relative to dry oxide as a function of fill height for each of the simulated moisture loadings for both PuO ₂ and MOX items.	59
Figure 58. Multiplication relative to dry oxide as a function of fill height for each of the simulated moisture loadings for the PuO ₂ containers.	59
Figure 59. Simulated bias resulting from the assay of “damp” PuO ₂ using the ENMC for increasing content of H ₂ O.	60
Figure 60. Simulated bias resulting from the assay of “damp” MOX material using the ENMC for increasing content of H ₂ O.	60
Figure 61. Simulated bias resulting from the assay of “damp” MOX material using the ENMC for increasing content of H ₂ O.	61
Figure 62. Example of uncertainties reported for traditional multiplicity assay results. Note that most analysis software currently in use reports the uncertainties with fully correlated covariance terms, which in this case underreports the uncertainties.	62
Figure 63. Example of additional uncertainty contributions to the multiplicity analysis for 722 g dry MOX powder assay using a PSMC.	64
Figure 64. Example of assay mass result total measurement uncertainty.	64

LIST OF TABLES

Table 1. Variables/Interferences in Multiplicity Analysis.	3
Table 2. Comparison of several neutron multiplicity counters. [5]	4
Table 3. Initial and final calibration parameters for a PSMC for use with MOX.	11
Table 4. Comparison of estimated and measured covariance matrices for a typical multiplicity assay.	16
Table 5. Isotopic data for decay correction.	24
Table 6. Example Pu isotopic decay correction.	25
Table 7. Isotopic data for decay correction (values for ²³⁸ Pu and ²⁴² Pu from Ref. [26], values for ²⁴⁴ Pu and ²⁴¹ Am are estimates).	25
Table 8. Nuclear data parameters and uncertainties.	26
Table 9. Simulated neutron detector parameters for the PSMC and ENMC systems for a ²⁴⁰ Pu point source.	36
Table 10. Simulated PSMC rates for the PuO ₂ baseline items.	36
Table 11. PME analysis results for the PuO ₂ baseline items simulated rates using ²⁴⁰ Pu point calibration.	37
Table 12. Detector parameters for point source and volumetric calibrations (ρ=2.5 g/cc).	38
Table 13. Simulated neutron detector parameters for the PSMC for a ²⁴⁰ Pu point source and a volumetric calibration based on 3.0 g/cc PuO ₂	45
Table 14. Simulated PSMC detector parameters for point source and volumetric calibrations (ρ=3.0 g/cc) used in Figure 44 through Figure 47.	52
Table 15. Bias parameters for several common low-Z (α, n) emitters.	56
Table 16. Uncertainty contributors to the multiplicity TMU.	62

ABBREVIATED TERMS

ENMC	Epithermal Neutron Multiplicity Counter
LEMC	Large Epithermal Neutron Multiplicity Counter
MCNP	Monte Carlo N-Particle software package
MOX	mixed oxide
NDA	nondestructive assay
NIST	National Institute of Standards and Technology
ORNL	Oak Ridge National Laboratory
PSMC	plutonium scrap multiplicity counter
PME	point model equations
Pu	plutonium
TMU	Total Measurement Uncertainty
U	uranium

ACKNOWLEDGMENTS

The authors would like to acknowledge and thank the Safeguards Technology Development Program within the Office of International Nuclear Safeguards, National Nuclear Security Administration (NNSA), United States Department of Energy (DOE) for providing funding for this work.

1. INTRODUCTION

Neutron multiplicity counting is the most commonly used nondestructive assay technique for determining the plutonium mass within containers of scrap PuO₂ or mixed oxide (MOX). In multiplicity analysis, the ²⁴⁰Pu_{eff} mass, leakage multiplication, and alpha ratio (the ratio of [α, n]-to-spontaneous fission neutron production) are the three primary unknown sample properties. They must be determined simultaneously. To solve for these three unknowns in a multiplicity assay, three measured values are needed: the singles, doubles, and triples neutron count rates. While the analysis is limited to solving for three unknowns, there are many additional factors that impact the observed count rates and contribute to the measurement uncertainty.

In this study we investigate the various uncertainty contributors for the multiplicity analysis through a combination of traditional uncertainty propagation techniques supplemented by Monte Carlo simulations to address the dependences not explicitly expressed by the point source model. Uncertainties arising from counting statistics, calibration parameters, calibration method, nuclear data, and various material characteristics (isotopic abundances, chemical form, density, and impurities) are considered. A Total Measurement Uncertainty (TMU) estimate is then developed from these uncertainty contributors.

This study is confined to multiplicity analysis of items commonly encountered in international safeguards applications. That is, the study focused on Pu oxides and MOX materials for the masses ranging up to 4000 grams total Pu. Multiplicity measurements were simulated using MCNP V6 [1] based on the Plutonium Scrap Multiplicity Counter (PSMC) [2] [3], Epithermal Multiplicity Counter (ENMC) [4], Pyrochemical Multiplicity Counter, and Large Epithermal Multiplicity Counter (LEMC) [5] for this study; however, this report focuses on the parameterization of the uncertainties for the PSMC. The performance differences between the PSMC and the other multiplicity counting systems are relatively small, primarily manifesting in the impact on measurement precision so that the evaluation developed for the PSMC can be applied to the other multiplicity counting systems.

Finally an analysis tool, the Multiplicity TMU Estimator, was developed from this study to serve as an aid for evaluation of the total measurement uncertainty of multiplicity assay results obtained from the commonly used INCC [6] acquisition and analysis software.

2. THE POINT MODEL EQUATIONS

Multiplicity analysis is based on the point model [7], using three measured rates (single neutron rate [*S*] and double [*D*] and triple [*T*] neutron coincidences) to solve for three unknown properties of the sample:

$$S = m_{240} \cdot \Phi \cdot M \cdot \varepsilon \cdot \overline{v_{s1}} \cdot (1 + \alpha),$$

$$D = \frac{m_{240} \cdot \Phi \cdot M^2 \cdot \varepsilon^2 \cdot f_d}{2} \cdot \left\{ \overline{v_{s2}} + \left(\frac{M-1}{v_{il}-1} \right) \cdot \overline{v_{s1}} \cdot \overline{v_{i2}} \cdot (1 + \alpha) \right\}, \text{ and}$$

$$T = \frac{m_{240} \cdot \Phi \cdot M^3 \cdot \varepsilon^3 \cdot f_t}{6} \cdot \left\{ \overline{v_{s3}} + \left(\frac{M-1}{v_{il}-1} \right) \cdot \left[3 \cdot \overline{v_{s2}} \cdot \overline{v_{i2}} + \overline{v_{s1}} \cdot \overline{v_{i3}} \cdot (1 + \alpha) \right] + 3 \left(\frac{M-1}{v_{il}-1} \right)^2 \overline{v_{s1}} \cdot (1 + \alpha) \cdot \overline{v_{i2}}^2 \right\},$$

where

- m_{240} = the ²⁴⁰Pu_{eff} mass,
- Φ = the spontaneous fission rate per gram ²⁴⁰Pu,

M = the self-leakage multiplication,
 ε = the neutron detection efficiency,
 f_d = the doubles gate fraction,
 f_t = the triples gate fraction,
 α = the ratio of uncorrelated to correlated neutron emission, and
 $\overline{V_{s1}}, \overline{V_{s2}}, \overline{V_{s3}}$ and $\overline{V_{i1}}, \overline{V_{i2}}, \overline{V_{i3}}$ = the spontaneous and induced fission prompt factorial moments, respectively.

With three measured rates, we can elect to solve for any of the following combinations of three unknowns.

- Known efficiency: solve for m_{240} , α , M
- Known alpha: solve for m_{240} , ε , M
- Known multiplication: solve for m_{240} , α , ε
- Known mass: solve for M , α , ε

This study is limited to the development of the TMU approach for the known efficiency analysis.

2.1 LIMITATIONS OF THE POINT MODEL

The point model requires many simplifying assumptions to be true in order to be successfully applied. However, these assumptions are rarely met in practice. Even for seemingly simple cases, such as a hypothetical non-multiplying point source, the model fails and adjustments to nuclear data or detector parameters must be made to obtain accurate assay results. This fundamental limitation of the point model is easily demonstrated through use of MCNP simulations.

The point model requires not only that the spontaneous and induced fission neutron energy distributions be identical but also that the (α, n) neutron energy distribution is the same as the fission distributions. When these energy distributions differ, the three different sources of neutrons within the sample are characterized by different induced fission rates, induced fission moments, and detection efficiencies. These differences are not accounted for by the model. These limitations of the point model are well known; however, it is generally assumed that the impact is negligible for low-mass, low-multiplication, small-volume samples (e.g., a point source). But let us consider the measurement of a small ($\ll 1$ g) fuel-grade Pu oxide sample using a standard multiplicity assay system such as the PSMC in MCNP simulation.

The source is defined as a 1 mg total Pu mass of fuel-grade material ($^{240}\text{Pu}_{\text{eff}} = 25\%$ with 1% ^{241}Am content) with $\alpha = 0.76$. The source is placed at the center of the PSMC assay cavity. The (α, n) neutron energy distribution is estimated using Sources 4C, and the ^{240}Pu spontaneous fission distribution is defined as a Watt distribution. The first deviation from the model observed is that the neutron detection efficiency for the ^{240}Pu spontaneous fission neutrons is $1.03\times$ greater than the detection efficiency for the (α, n) neutrons. This is because the average neutron energy from the oxygen (α, n) neutrons is greater (2.5 vs 1.9 MeV) than the spontaneous fission neutron energy. This raises the question of what characteristic detection efficiency to use for the counter? The common approach, using the average neutron detection efficiency for the PuO_2 item (whether from simulation or measurement), would result in a $\sim 2\%$ bias in the reported mass value for the hypothetical non-multiplying source. Instead the neutron detection efficiency for ^{240}Pu spontaneous fission neutrons must be used to provide the correct mass result. This is obvious from the point model equations (PME), where the contribution from (α, n) to the coincidence rate is zero for non-multiplying items.

For more realistic items with measurable extent and multiplication, the situation is more complicated. For these items, the detection efficiency and multiplication vary as a function of position within the item, the impact of (α , n) is no longer negligible, and moderators in the item impact both the multiplication and detection efficiency, along with many other interferences.

The items in Table 1 represent a non-inclusive list of potential interferences to the PME-based multiplicity analysis. As can be seen in the table, while the typical multiplicity analysis measures three count rates (Singles, Doubles and Triples), there are many more potential unknowns.

These deficiencies in the point model are accommodated by arbitrary adjustments (arbitrary in the sense of that these are purely empirical corrections with no basis in model) to the three characteristic neutron detector parameters (ϵ , f_d and f_t). This approach requires the use of representative standards to determine the revised parameters and that the items under assay closely resemble these standards. The “calibration-free” multiplicity analysis is highly dependent on implementation of a proper calibration methodology.

Table 1. Variables/Interferences in Multiplicity Analysis.

Mass of the Fissile Isotopes	Matrix Effects & Packaging
Multiplication	Moderating
Item Geometry	Reflective
Item Density	Absorbing
Item Composition	Neutron Counter Parameters
Isotopic Abundance	Efficiency (x, y, z, E)
Alpha – relative Measure of (α , n) Rate	Die-away Time
Isotopics Distribution	Electronics Dead-time
Age of the Pu	Presence of Other Fission Sources
Elemental Impurities	^{242}Cm , ^{244}Cm , ^{248}Cm
$^{240}\text{Pu}_{\text{eff}}$ / g– Weighted Neutron Emission Rates	^{252}Cf
Isotopics Distribution	^{235}U , ^{238}U
Age of the Pu	Nuclear Data (used in the algorithm)
Actinide Impurities	

2.1.1 Extensions to the Point Model

Various extensions to the PME have been investigated over the years; the two most common techniques are the Weighted Point Model [8] [9] [10] [11] [12] [13] [6], which attempts to compensate for variation in multiplication through the item, and the Dual Energy Point Model [14] [6] [15] [16] [17], which addresses a portion of the impact of neutron energy dependence of the fission and (α , n) events. While implementations of these extension are available in analysis software such as INCC, they are not widely used at this time.

2.2 CALIBRATIONS

There are several potential approaches to the calibration of a multiplicity counting system [18] [15]; however, the optimal method depends on the material characteristics of the item (e.g., density, U/Pu ratio, etc.). Because the multiplicity analysis only lets us solve for three unknowns (typically m, M and alpha), the range of material characteristics of the item to be assayed must be constrained and each material type requires its own calibration to yield an accurate result. The non-ideal detector response (e.g., spatial and energy dependences) further confound the analysis.

Typically, initial calibration parameters (efficiency, doubles and triples gate fractions) are determined using ^{252}Cf . The efficiency is determined using a National Institute of Standards and Testing (NIST) traceable ^{252}Cf source. These initial values are adjusted using the Monte Carlo N-Particle software package (MCNP) [1, 19] to provide the efficiency for a ^{240}Pu point fission source in the center of the assay cavity (note there is an unquantified uncertainty inherent in the use of the MCNP-based efficiency scaling factor). Several representative Pu standards are then assayed to adjust the doubles and triples gate fractions. The uncertainty characteristics depend upon the calibration methodology and characteristics of the representative standards employed, and as the deviations from the calibration conditions increase, the associated uncertainties will also increase.

The initial neutron multiplicity counter calibration will determine the following

- Neutron detection efficiency for a point source of ^{252}Cf positioned in the cavity center
- Characteristic Die-Away Time
- Doubles and Triples Gate Fractions (Gate Utilization parameters)
- Axial Response Profile
- Radial Response Profile
- Dead-time Parameters

Examples of typical initial characterization parameters are provided in Table 2 for several multiplicity counters. (We note that rarely do the characterization documents included uncertainties for these parameters.) Following the initial characterization, parameters specific to the items to be assayed will be determined either using representative standards or MCNP simulations benchmarked using the ^{252}Cf measurements. This follow-on characterization will determine the following.

- Neutron detection efficiency for Pu assay
- Revised Gate Fractions
- Sensitivity to Interferences
 - Potential Correction Factors

Table 2. Comparison of several neutron multiplicity counters. [5]

	ENMC [4]	PSMC-01	PSMC-HE	LEMC
Assay Cavity (Dia. × H in cm)	20 × 43	20 × 40	21 × 40	40 × 50
He-3 Tubes	121	80	80	126
He-3 Partial Pressure (atm.)	10	4	10	10
Amptek A111 amp/SCA boards	27	19	20	27
Rings	4	4	4	3
Efficiency (ϵ)	65%	55%	62%	51%
Die-Away (μs)	19.1	49	36	24
Pre-Delay (μs)	1.5	4.5	3	1.5
Gate Width (μs)	24	64	46	32
Doubles Gate Fraction	0.621	0.621	0.593	0.652
Triple Gate Fraction	0.404	0.392	0.362	0.435
Sensitivity Reals/g Pu-240	239	171	203	154
Multiplicity Dead-time (ns)	37.5	54.1	48.1	41.5

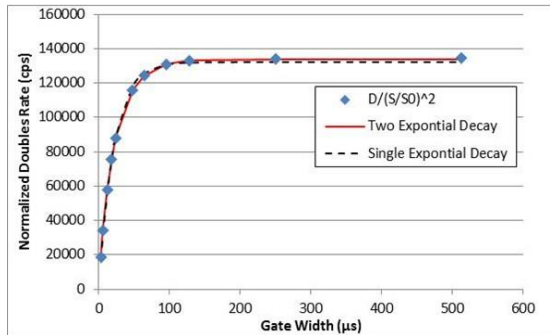
2.2.1 Die-Away Time

The die-away time represents the characteristic time required for fast neutrons emitted in the assay cavity to slow down to thermal (or epithermal) energies and be detected, absorbed in the counter body, or exit the counter. This value itself is only used in the dead-time correction algorithm; however, the die-away time of the counter defines the optimal coincidence gate settings and the doubles and triples gate fractions (gate utilization factors). These gate fractions and the neutron detection efficiency are key parameters in the multiplicity analysis, yet traditionally no errors are assigned to these values.

The doubles and triples gate fractions, f_d and f_t , are typically determined by assay of a ^{252}Cf source for a series of gate width settings (or, if available, extracted from a list mode data set). The fit to the data must include a sufficient number of exponential components to accurately reproduce the curvature of the data (typically two or three distinct exponential components are necessary). For a typical cadmium-lined neutron multiplicity counter, the doubles rate, D , as a function of gate width is given by the following expression:

$$D = \sum_i^n D_i \cdot e^{-\frac{P}{\tau_i}} \cdot \left(1 - e^{-\frac{G}{\tau_i}}\right) \cong D_1 \cdot e^{-\frac{P}{\tau_1}} \cdot \left(1 - e^{-\frac{G}{\tau_1}}\right) + D_2 \cdot e^{-\frac{P}{\tau_2}} \cdot \left(1 - e^{-\frac{G}{\tau_2}}\right),$$

where P is the pre-delay, G is the gate width, and τ_1 and τ_2 are the decay times and D_1 and D_2 are the relative contributions of the two exponentials. Figure 1 shows a typical plot of a gate width measurement for an epithermal neutron coincidence counter. A proper fit to the data using the above equation provides an estimate of the uncertainty as well as the exponential parameters. Typical uncertainties in the gate fractions would be 0.25% for the doubles gate fraction and 0.5% for the triples. However, it should be noted that although the gate fractions are characteristics of the coincidence counter and can be determined fairly precisely (e.g. $\pm 0.25\%$ for f_d), these values may not ultimately be used in the mass assay. As will be discussed later, the gate fractions are “adjusted” to accommodate the limitations of the point model.



Measured Gate Fractions			
	Single Exponential	Two Exponential	
f_d	0.6217	0.6088 ± 0.0016	~0.25%
f_t	0.3912	0.3785 ± 0.0019	~0.5%
x^2/n	943	2.1	

Figure 1. Example doubles gate fraction curve from a high-efficiency multiplicity counter [20].

Alternatively, the gate fractions can be determined from the dead-time-corrected rates ratios of a ^{252}Cf source. The doubles gate fraction is given by

$$f_d = \frac{2}{\varepsilon} \cdot \frac{\nu_{s1}}{\nu_{s2}} \cdot \frac{D}{S}$$

and the triples gate fraction by

$$f_t = \frac{6}{\varepsilon^2} \cdot \frac{\nu_{s1}}{\nu_{s3}} \cdot \frac{T}{S}$$

The resulting gate fractions for the same measurement depicted in Figure 1 are

$$f_d = 0.5950 \pm 0.0060,$$

$$f_i = 0.3434 \pm 0.0036, \text{ and}$$

$$\text{Cov}(f_d, d_i) = 2.1\text{E-}5.$$

In this method, the uncertainty is limited by the uncertainty in the declared activity for the ^{252}Cf source and the uncertainties of ν_{s1} , ν_{s2} , and ν_{s3} .

More recently, list mode data acquisition systems have begun to see more use so that the die-away time can be determined from a single measurement. With list mode acquisition, the die-away time will be determined by fitting the coincidence rate for a fixed gate width while effectively increasing the pre-delay.

2.2.2 Dead-Time Parameters

The characteristic dead-time parameters for a multiplicity counter are determined using a series of ^{252}Cf sources of increasing count rate. Because the ^{252}Cf sources are non-multiplying and (α, n) of ^{252}Cf is negligible compared with the spontaneous fission neutron emission rate, the rates ratios for every ^{252}Cf source (the exception being aged sources where the longer lived fissioning isotopes begin to have an impact) are given by

$$\frac{D}{S} = \frac{\varepsilon \cdot f_d}{2} \cdot \frac{\nu_{s2}}{\nu_{s1}}, \quad \frac{T}{S} = \frac{\varepsilon^2 \cdot f_t}{6} \cdot \frac{\nu_{s3}}{\nu_{s1}}, \quad \text{and} \quad \frac{T}{D} = \frac{\varepsilon \cdot f_t}{3 \cdot f_d} \cdot \frac{\nu_{s3}}{\nu_{s2}},$$

which are constant for a given neutron counting system. Because the dead-time-corrected singles::doubles, doubles::triples, and singles::triples count ratios rates should be the same for each source, we attribute the difference to electronic dead-time. Fitting these ratios as a function of count rate allows the characteristic dead-time parameters and associated uncertainties for the counter to be determined. As an example, Figure 2 shows the Triples/Doubles ratio for a series of ^{252}Cf sources of increasing activity prior to dead-time correction. The characteristic dead-time parameter for the counter is 0.25 times the slope of the Triples/Doubles.

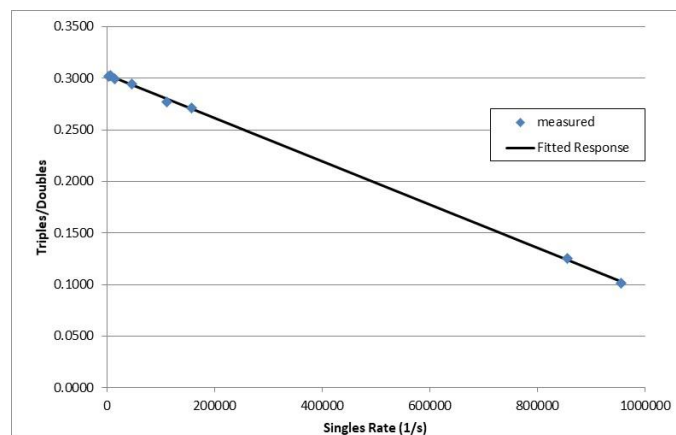


Figure 2. Plot of the non-dead-time-corrected triples/doubles rate ratios as a function of the singles count rate for a standard PSMC.

The typical dead-time parameters and uncertainties for a PSMC without an internal de-randomizer board are (as defined for use with the INCC software [6] analysis)

$$\begin{aligned} a &= 0.3093 \pm 0.011 \mu\text{s}, \\ b &= 0.0998 \text{ ps}, \\ c &= 19 \pm 19 \text{ ns}, \\ d &= \text{NA}, \text{ and} \\ \tau &= 109.1 \pm 0.5 \text{ ns}. \end{aligned}$$

2.2.3 Axial and Radial Response Profiles

The axial response profile of a multiplicity counter refers to the variation in neutron detection efficiency with the height of a point source above the assay cavity floor. For a well-designed neutron counting system, the response profile will be relatively flat over the volume of the largest item to be assayed as these variations in efficiency are not captured by the PME analysis. A representative axial response profile for a PSMC is shown in Figure 3. For use in estimating the impact on TMU, we have developed an empirical algorithm that predicts the axial response profile based on the assay cavity height and tube ring diameters. This algorithm has been found to reproduce the response profile reasonably well for many systems in part due to the similarity in design of most multiplicity counting systems. However, this response function was developed only for the purposes of estimating, not correcting for the axial response bias.

The response function is given as

$$\varepsilon(z) = \left[4\pi - \frac{2 \cdot R_{cav}^2 \cdot (T_L^2 + 4 \cdot z_0^2)}{(T_L^2 - 4 \cdot z_0^2)^2} \right] / [4\pi - 2 \cdot (R_{cav}/T_L)^2] , \quad (1)$$

where $T_L = 1.1 \cdot (H + R_{cav})$,

H is the internal cavity height,

R_{cav} is the effective cavity radius which is equal to the radius of the outermost tube ring, and

z_0 is the distance of the source from the vertical center of the cavity.

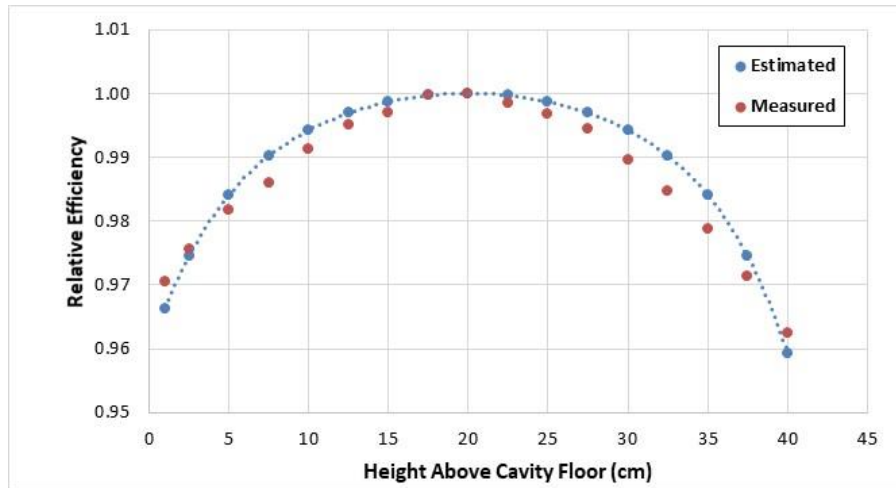


Figure 3. Measured axial response profiles for a PSMC compared with the estimates from Eq. (1).

The radial response profile refers to the change in neutron detection efficiency for a point source as a function of distance from the axial centerline of the cavity, generally at the vertical center of the assay cavity. A similar algorithm was developed to represent the radial response profile given by

$$\varepsilon(r) = \frac{T_L^2}{(4\pi - 2*(R_{cav}^2 + 4*R_0^2))} \cdot \frac{1}{(4\pi - 2*(R_{cav}/T_L)^2)^2}, \quad (2)$$

where R_0 is the radial offset (distance to the centerline).

We realized later that the product of the axial and radial response profiles provided a reasonable representation of the variation in efficiency throughout the assay cavity volume. The radial response profile is given by

$$\varepsilon(r, z) = \varepsilon(r) \cdot \varepsilon(z) \quad (3)$$

or

$$\varepsilon(r, z) = \frac{T_L^2}{(4\pi - 2*(R_{cav}^2 + 4*R_0^2))} \cdot \frac{1}{(4\pi - 2*(R_{cav}/T_L)^2)^3} \cdot \left[4\pi - \frac{2*R_{cav}^2*(T_L^2 + 4*z_0^2)}{(T_L^2 - 4*z_0^2)^2} \right]. \quad (4)$$

The plots in Figure 4 provide a comparison of the predicted and measured radial response profiles for the LEMC at the cavity centerline and near the top of the assay cavity (with the plug installed). The response function given in Eq. (4) will be used to estimate the fill height dependence of the assay result.

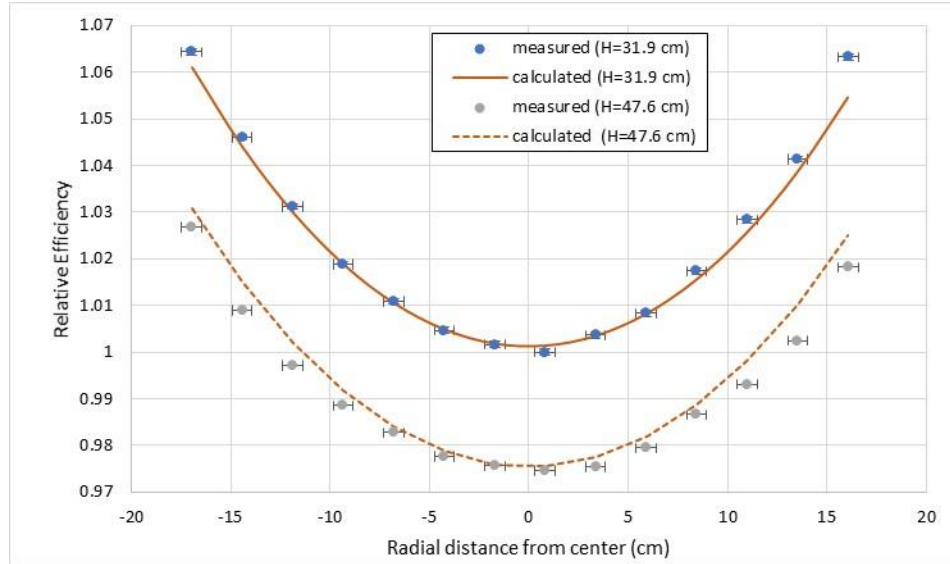


Figure 4. Comparison of predicted and measured radial response profiles for the LEMC.

The expressions for radial and axial response can be used to estimate the detector response to partially filled containers. For example, Figure 5 shows the MCNP simulated neutron detection efficiency averaged over the volume of a 10 cm diameter container of very low-density (non-multiplying) PuO_2 as a function of fill height relative to a point source in the center of the assay cavity. The figure also shows the volume average neutron detection efficiency as a function of fill height for the same counter and container using the expression above for $\varepsilon(r, z)$ integrated over the material volume.

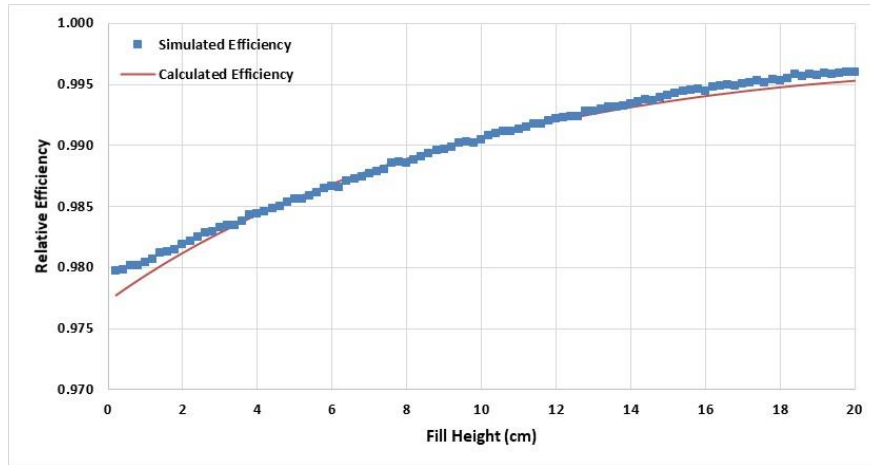


Figure 5. MCNP simulated average neutron detection efficiency as a function of fill height for a non-multiplying MOX container in the PSMC relative to a point ^{240}Pu point source in the center of the assay cavity.

The doubles and triples gate fractions have also been examined as a function of fill height using MCNP simulations. The gate fractions were found to be independent of fill height (Figure 6) for the non-multiplying container of MOX material. Figure 7 presents the measured doubles gate fraction for a ^{252}Cf point source determined at 19 vertical locations for each of three different radial positions within the LEMC illustrating the independence of the gate fraction on the measurement position within the counter.

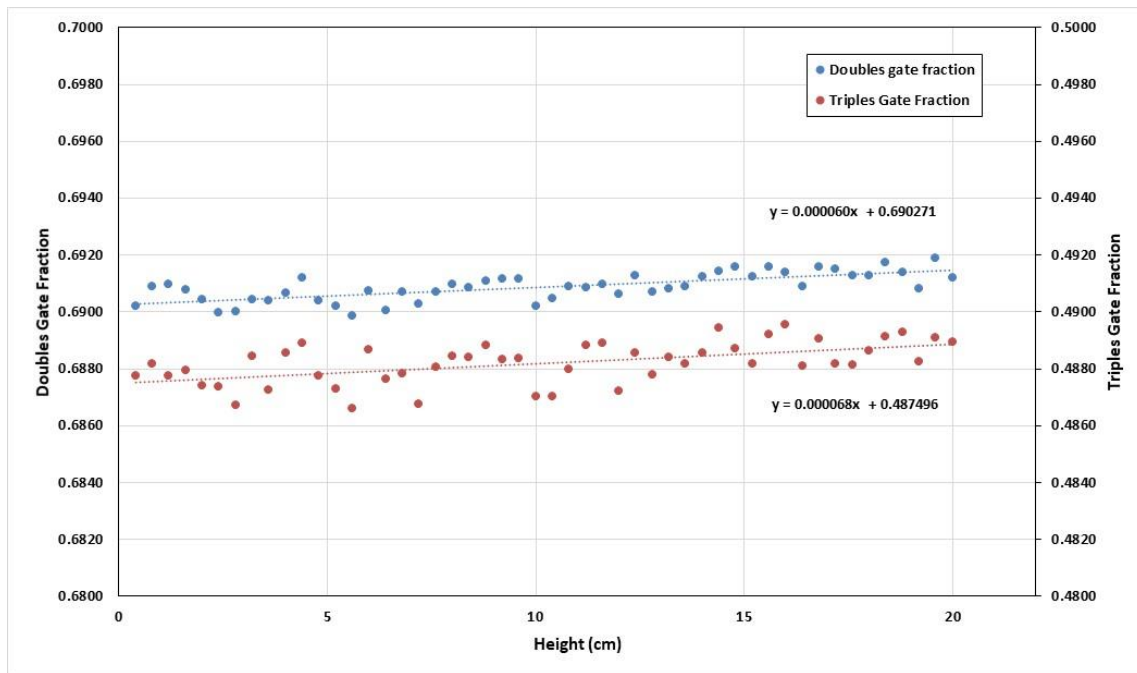


Figure 6. Doubles and Triples gate fractions as a function of fill height for non-multiplying MOX items, illustrating the minimal dependence on height ($\sim 0.01\%/cm$).

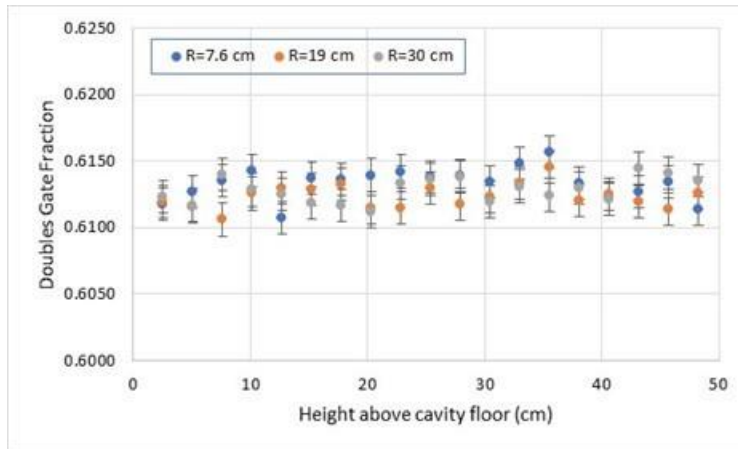


Figure 7. Doubles gate fraction as a function of position within the LEMC for a ^{252}Cf point source.

2.2.4 Efficiency Determination Using a ^{252}Cf Point Source

Often the neutron detection efficiency is established using a ^{252}Cf source placed at the center of the assay cavity. The ^{252}Cf source seems ideal because the small masses ($< 1\text{E-}6$ g) produce no measurable multiplication, the relative (α, n) yield is essentially zero, and the Cf source material is confined to a very small volume. However, due to the short half-lives of the Cf isotopes, the neutron emission rate, declaration date, relative isotopic abundances, and declaration date for the isotopic abundances must be known. Certified testing facilities such as the NIST will typically determine the yield for a given source to 1% uncertainty (1 sigma). However, this uncertainty will increase as the source ages due to uncertainties in the isotopic declarations, isotopic neutron yields, and half-lives. Use of multiple traceable sources can reduce this error somewhat, but unless the sources are certified by independent test facilities, the systematic uncertainty quoted by the facility limits the overall accuracy of the efficiency determination.

It is common practice to determine the ^{240}Pu spontaneous fission neutron detection efficiency using MCNP results benchmarked to the ^{252}Cf value. That is, the ratio of the neutron detection efficiencies determined using MCNP for ^{240}Pu and ^{252}Cf is multiplied by the measured ^{252}Cf detection efficiency to provide the ^{240}Pu detection efficiency. This approach seems reasonable; however, it is not known how large an uncertainty is introduced through the MCNP ratio, although this error contribution is typically ignored.

2.2.5 Efficiency Determination Using Plutonium Button Sources

Button sources are typified by small size, reproducible geometry, and low fissile mass content. Efficiency calibration using Pu button sources (e.g., the PIDIE sources [21]) offers the advantage that they are macroscopic (the source material can be weighed using high-performance balances, and the isotopic composition can be determined through sampling and mass spectrometry). However, the neutron emission from these sources will be impacted by the chemical form of the source material and, to some extent, by self-multiplication. The presence of (α, n) emission and multiplication will impact the average neutron energy and the observed neutron detection efficiency. Sources with minimal (α, n) contribution (e.g., pure $^{240}\text{PuO}_2$ or PuGa alloys) are preferred. Calibration with low mass, diffuse Pu sources can provide a better benchmark for evaluation of assay interferences, providing the ^{240}Pu spontaneous fission detection efficiency to accuracies of less than 0.2%.

2.2.6 Calibration with Representative Standards

Using certified ^{252}Cf or ^{240}Pu standards can provide highly accurate values for the neutron counter's characteristic parameters (i.e., dead-time, efficiency and gate fractions); however, if we were to use these values in the analysis of the item under assay, the results would likely be disappointing. For example, a PSMC was calibrated using ^{252}Cf sources and the detection efficiency adjusted via MCNP simulations [3]. The results of the initial ^{252}Cf -based calibration and final calibration using MOX standards are presented in Table 3. Note that there were no uncertainties reported for these values. The necessary modifications to the parameters were each several times the typical 1 sigma uncertainty for each of those parameters.

Table 3. Initial and final calibration parameters for a PSMC for use with MOX.

Parameter	Initial (^{252}Cf)	Final (MOX)
Efficiency	55.60%	54.3%
Doubles Gate Fraction	0.6117	0.615
Triples Gate Fraction	0.3896	0.400

The updated calibration parameters presented in Table 3 were based on the assay of three well-characterized working standards (the isotopic distribution was determined by mass spec, the total Pu mass by weighting and knowledge of the chemical form). While the composition of the items was well known, the items were fabricated using the same source material so that the chemical form, isotopic abundances, and impurities were the same. This type of calibration is commonplace for multiplicity counting systems where only two quantities were varied, multiplication and m_{240} , so that final calibration parameters do not necessarily provide a unique solution (note that in this case additional material types were later assayed to examine the system response to a broader range of variables). However, if the material properties (density, chemical form, U/Pu ratio, etc.) are fairly constant, then a traditional calibration approach (simply increasing the contents of the container) is viable. If, for instance, the U/Pu ratio is expected to vary significantly (say from U/Pu=1 to U/Pu=3), then it is more advantageous to create standards of constant fill height.

3. UNCERTAINTY CONTRIBUTIONS

To examine the TMU, we must first isolate the individual error contributors. The following error contributions are considered to have been found to have a significant impact on the multiplicity analysis of typical PuO_2 and MOX materials.

Multiplicity Analysis Error Contributors

Measurement Precision	Material Properties
Detector Characteristics	Fill Height
Dead-time	Density
Gate Fractions	U/Pu Ratio
Efficiency	(α , n) emission
Axial Response Profile	Isotopic Abundances
Radial Response Profile	Moderation
Nuclear Data	Container Positioning
$^{240}\text{Pu}_{\text{eff}}$ conversion factors	Container Wall Effects
Fission moments	

3.1 COUNTING STATISTICS

Counting statistics and measurement precision are often assumed to be the same for multiplicity assay; however, this is not the case. There are several additional random error components that contribute to the TMU, and these will be considered in the later sections of this report.

A multiplicity assay is typically acquired as a series of short (~20 s) intervals. The uncertainty in the singles, doubles, and triples rates may be determined from the standard deviation of the rates reported for each measurement cycle. It is also possible to calculate the uncertainties from the summed rates or directly from the histograms. Examination of the collection of cycle-by-cycle rates offers the advantage that unexpected factors (e.g., electronic noise) will be directly incorporated into the uncertainty. Additionally, calculation of the covariance matrix is straightforward.

Because the singles, doubles, and triples rates reflect different order moments of the same multiplicity distributions, these rates are expected to be correlated and it is important to calculate the covariance matrix for each assay. The simplest approach is to analyze the cycle-by-cycle rates assuming these rates in each cycle are statistically meaningful and a sufficient number of cycles are available. The uncertainty of and covariance for the (singles, doubles, or triples) rates are

$$\sigma_j = \frac{1}{n-1} \sum_{i=1}^n (\langle r_j \rangle - r_{j,i})^2$$

and

$$\text{cov}(r_j, r_k) = \frac{1}{n-1} \sum_{i=1}^n (\langle r_j \rangle - r_{j,i}) \cdot (\langle r_k \rangle - r_{k,i}),$$

where $r_{j,i}$ and $r_{k,i}$ are the j^{th} and k^{th} rates (e.g., S, D, or T) of the i^{th} cycle and n is the total number of measurement cycles.

If the cycle-by-cycle histogram or rates data are unavailable, the singles and doubles rates' uncertainties may also be estimated using the following expressions [22] [23]:

$$\sigma_S = \sqrt{\xi^{1/2} \cdot (S + B_S)/t_m + \sigma_{B_S}^2},$$

and

$$\sigma_D = \sqrt{(2 \cdot S^2 \cdot G + D + B_D)/t_m \cdot \left(1 + 8 \cdot \gamma \cdot \frac{D}{f_d \cdot S}\right)^{1/2} + \sigma_{B_D}^2},$$

where $\xi = \sqrt{1 + \frac{D}{S \cdot f_d}}$ and

$$\gamma = 1 - (1 - e^{-G/\tau})/(G/\tau).$$

The uncertainty in the triples rates can be determined from the multiplicity histogram as described in Ref. [6], or it can be approximated as described by Croft et al. [23] as the following expression:

$$\sigma_T = \sqrt{1 + n \cdot g_2 \cdot \frac{D/f_2}{S}} \cdot \sqrt{(T + 2 \cdot A_T)/t} \cdot$$

However, we find that for MOX and ^{252}Cf measurements the following relation adequately represents the observed triples standard deviation:

$$\sigma_T \cong \sqrt{2 \cdot \frac{(S^3 \cdot G^2 + T + B_T)}{t_m} + \sigma_{B_T}^2} \cdot$$

Alternatively, the triples uncertainty can be determined by dithering the elements of the multiplicity histograms. In this approach, a collection of histograms is built up where the counts in each bin of the histogram are randomly adjusted about the recorded value based on a normal distribution. Then the complete histogram is renormalized also using a normal distribution based on the total number of counts in the acquisition. Typically, 1000 randomized histograms are created and analyzed to provide 1000 sets of singles, doubles, and triples rates and the average rates' uncertainties and covariance matrix. We find the rates' uncertainties determined from the dithering process provide reasonable agreement, with the uncertainties determined from the standard deviation of the measured rates. Currently the dithered results are used as a check on the measured values to identify inconsistencies in the data. We note that the covariance matrix derived from the dithered rates often bears little resemblance to the measured covariance matrix; however, they provide equivalent impact on the overall mass uncertainty.

For uncertainty analysis, the observed standard deviation of the cycle-by-cycle rates provides a more realistic representation of the uncertainty and is preferred over the analytical representations.

3.1.1 Impact of the Counting Statistics on the Mass Result

Much of the following discussion can be found in the INCC software manual; however, we solve for the multiplication first, alpha second, and mass third, resulting in slightly different expressions of the same values (note that the results are the same).

3.1.1.1 Solving for Multiplication

The point model equations are arranged to eliminate m_{240} and α to provide a third-order polynomial in terms of M .

$$k_1 + k_2 \cdot M + k_3 \cdot M^2 + M^3 = 0 ,$$

where

$$k_1 = \frac{-6 \cdot T \cdot v_{s2} \cdot (v_{i1} - 1)}{(v_{s2} \cdot v_{i3} - v_{s3} \cdot v_{i2}) \cdot \varepsilon^2 \cdot f_t \cdot S} ,$$

$$k_2 = \frac{2 \cdot D \cdot [v_{s3} \cdot (v_{i1} - 1) - 3 \cdot v_{s2} \cdot v_{i2}]}{(v_{s2} \cdot v_{i3} - v_{s3} \cdot v_{i2}) \cdot \varepsilon \cdot f_d \cdot S} , \text{ and}$$

$$k_3 = \frac{6 \cdot D \cdot v_{s2} \cdot v_{i2}}{(v_{s2} \cdot v_{i3} - v_{s3} \cdot v_{i2}) \cdot \varepsilon \cdot f_d \cdot S} - 1 .$$

It is possible to solve this cubic equation directly for the multiplication from the roots of the cubic equation [24]; however, the INCC software solves for the multiplication by iteration (Newton-Raphson method) of the following equation:

$$z = \frac{-k_1 + k_3 \cdot M^2 + 2 \cdot M^3}{k_2 + 2 \cdot k_3 \cdot M + 3 \cdot M^2},$$

until $|M - z| < 1E-9$ [6]. While, perhaps, less elegant than solving the cubic equation,* this approach tends to avoid the non-physical roots of the equation. Once M has been determined, the values for m_{240} and α are calculated along with the uncertainties and covariance terms.

The partial derivatives of the multiplication with respect to the singles, doubles, and triples rates are provided below (although we have not exposed the explicit rates dependences in partial derivatives of M , this section follows the INCC user manual section “Conventional Multiplicity Assay” [6]). For example, the partial derivative of M with respect to the singles rates S is determined from the equation above for multiplication.

$$\frac{\partial k_1}{\partial S} + \frac{\partial k_2}{\partial S} M + k_2 \frac{\partial M}{\partial S} + \frac{\partial k_3}{\partial S} M^2 + k_3 2M \frac{\partial M}{\partial S} + 3M^2 \frac{\partial M}{\partial v_{i1}} = 0,$$

which is rearranged to provide

$$\frac{\partial M}{\partial S} = -\frac{\frac{\partial k_1}{\partial S} + \frac{\partial k_2}{\partial S} M + \frac{\partial k_3}{\partial S} M^2}{k_2 + 2 \cdot k_3 M + 3 \cdot M^2}.$$

The partial derivatives of k_1 , k_2 , and k_3 with respect to the singles rate are

$$\frac{\partial k_1}{\partial S} = \frac{6 \cdot T \cdot v_{s2} \cdot (v_{i1} - 1)}{(v_{s2} \cdot v_{i3} - v_{s3} \cdot v_{i2}) \cdot \varepsilon^2 \cdot f_t \cdot S^2} = \frac{-k_1}{S},$$

$$\frac{\partial k_2}{\partial S} = -\frac{2 \cdot D \cdot [v_{s3} \cdot (v_{i1} - 1) - 3 \cdot v_{s2} \cdot v_{i2}]}{(v_{s2} \cdot v_{i3} - v_{s3} \cdot v_{i2}) \cdot \varepsilon \cdot f_d \cdot S^2} = \frac{-k_2}{S},$$

* The cubic equation for multiplication can be solved using the Trigonometric method described in CRC Standard Mathematical Tables [21].

$$k_1 + k_2 \cdot M + k_3 \cdot M^2 + M^3 = 0$$

$$a = (3 \cdot k_2 - k_3^2)/3$$

$$b = (2 \cdot k_3^3 - 9 \cdot k_3 \cdot k_2 + 27 \cdot k_1)/3$$

$$d = 2 \cdot \sqrt{-a/3}$$

$$\theta = \arccos\left(3 \cdot \frac{b}{a \cdot d}\right)/3$$

The three roots of the equation are

$$M = d \cdot \cos\left(\frac{\theta}{3} + n \cdot \frac{\pi}{3}\right) - \frac{k_3}{3}, \text{ where } n = 0, 2, \text{ or } 4.$$

The appropriate root reliably occurs for $n = 0$; this may be verified using the iterative method discussed above.

$$M = d \cdot \cos\left(\frac{\theta}{3}\right) - \frac{k_3}{3}.$$

and

$$\frac{\partial k_3}{\partial S} = \frac{-6 \cdot D \cdot v_{s2} \cdot v_{i2}}{(v_{s2} \cdot v_{i3} - v_{s3} \cdot v_{i2}) \cdot \varepsilon \cdot f_d \cdot S^2} = \frac{-(k_2 + 1)}{S}$$

so that

$$\frac{\delta M}{\delta S} = \frac{(k_1 + k_2 \cdot M + (k_3 + 1) \cdot M^2)}{S \cdot (k_2 + 2 \cdot M \cdot k_3 + 3 \cdot M^2)}.$$

Similarly for $\frac{\delta M}{\delta D}$ and $\frac{\delta M}{\delta T}$ we find

$$\frac{\delta M}{\delta D} = \frac{-(k_2 \cdot M + (k_3 + 1) \cdot M^2)}{D \cdot (k_2 + 2 \cdot M \cdot k_3 + 3 \cdot M^2)} \text{ and}$$

$$\frac{\delta M}{\delta T} = \frac{-k_1}{T \cdot (k_2 + 2 \cdot M \cdot k_3 + 3 \cdot M^2)},$$

and the measurement precision in the multiplication is calculated in the traditional way:

$$\sigma_M = \sqrt{\left(\frac{\delta M}{\delta S} \cdot \sigma_S\right)^2 + \left(\frac{\delta M}{\delta D} \cdot \sigma_D\right)^2 + \left(\frac{\delta M}{\delta T} \cdot \sigma_T\right)^2 + 2 \cdot \left(\frac{\delta M}{\delta S} \cdot \frac{\delta M}{\delta D} \cdot \text{cov}(S, D) + \frac{\delta M}{\delta S} \cdot \frac{\delta M}{\delta T} \cdot \text{cov}(S, T) + \frac{\delta M}{\delta D} \cdot \frac{\delta M}{\delta T} \cdot \text{cov}(D, T)\right)}.$$

3.1.1.2 Determining the ^{240}Pu effective mass

Once the value of M is known, α and the ^{240}Pu mass (m_{240}) can be determined. The ^{240}Pu mass is given by

$$m_{240} = \frac{\frac{2 \cdot D}{\varepsilon \cdot f_d} - \frac{M \cdot (M - 1) \cdot v_{i2} \cdot S}{(v_{i1} - 1)}}{\varepsilon \cdot M^2 \cdot v_{s2} \cdot \Phi}.$$

To determine the uncertainty in the assay value for m_{240} , we take the following partial derivatives:

$$\frac{\delta m_{240}}{\delta M} = -\left(\frac{4D}{f_d \cdot \varepsilon^2 \cdot v_{s2} \cdot \Phi \cdot M^3} + \frac{v_{i2} \cdot S}{(v_{i1} - 1) \cdot \varepsilon \cdot v_{s2} \cdot \Phi \cdot M^2}\right),$$

$$\frac{\delta m_{240}}{\delta S} = -\frac{(1 - 1/M) \cdot v_{i2}}{(v_{i1} - 1) \cdot \varepsilon \cdot v_{s2} \cdot \Phi} + \frac{\delta m_{240}}{\delta M} \cdot \frac{\delta M}{\delta S},$$

$$\frac{\delta m_{240}}{\delta D} = \frac{2}{v_{s2} \cdot \Phi \cdot \varepsilon^2 \cdot f_d \cdot M^2} + \frac{\delta m_{240}}{\delta M} \cdot \frac{\delta M}{\delta D},$$

$$\frac{\delta m_{240}}{\delta T} = \frac{\delta m_{240}}{\delta M} \cdot \frac{\delta M}{\delta T}.$$

The uncertainty in m_{240} is generally given as

$$\sigma_{m_{240}} = \left[\left(\frac{\delta m_{240}}{\delta S} \cdot \sigma_S \right)^2 + \left(\frac{\delta m_{240}}{\delta D} \cdot \sigma_D \right)^2 + \left(\frac{\delta m_{240}}{\delta T} \cdot \sigma_T \right)^2 + 2 \left(\frac{\delta m_{240}}{\delta S} \cdot \frac{\delta m_{240}}{\delta D} \cdot \text{cov}(S, D) + \frac{\delta m_{240}}{\delta S} \cdot \frac{\delta m_{240}}{\delta T} \cdot \text{cov}(S, T) + \frac{\delta m_{240}}{\delta D} \cdot \frac{\delta m_{240}}{\delta T} \cdot \text{cov}(D, T) \right) \right]^{1/2}.$$

The covariance terms should be determined from variations in the measured rates. In most software packages the covariance is represented by the product of the two uncertainties (e.g., $\sigma_S \cdot \sigma_T$) assuming the rates are fully correlated. Table 4 shows a comparison of the estimated or fully correlated (i.e., $\sigma_S \cdot \sigma_T$) covariance matrix and the measured (partially correlated) values for a given assay. In this example case the $\sigma_{m_{240}}$ was 1.52 g using the measured and 1.13 g using the estimated covariance terms—a 35% difference. Hence, it is important to use the measured values when possible.

Table 4. Comparison of estimated and measured covariance matrices for a typical multiplicity assay.

Rates	Estimated (fully correlated) Covariance Matrix	Measured (Partially Correlated) Covariance Matrix
183415.13 ± 24.15	583.3 1762.4 3805.7	583.3 410.4 1275.5
4671.61 ± 72.97	1762.4 5325.2 11499.3	410.4 5325.3 5055.2
13172.46 ± 157.58	3805.7 11499.3 24831.8	1275.5 5055.2 24832.0

3.1.1.3 Determining the value α

With both m_{240} and M already determined, the value of alpha, α , is calculated as follows:

$$\alpha = \frac{S}{m_{240} \cdot \Phi \cdot \varepsilon \cdot v_{s1} \cdot M} - 1.$$

To determine the uncertainty in the assay value for alpha, we take the following partial derivatives:

$$\frac{\delta \alpha}{\delta S} = (\alpha + 1) \cdot \left(\frac{1}{S} - \frac{1}{M} \cdot \frac{\delta M}{\delta S} - \frac{1}{m_{240}} \cdot \frac{\delta m_{240}}{\delta S} \right),$$

$$\frac{\delta \alpha}{\delta D} = -(\alpha + 1) \cdot \left(\frac{1}{M} \cdot \frac{\delta M}{\delta D} + \frac{1}{m_{240}} \cdot \frac{\delta m_{240}}{\delta D} \right), \text{ and}$$

$$\frac{\delta \alpha}{\delta T} = -(\alpha + 1) \cdot \left(\frac{1}{M} \cdot \frac{\delta M}{\delta T} + \frac{1}{m_{240}} \cdot \frac{\delta m_{240}}{\delta T} \right),$$

and the uncertainty contribution in the assay value of α due to counting statistics is given by

$$\sigma_\alpha = \sqrt{\left(\frac{\delta \alpha}{\delta S} \cdot \sigma_S \right)^2 + \left(\frac{\delta \alpha}{\delta D} \cdot \sigma_D \right)^2 + \left(\frac{\delta \alpha}{\delta T} \cdot \sigma_T \right)^2 + 2 \cdot \left(\frac{\delta \alpha}{\delta S} \cdot \frac{\delta \alpha}{\delta D} \cdot \text{cov}(S, D) + \frac{\delta \alpha}{\delta S} \cdot \frac{\delta \alpha}{\delta T} \cdot \text{cov}(S, T) + \frac{\delta \alpha}{\delta D} \cdot \frac{\delta \alpha}{\delta T} \cdot \text{cov}(D, T) \right)}.$$

3.1.2 Predicted Measurement Precision

Predicting the expected measurement precision for a series of items can be useful for planning a measurement campaign and for quality control. The measurement precision of the multiplicity analysis is dependent on the ^{240}Pu effective mass, multiplication, and relative (α , n) emission rate. For a given material stream and container type, we expect the multiplication as a function of mass to be consistent from item to item. Using MCNP or historical data for the multiplicity counter, an expression for the typical multiplication can be created. The following expression is a generic form of the empirical relationship we have used to evaluate the precision:

$$M_{typ}(m_{Pu}) = 1 + k_{M1} \cdot \left(\frac{m_{Pu}}{m_{ref}} \right)^{k_{M1}},$$

where k_{M1} and k_{M2} are empirically determined constants, and m_{ref} is a reference total Pu mass. For example, for a series of simulated measurements of 2.5 g/cc PuO_2 powder packaged in a 10 cm ID container, the MCNP-simulated multiplication as a function of mass is shown in Figure 8. For the series of simulations shown in the figure, $k_{M1} = 0.003$ and $k_{M1} = 0.5$.

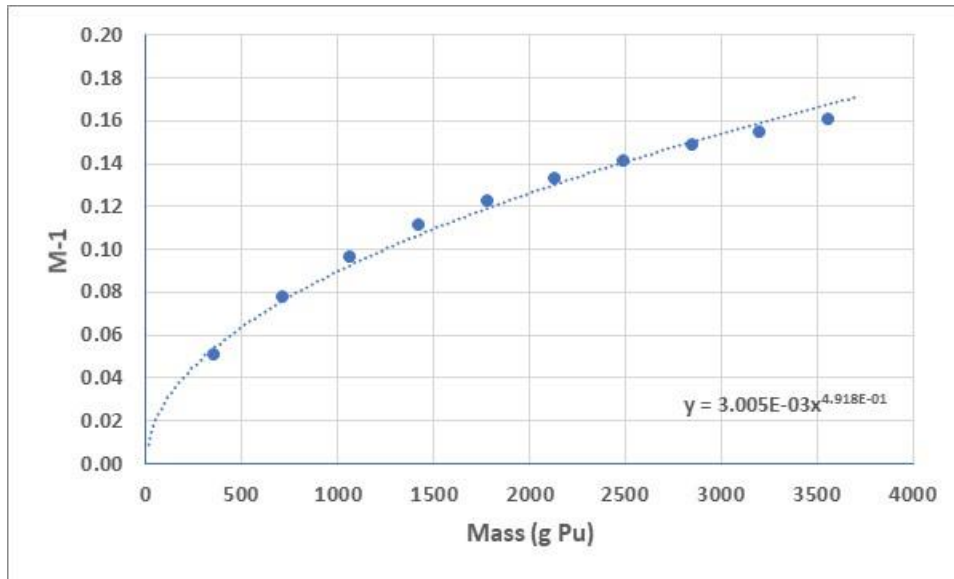


Figure 8. MCNP-simulated multiplication as a function of Pu mass for a 2.5 g/cc and a 10 cm ID container.

With an estimated multiplication function, the measurement precision as function of Pu mass may be calculated for various values of α . Figure 9 provides the predicted measurement precision of containers of PuO_2 in a PSMC for an acquisition time of 10 minutes. Comparison of the current assay result against the expected values can provide an indication of potential measurement interferences should the observed and predicted differ significantly.

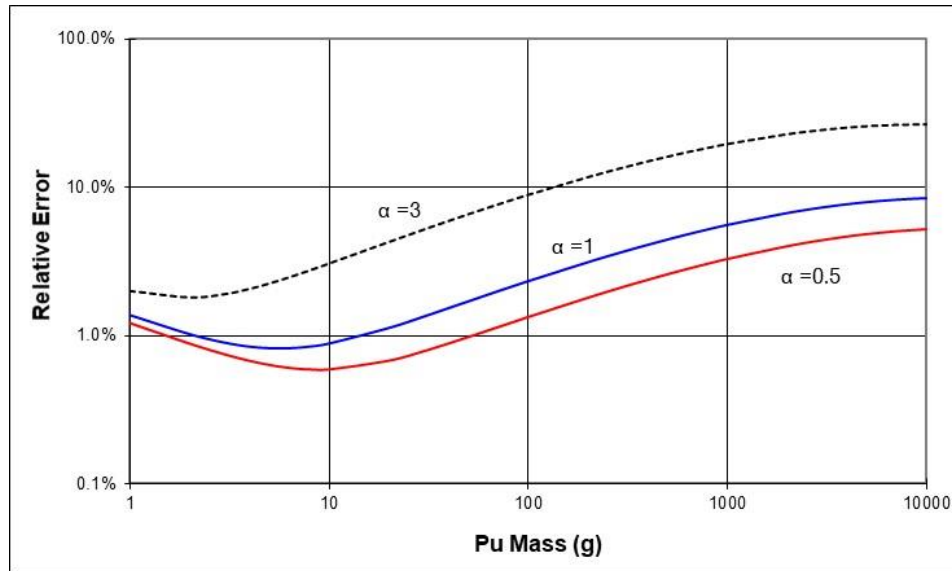


Figure 9. Expected measurement precision as a function of Pu mass for high-burnup MOX ($^{240}\text{Pu}_{\text{eff}} = 0.33 \text{ g/g}$) in the PSMC (600 s count time).

3.2 DETECTOR PARAMETERS

3.2.1 Dead-time Parameters

Neutron multiplicity counters will typically have a large number of pre-amplifiers and integrated de-randomizer circuits, resulting in small characteristic electronic dead-times (20 to 100 ns) and operated with singles count rates of 1E6 cps or lower. The singles rate dead-time correction will be a few percent or lower and have a minimal impact on the measurement. However, correction for the doubles and triples rate will be several times larger and the uncertainty in the corrections can introduce a bias into the assay result. To some extent the bias may be compensated by adjustment of the gate fractions; however, due to the complex nature of the dead-time correction [25], the required adjustment will vary with the item's alpha, mass, and multiplication. Figure 10 provides a comparison of the biases introduced into the mass assay results for several ^{252}Cf sources and MOX items from a 1% change in the characteristic dead-time parameter using a PSMC.

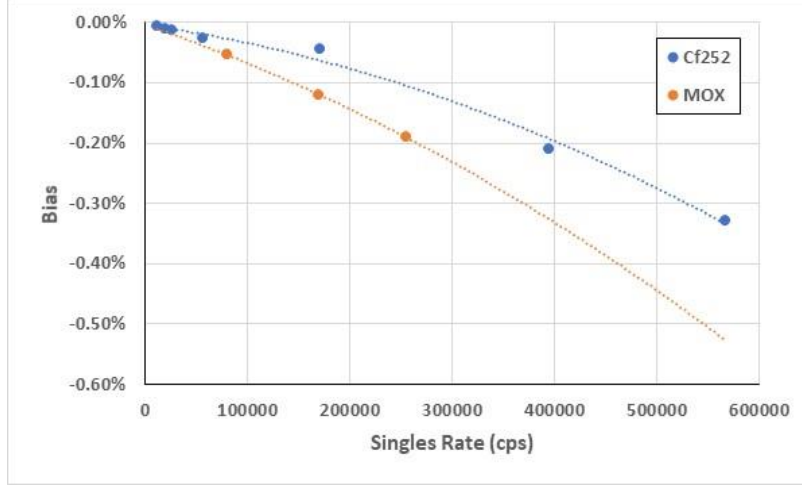


Figure 10. Bias in the mass assay result as a function of singles rate introduced by a 1% change in the characteristic dead-time parameter.

The uncertainties in the dead-time parameters have largely been ignored in neutron coincidence counting and are rarely quantified and reported. Representative uncertainties for the coincidence dead-time parameter, a , and multiplicity dead-time parameter, τ , are given in reference [26]. The typical uncertainties for the coincidence dead-time parameter are approximately 0.25%, while for the characteristic multiplicity dead-time parameter, the uncertainties will range from 0.5 to 1%. The uncertainty in the triples rate dead-time parameter, c , is typically 1 to 2%.

A description of the dead-time correction algorithms can be found in Refs. [6] and [25]. It should be noted that INCC software utilizes the Totals, Reals, and Triples rates rather than the Singles, Doubles, and Triples. While there is no significant difference in the computation of the singles and totals rates, the dead-time corrections for the Reals and Doubles rates are different quantities. The reals rates are determined from the multiplicity histograms using the following expression:

$$R = \left[\left(\sum_{i=1}^n (P_i - Q_i) \cdot i \right) \cdot T_m \right] \cdot e^{(a+b \cdot T_m) \cdot T_m},$$

while the doubles rates are determined using the more complex equation

$$D = \left\{ \sum_{i=1}^n (P_i - Q_i) \cdot \left[1 + \sum_{j=0}^{i-2} \binom{i-1}{j+1} \frac{(j+1)^j \varphi^j}{[1 - (j+1) \cdot \varphi]^{j+2}} \right] \right\} \cdot T_m \cdot e^{\tau \cdot T_m} \cdot e^{c \cdot T_m},$$

which is more closely related to the expression for the dead-time corrected triples rates.

$$T = \left[\sum_{i=2}^n \beta_i (P_i - Q_i) - \sum_{i=1}^n \alpha_i (P_i - Q_i) \cdot \sum_{i=1}^n \alpha_i \cdot Q_i \right] \cdot e^{-\tau \cdot T_m} \cdot e^{-d \cdot T_m} \cdot T_m,$$

where

$$\alpha_i = 1 + \sum_{j=0}^{i-2} \binom{i-1}{j+1} \frac{(j+1)^j \varphi^j}{[1 - (j+1) \cdot \varphi]^{j+2}}$$

and

$$\beta_i = \alpha_i - 1 + \sum_{j=0}^{i-3} \binom{i-1}{j+2} \frac{(j+1)(j+2)^j \varphi^j}{[1 - (j+2) \cdot \varphi]^{j+3}}.$$

In principle, the inherent information in covariance between the Doubles and Triples rate is lost by replacing the Doubles rate with the Reals rate. (This author believes the replacement of the Singles and Doubles rates with the Totals and Reals in the analysis was part of an effort to simplify the multiplicity report format and eliminate confusion as to why there were slight differences between the reported Reals and Doubles rates.) However, because it has been in common use since the late 1990s, we have adopted the method described in the INCC software manual for this evaluation.

The uncertainty of the dead-time correction impacts the Singles, Doubles, and Triples rates as a systematic rather than a random contribution. The contributions were evaluated by determining the partial derivatives of the mass response with respect to the individual dead-time parameters computationally (rather than analytically). Evaluation of a standard PSMC, the total contribution from the dead-time correction was found to be ~0.1% for singles count rates of less than 250 kcps.

3.2.2 Efficiency and Gate Fractions

This section discusses only the error contribution associated with the uncertainties of the neutron detection efficiency and gate fractions (σ_ε , σ_{f_d} and σ_{f_t}). The more problematic errors associated with the application of the point model will be discussed in the later sections of this report. This section only considers the direct error propagation of the detection efficiency and gate fractions through the point model analysis.

$$m_{240} = \frac{2 \cdot D}{\varepsilon \cdot f_d} \frac{M \cdot (M - 1) \cdot \nu_{i2} \cdot S}{(\nu_{i1} - 1)} \cdot \frac{1}{\varepsilon \cdot M^2 \cdot \nu_{s2} \cdot \Phi}.$$

To evaluate the impact of the neutron counter detection parameters on m_{240} , we follow a methodology similar to that in Section 3.1.1 for the measurement precision. First, the partial derivatives of the multiplication with respect to the efficiency, doubles gate fraction, and triples gate fraction are determined:

$$\frac{\delta M}{\delta \varepsilon} = \frac{(2 \cdot k_1 + k_2 \cdot M + (k_3 + 1) \cdot M^2)}{\varepsilon \cdot (k_2 + 2 \cdot M \cdot k_3 + 3 \cdot M^2)},$$

$$\frac{\delta M}{\delta f_d} = \frac{-(k_2 \cdot M + (k_3 + 1) \cdot M^2)}{f_d \cdot (k_2 + 2 \cdot M \cdot k_3 + 3 \cdot M^2)},$$

$$\frac{\delta M}{\delta f_t} = \frac{k_1}{f_t \cdot (k_2 + 2 \cdot M \cdot k_3 + 3 \cdot M^2)}.$$

The error contribution to the reported $^{240}\text{Pu}_{\text{effective}}$ mass, m_{240} , due to the uncertainty in the efficiency value is expressed as

$$\sigma_{m_{240},\varepsilon} = \sqrt{\left(\frac{\delta m_{240}}{\delta \varepsilon} \sigma_{\varepsilon} + \frac{\delta m_{240}}{\delta M} \cdot \frac{\delta M}{\delta \varepsilon}\right)^2 \sigma_{\varepsilon}^2},$$

where

$$\frac{\delta m_{240}}{\delta \varepsilon} = \frac{-4 \cdot D}{f_d \cdot M^2 \cdot \nu_{s2} \cdot \Phi \cdot \varepsilon^3} + \frac{(M-1)}{M} \cdot \frac{\nu_{i2} \cdot S}{(\nu_{i1} - 1) \cdot \nu_{s2} \cdot \Phi \cdot \varepsilon^2}$$

and

$$\frac{\delta m_{240}}{\delta M} = \frac{-4 \cdot D}{f_d \cdot \nu_{s2} \cdot \Phi \cdot \varepsilon^2 \cdot M^3} - \frac{\nu_{i2} \cdot S}{(\nu_{i1} - 1) \cdot \nu_{s2} \cdot \Phi \cdot \varepsilon \cdot M^2}.$$

Figure 11 shows the impact on the assay result from a relative 1% uncertainty in the neutron detection efficiency as a function of total Pu mass for different alpha values. As can be seen in the figure, the resulting bias is not only dependent on the Pu mass but also on alpha due to the increasing multiplication. More importantly, as can be seen, the resulting bias is not always positive or negative.

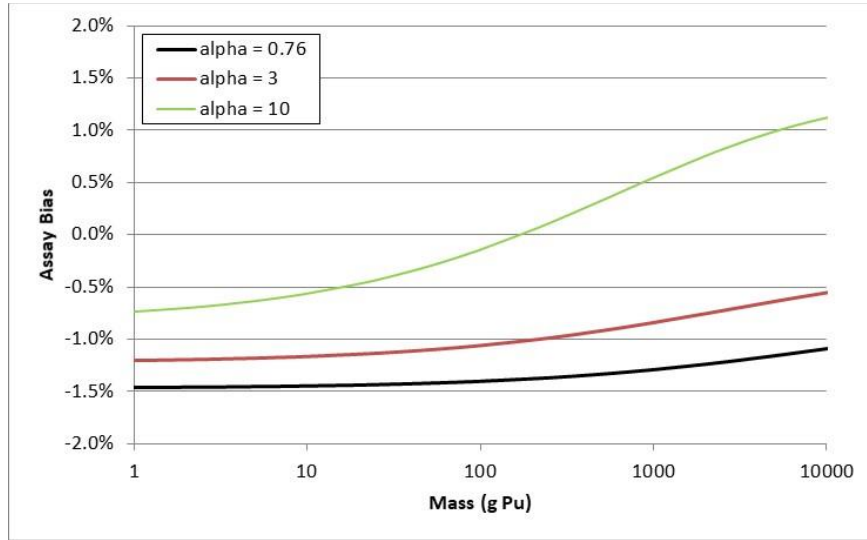


Figure 11. Bias introduced in the reported assay mass value for the measurement of high-burnup MOX materials in the PSMC where the efficiency has been biased high by 1%.

The error contributions to the reported $^{240}\text{Pu}_{\text{effective}}$ mass, m_{240} , due to the uncertainty in the doubles gate fraction is given as

$$\sigma_{m_{240},f_d} = \sqrt{\left(\frac{\delta m_{240}}{\delta f_d} + \frac{\delta m_{240}}{\delta M} \cdot \frac{\delta M}{\delta f_d}\right)^2 \sigma_{f_d}^2},$$

where

$$\frac{\delta m_{240}}{\delta f_d} = \frac{-2 \cdot D}{f_d^2 \cdot M^2 \cdot \nu_{s2} \cdot \Phi \cdot \varepsilon^2}.$$

Figure 12 shows the impact on the assay result from a 0.25% relative uncertainty in the doubles gate fraction as a function of total Pu mass for different alpha values.

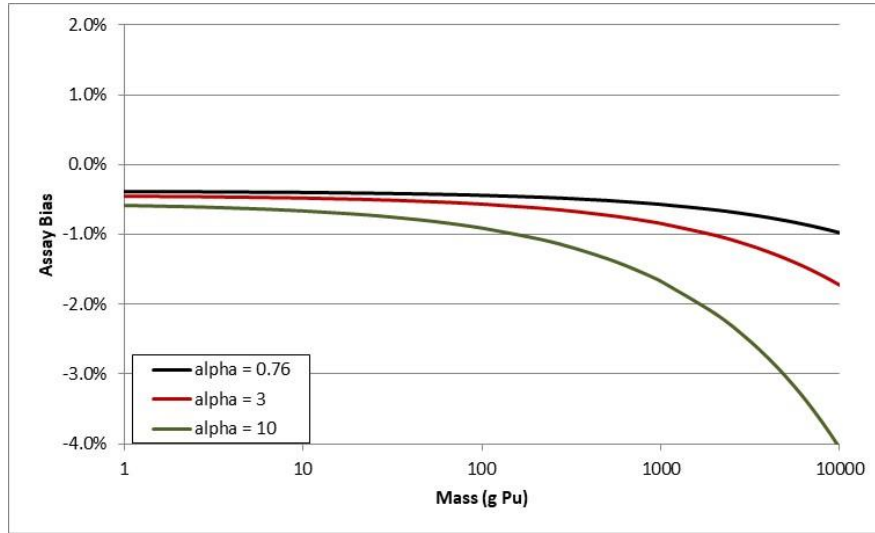


Figure 12. Bias introduced in the reported assay mass value for the measurement of high-burnup MOX materials in the PSMC if the doubles gate fraction is biased low by 0.25%.

The error contributions to the reported $^{240}\text{Pu}_{\text{effective}}$ mass, m_{240} , due to the uncertainty in the triples gate fraction is given as

$$\sigma_{m_{240},f_t} = \frac{\delta m_{240}}{\delta M} \cdot \frac{\delta M}{\delta f_t} \cdot \sigma_{f_t}.$$

Figure 13 shows the impact on the assay result from a 0.5% relative uncertainty in the triples gate fraction as a function of total Pu mass for different alpha values.

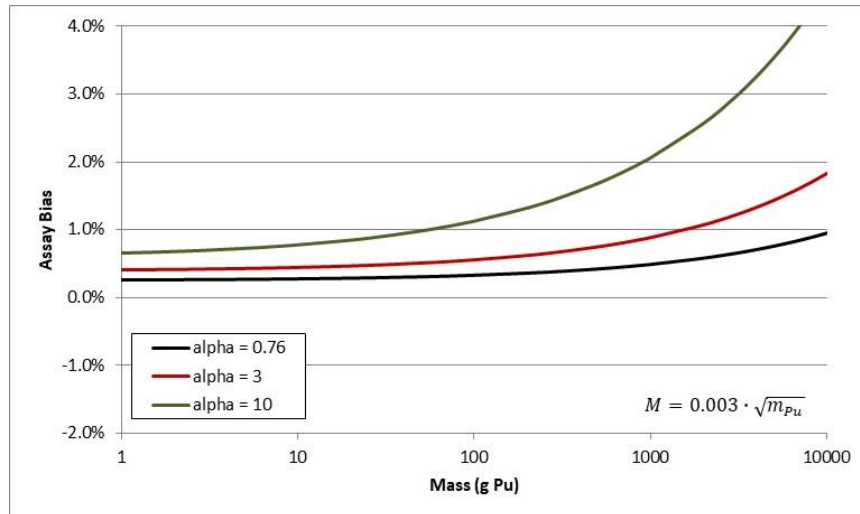


Figure 13. Bias introduced in the reported assay mass value for the measurement of high-burnup MOX materials in the PSMC if the triples gate fraction is biased low by 0.5%.

Figure 11 through Figure 13 examine the impact of the detector parameters on the assay result as a function of mass and do not take covariance into account. Examination of the point model equations shows that gate fractions are always present as a product with the efficiency. From this it seems likely that the gate fractions and efficiency will be correlated and that the covariance terms will be important. However, calibrations with ^{252}Cf sources which have no significant multiplication or alpha result in insignificant covariance between the doubles and triples gate fractions. For example, the results of a ^{252}Cf -based calibration of a multiplicity gave the following values for f_d and f_t .

$$\begin{aligned} f_d &= 0.6325 \pm 0.0011 \\ f_t &= 0.4097 \pm 0.0016 \quad \text{cov}(f_d, f_t) = 1.32\text{E-}05 \end{aligned}$$

If the gate fractions are later adjusted to accommodate for the limitations of the point model during representative calibrations, the covariance may or may not be negligible.

3.3 ^{240}Pu -EFFECTIVE SCALING FACTOR

The isotopic distribution of the Pu introduces uncertainties in a number of ways such as the intensity and energies of the emitted (α , n) neutrons. However, the multiplicity analysis only makes use of the isotopic distribution to determine the ^{240}Pu -effective mass scaling factor, m_{eff} . The multiplicity analysis is performed in terms of an effective ^{240}Pu mass because it is generally the dominant source of spontaneous fission within a Pu sample. The ^{240}Pu -effective mass represents the mass of ^{240}Pu that would provide the same coincidence rate as the sum of all fissioning isotopes contained within the item.

The ^{240}Pu -effective scaling factor, m_{eff} , is given by

$$m_{eff} = f_{Am} \cdot k_{Am} + \sum_n k_{Pu_n} \cdot f_{Pu_n},$$

where k_{Am} and k_{Pu} represent the specific $^{240}\text{Pu}_{eff}$ weighting factors for each isotope (based on the spontaneous fission rate and ν_2), and f_{Am} and f_{Pu} are the relative Am and Pu isotopic abundances (in wt%) at time of assay, respectively.

The uncertainty contributors impacting the value of $^{240}\text{Pu}_{eff}$ arise from the isotopic declaration, isotopic decay parameters, and weighting factors.

$$\sigma_{m_{eff}}^2 = (k_{Am}^2 \cdot \sigma_{f_{Am}}^2 + f_{Am}^2 \cdot \sigma_{k_{Am}}^2) + \sum_n (k_{Pu_n}^2 \cdot \sigma_{f_{Pu_n}}^2 + f_{Pu_n}^2 \cdot \sigma_{k_{Pu_n}}^2).$$

3.3.1 Isotopics Decay Correction and Uncertainty

The relative isotopic abundances will be provided either by mass spectrometry, alpha spectroscopy, or gamma-ray spectroscopy. The item assay may not take place until years following the isotopic declaration so that a decay correction must be applied. Keeping in mind that the relative abundances are given with respect to the current total Pu mass, the decay-corrected Pu isotopic mass fractions are given by the following expression:

$$f_{Pu_n} = f_{Pu_n,0} \cdot e^{-\lambda_{Pu_n} \cdot t} / \sum_n f_{Pu_n,0} \cdot e^{-\lambda_{Pu_n} \cdot t}.$$

The ^{241}Am decay must include the ingrowth from the decay of ^{241}Pu , so the decay-corrected ^{241}Am abundance relative to the total Pu mass is given by

$$f_{Am_{241}} \cong \frac{f_{Am_{241},0} \cdot e^{-\lambda_{Am_{241}} \cdot t} + \frac{\lambda_{Pu_{241}}}{\lambda_{Am_{241}} - \lambda_{Pu_{241}}} \cdot f_{Pu_{241},0} \cdot e^{-\lambda_{Pu_{241}} \cdot t} \cdot (e^{-\lambda_{Pu_{241}} \cdot t} - e^{-\lambda_{Am_{241}} \cdot t})}{\sum_n f_{Pu_n,0} \cdot e^{-\lambda_{Pu_n} \cdot t}},$$

where $f_{Pu_n,0}$ are the mass fractions of the various Pu isotopes at time of the Pu declaration,
 f_{Pu_n} are the mass fractions of the various Pu isotopes decay corrected to the assay date and normalized so that the sum of the Pu mass fractions will equal 1,
 n is the atomic number of the Pu isotope (e.g., 238, 239, ...),
 $f_{Am_{241},0}$ is the mass fraction of ^{241}Am relative to the sum of the decay-corrected Pu isotopes on the Am declaration date with buildup of ^{241}Am from ^{241}Pu decay,
 $f_{Am_{241}}$ is mass fraction of the decay-corrected ^{241}Am relative to the sum of the decay-corrected Pu isotopes at the assay date, and
 t is the time between the assay date and the relevant declaration date.

The half-lives and uncertainties of the isotopes generally of concern to multiplicity measurements are presented in Table 5.

Table 5. Isotopic data for decay correction.

Isotope	Half Life (y) [27]	λ (1/s)
Pu-238	87.74 \pm 0.09	2.50E-10 \pm 2.6E-13
Pu-239	24100 \pm 30	9.11E-13 \pm 1.1E-15
Pu-240	6560 \pm 7	3.35E-12 \pm 3.6E-15
Pu-241	14.35 \pm 0.10	1.53E-09 \pm 2.1E-11
Pu-242	376000 \pm 2000	5.84E-14 \pm 3.1E-16
Pu-244	8.26E+07 \pm 9.0E+05	2.66E-16 \pm 2.9E-18
Am-241	433.6 \pm 0.50	5.07E-11 \pm 5.8E-14
Cf-252	2.645 \pm 0.01	8.30E-09 \pm 2.5E-11

The uncertainties in the isotopic decay corrections for each of the Pu isotopes and ^{241}Am are given by the following:

$$\sigma_{f_{Pu_n}} = \sqrt{\left(\left(\frac{f_{Pu_n}}{f_{Pu_n,0}} \right) \cdot \sigma_{f_{Pu_n,0}} \right)^2 + \left(\left(\frac{f_{Pu_n} - f_{Pu_n,0}}{f_{Pu_n,0}} \right) \cdot t \cdot \sigma_{\lambda_{Pu_n}} \right)^2},$$

and

$$\sigma_{f_{Am_{241}}} = \sqrt{\left(\frac{f_{Am_{241}}}{f_{Am_{241},0}} \right)^2 \cdot \sigma_{f_{Am_{241},0}}^2 + \left(\frac{f_{Am_{241}}}{f_{Am_{241},0}} \right)^2 \cdot t^2 \cdot \sigma_{\lambda_{Am_{241}}}^2 + (f_{Am_{241}} - f_{Am_{241},0} \cdot e^{-\lambda_{Am_{241}} \cdot t}) \cdot \sigma_{f_{Pu_{241}}}^2}.$$

3.3.2 $^{240}\text{Pu}_{\text{effective}}$ Uncertainty due to the Isotopic Declaration and Decay Correction

The multiplicity analysis is performed in terms of an effective ^{240}Pu mass because it is generally the dominant source of spontaneous fission within a Pu sample. The spontaneous fission contributions of ^{238}Pu and ^{242}Pu are weighted based on their isotopic abundance and relative spontaneous fission rates. The values for ^{238}Pu and ^{242}Pu are taken from Ref. [28].

There is a significant difference in the uncertainty arising from isotopic data provided from destructive and nondestructive means. While the uncertainties in the isotopic abundances obtained from destructive analysis methods (e.g., isotope dilution mass spectrometry) may be of the order of 0.1%, gamma-ray spectroscopy methods will typically provide uncertainties on the order of 1% (10× larger). Table 6 provides example results for a high-burnup/high- ^{241}Am item determined using a commonly accepted gamma-ray isotopics code.

Table 6. Example Pu isotopic decay correction.

Isotope	Declared Abundance	Decay Corrected to Assay Date
Pu-238	1.167 ± 0.008	1.147 ± 0.010
Pu-239	64.115 ± 0.321	64.596 ± 0.456
Pu-240	26.137 ± 0.178	26.326 ± 0.253
Pu-241	5.059 ± 0.031	4.382 ± 0.039
Pu-242	3.521 ± 0.352	3.548 ± 0.501
Am-241	3.232 ± 0.020	3.853 ± 0.037
	Pu Date: Apr 19 1992 Am Date: Apr 19 1992	Assay Date: Jun 06 1995
$^{240}\text{Pu}_{\text{eff}}$		0.3531 ± 0.0090

3.3.3 $^{240}\text{Pu}_{\text{effective}}$ Conversion Constants Contribution

As stated in the previous section, the multiplicity analysis is performed in terms of an effective ^{240}Pu mass because it is generally the dominant source of spontaneous fission within a Pu sample. The uncertainty in the $^{240}\text{Pu}_{\text{eff}}$ value includes an additional contribution due to the uncertainty in the nuclear data. The spontaneous fission contribution weighting factors each have an associated uncertainty and are presented in Table 7.

Table 7. Isotopic data for decay correction (values for ^{238}Pu and ^{242}Pu from Ref. [28], values for ^{244}Pu and ^{241}Am are estimates).

Isotope	^{240}Pu Equivalent
Pu-238	2.566 ± 0.235
Pu-240	1 ± 0
Pu-242	1.702 ± 0.036
Pu-244	1.75 ± 0.17
Am-241	0.0017 ± 0.0001

The corresponding uncertainty contribution for the $^{240}\text{Pu}_{\text{effective}}$ fraction, σ_{eff} , is expressed as

$$\sigma_{m_{eff}}^2 = f_{Am}^2 \cdot \sigma_{k_{Am}}^2 + \sum_n f_{Pu_n}^2 \cdot \sigma_{k_{Pu_n}}^2 .$$

Generally the contributions from ^{241}Am and ^{244}Pu may be ignored so that the value of σ_{eff} and error contributors and given by the following expression [28], [20]

$$m_{eff} = (2.566 \pm 0.235) \cdot f_{Pu_{238}} + f_{240} + (1.702 \pm 0.036) \cdot f_{242} .$$

To illustrate the magnitude of this bias, consider high-burnup MOX materials with 1.5 wt% ^{238}Pu , 5 wt% ^{242}Pu , and 1 wt% ^{241}Am . The error contribution to the mass result is

$$\frac{\sigma_{m_{eff}}}{m_{eff}} = \sqrt{(0.235 \cdot 0.015)^2 + (0.036 \cdot 0.05)^2} = \sim 0.5\% .$$

We should note that the values for $^{240}\text{Pu}_{\text{effective}}$ differ from those listed in the INCC User's Manual [6], which in turn are based on values derived from the PANDA manual [29]. However, there are no error estimates associated with the PANDA values, which appears to leave out a potential significant source of bias. However, for material streams with a limited range of isotopic abundances, this bias may to some extent be reduced by the use of representative standards for calibrations. That is, the necessary bias correction is subsumed into the adjustment of the detection efficiency and gate fraction (away from the point source calibration values).

3.4 FISSION PARAMETERS

The values listed in Table 8 represent a current evaluation of the nuclear data parameters for ^{239}Pu and ^{240}Pu for use in safeguards neutron multiplicity analysis based on the analysis of data from [28, 30, 31]. Based on the data set used to derive the evaluated parameters, a preliminary evaluation of the associated uncertainty values was performed. The multiplicity analysis also requires similar data for ^{238}Pu and ^{242}Pu , but there is insufficient data in the literature to provide similarly robust evaluations. These values and uncertainties were examined through a sensitivity analysis to evaluate the impact on the final assay mass result and compared with the statistical uncertainties for typical assay results.

Table 8. Nuclear data parameters and uncertainties.

Isotope	Constant	Value	Relative Error
^{240}Pu	Φ	473.5 ± 3.9 fission/n	(0.82%)
^{240}Pu	ν_{s1}	2.154 ± 0.005 n/fission	(0.2%)
^{240}Pu	ν_{s2}	3.789 ± 0.013 1/fission	(0.3%)
^{240}Pu	ν_{s3}	5.210 ± 0.067 1/fission	(1.3%)
^{240}Pu	$\text{covar}(\nu_{s2}, \nu_{s3})$	0.000768	
^{239}Pu	ν_{i1}	3.1635 ± 0.0680 n/fission	(0.2%)
^{239}Pu	ν_{i2}	8.3050 ± 0.0407 1/fission	(0.5%)
^{239}Pu	ν_{i3}	17.782 ± 0.151 1/fission	(0.8%)

The error contribution for the nuclear data constants is examined by first determining the partial derivatives of the m_{240} mass and multiplication with respect to each constant. First, we note that the constant, ν_{s1} , does not appear in the expressions for multiplication or m_{240} effective mass and no impact

on the assay mass result using the standard point model analysis. From the expression for the ^{240}Pu effective mass,

$$m_{240} = \frac{\frac{2 \cdot D}{\varepsilon \cdot f_d} - \frac{M \cdot (M - 1) \cdot v_{i2} \cdot S}{(v_{i1} - 1)}}{\varepsilon \cdot M^2 \cdot v_{s2} \cdot \Phi},$$

the partial derivatives with respect to the fission moment are determined to be

$$\begin{aligned} \frac{\delta m_{240}}{\delta v_{s1}} &= 0 ; \quad \frac{\delta M}{\delta v_{s1}} = 0, \\ \frac{\delta m_{240}}{\delta v_{s2}} &= -\frac{m_{240}}{v_{s2}} + \frac{\delta m_{240}}{\delta M} \cdot \frac{\delta M}{\delta v_{i3}}, \\ \frac{\delta m_{240}}{\delta v_{i3}} &= \frac{\delta m_{240}}{\delta M} \cdot \frac{\delta M}{\delta v_{i3}}, \end{aligned}$$

and requiring the partial derivatives of M. These are given as

$$\begin{aligned} \frac{\delta M}{\delta v_{s2}} &= \frac{f_1 \cdot \frac{v_{i3}}{k_4} - \frac{k_1}{v_{i2}} - (k_3 + 1) \cdot \frac{M^2}{v_{s2}} + \frac{6 \cdot D \cdot v_{i2}}{k_4 \cdot \varepsilon \cdot f_d \cdot S} \cdot M}{f_2}, \\ \frac{\delta M}{\delta v_{s3}} &= -\frac{f_1 \cdot \frac{v_{i2}}{k_4} + \frac{2 \cdot D \cdot (v_{i1} - 1)}{k_4 \cdot \varepsilon \cdot f_d \cdot S}}{f_2}, \\ \frac{\delta m_{240}}{\delta M} &= \frac{-4 \cdot D}{f_d \cdot v_{s2} \cdot \Phi \cdot \varepsilon^2 \cdot M^3} - \frac{v_{i2} \cdot S}{(v_{i1} - 1) \cdot v_{s2} \cdot \Phi \cdot \varepsilon \cdot M^2}, \end{aligned}$$

where we have defined

$$k_4 = (v_{s2} \cdot v_{i3} - v_{s3} v_{i2}),$$

$$f_1 = k_1 + k_2 \cdot M + (k_3 + 1) \cdot M^2, \text{ and}$$

$$f_2 = k_2 + 2 \cdot M \cdot k_3 + 3 \cdot M^2 \text{ for convenience.}$$

The resulting uncertainties are given by the following expressions.

$$\begin{aligned} \sigma_{m_{240}, v_{s1}} &= 0, \\ \sigma_{m_{240}, v_{s2}} &= \sqrt{\left(\frac{\delta m_{240}}{\delta v_{i2}} + \frac{\delta m_{240}}{\delta M} \cdot \frac{\delta M}{\delta v_{i2}} \right)^2 \cdot \sigma_{v_{s2}}^2}, \\ \sigma_{m_{240}, v_{s3}} &= \sqrt{\left(\frac{\delta m_{240}}{\delta M} \cdot \frac{\delta M}{\delta v_{s3}} \right)^2 \cdot \sigma_{v_{s3}}^2}. \end{aligned}$$

To illustrate the potential impact on the multiplicity mass assay result, Figure 14 and Figure 15 plot the relative change in the mass assay result due to a 1% positive change in the values of ν_{s2} and ν_{s3} , respectively.

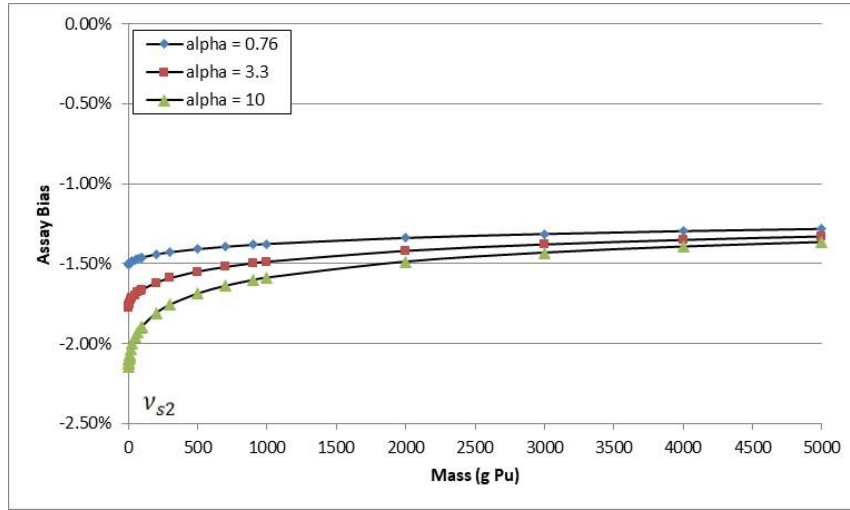


Figure 14. Impact of a 1% positive bias in the value of ν_{s2} on the mass assay result.

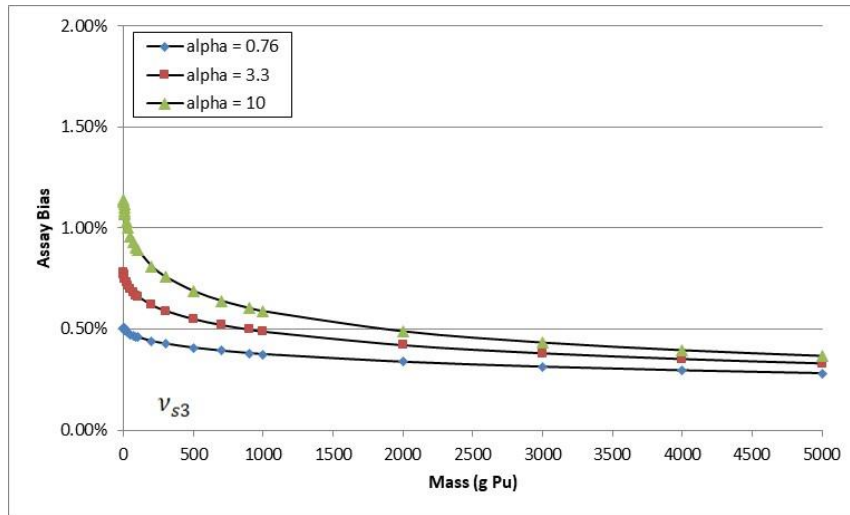


Figure 15. Impact of a 1% positive bias in the value of ν_{s3} on the mass assay result.

The values of ν_{s2} and ν_{s3} are correlated and the uncertainty contribution to the ^{240}Pu mass assay result.

$$\sigma_{m_{240}, \nu_S} = \sqrt{\left(\frac{\delta m_{240}}{\delta \nu_{s2}}\right)^2 \cdot \sigma_{\nu_{s2}}^2 + \left(\frac{\delta m_{240}}{\delta \nu_{s3}}\right)^2 \cdot \sigma_{\nu_{s3}}^2 + 2 \cdot \frac{\delta m_{240}}{\delta \nu_{s2}} \cdot \frac{\delta m_{240}}{\delta \nu_{s3}} \cdot \text{covar}(\nu_{s2}, \nu_{s3})}$$

Using the values for ν_{s2} and ν_{s3} in Table 8, the uncertainty due to the spontaneous fission moments as a function of mass (assuming $M = 0.003m^{1/2}$ and the $^{240}\text{Pu}_{\text{eff}} = 0.33 \text{ g/g}$) is plotted in Figure 16. From the figure it is seen that the uncertainty contribution due to the spontaneous fission moments is 1.5% or greater for typical MOX materials.

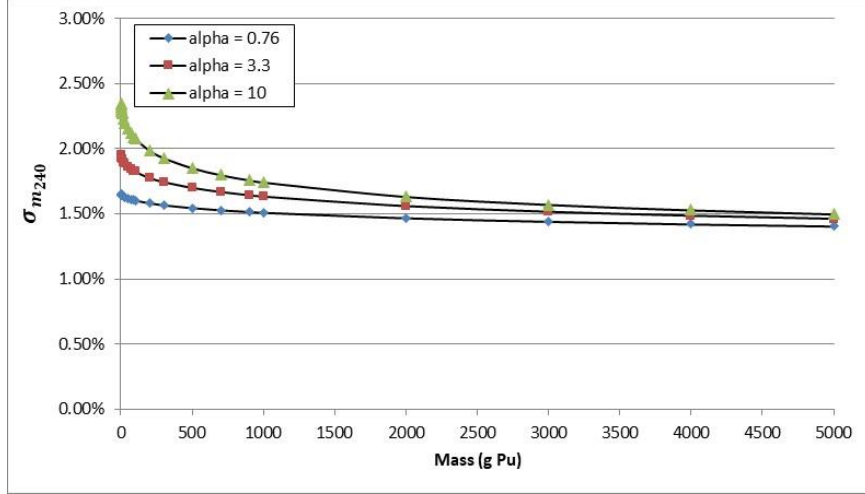


Figure 16. The m_{240} uncertainty contribution due to the spontaneous fission data.

Similarly, for the induced fission moments, the partial derivatives are

$$\frac{\delta m_{240}}{\delta v_{i1}} = \frac{\left(1 - \frac{1}{M}\right) \cdot v_{i2} \cdot S}{(v_{i1} - 1)^2 \cdot v_{s2} \cdot \Phi \cdot \varepsilon} + \frac{\delta m_{240}}{\delta M} \cdot \frac{\delta M}{\delta v_{i1}},$$

which can be expanded to

$$\frac{\delta m_{240}}{\delta v_{i1}} = \frac{1}{v_{s2} \cdot \Phi \cdot \varepsilon} \cdot \left\{ \frac{v_{i2} \cdot S}{(v_{i1} - 1)} \cdot \left[\frac{(M - 1)}{(v_{i1} - 1) \cdot M} - \frac{1}{M^2} \right] + \frac{4D}{f_d \cdot \varepsilon \cdot M^3} \right\} \cdot \frac{\delta M}{\delta v_{i1}},$$

where

$$\frac{\partial M}{\partial v_{i1}} = - \frac{\frac{\partial k_1}{\partial v_{i1}} + \frac{\partial k_2}{\partial v_{i1}} M}{k_2 + k_3 2M + 3M^2},$$

or

$$\frac{\delta M}{\delta v_{i1}} = - \frac{\frac{k_1}{(v_{i1} - 1)} + \frac{2 \cdot D \cdot v_{s3} \cdot M}{k_4 \cdot f_d \cdot \varepsilon \cdot S}}{f_2},$$

where k_4 and f_2 have been defined above.

$$\frac{\delta m_{240}}{\delta v_{i2}} = \frac{\left(1 - \frac{1}{M}\right) \cdot S}{(v_{i1} - 1) \cdot v_{s2} \cdot \Phi \cdot \varepsilon} + \frac{\delta m_{240}}{\delta M} \cdot \frac{\delta M}{\delta v_{i2}}.$$

$$\frac{\delta m_{240}}{\delta v_{i3}} = \frac{\delta m_{240}}{\delta M} \cdot \frac{\delta M}{\delta v_{i3}}.$$

$$\frac{\delta M}{\delta v_{i2}} = - \frac{f_1 \cdot \frac{v_{s3}}{k_4} + (k_3 + 1) \cdot \frac{M^2}{v_{i2}} - \frac{6 \cdot D \cdot v_{s2}}{k_4 \cdot \varepsilon \cdot f_d \cdot S} \cdot M}{f_2} .$$

$$\frac{\delta M}{\delta v_{i3}} = - \frac{f_1 \cdot \frac{v_{s2}}{k_4}}{f_2} .$$

The resulting uncertainties are given by the following expressions.

$$\sigma_{m_{240}, v_{i1}} = \sqrt{\left(\frac{\delta m_{240}}{\delta v_{i1}} + \frac{\delta m_{240}}{\delta M} \cdot \frac{\delta M}{\delta v_{i1}} \right)^2 \cdot \sigma_{v_{i1}}^2} .$$

$$\sigma_{m_{240}, v_{i2}} = \sqrt{\left(\frac{\delta m_{240}}{\delta v_{i2}} + \frac{\delta m_{240}}{\delta M} \cdot \frac{\delta M}{\delta v_{i2}} \right)^2 \cdot \sigma_{v_{i2}}^2} .$$

$$\sigma_{m_{240}, v_{i3}} = \sqrt{\left(\frac{\delta m_{240}}{\delta M} \cdot \frac{\delta M}{\delta v_{i3}} \right)^2 \cdot \sigma_{v_{i3}}^2} .$$

At present there are no covariance data for the induced fission moments, so a complete evaluation of the contribution to the total measurement uncertainty cannot be performed at this time. The relative impact on the assay mass result due to a hypothetical positive 1% increase in each of the induced fission moments is shown in Figure 17 through Figure 19.

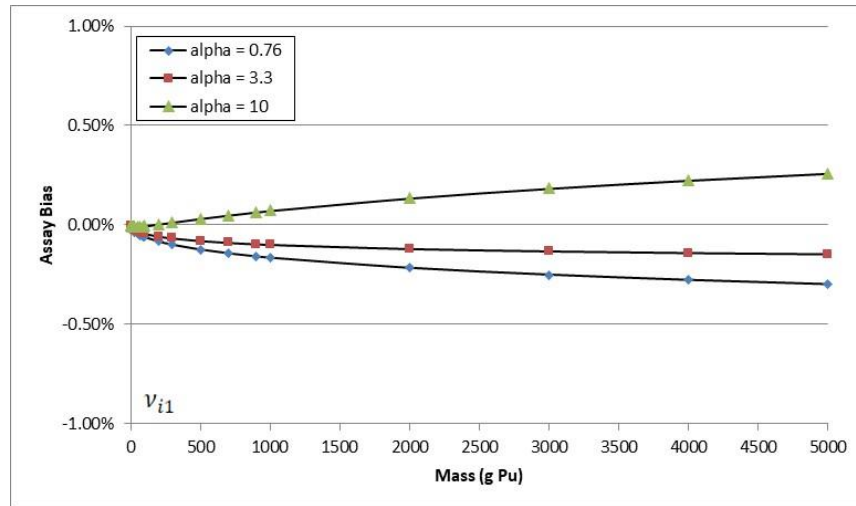


Figure 17. Impact of a 1% positive bias in the value of v_{i1} on the mass assay result.

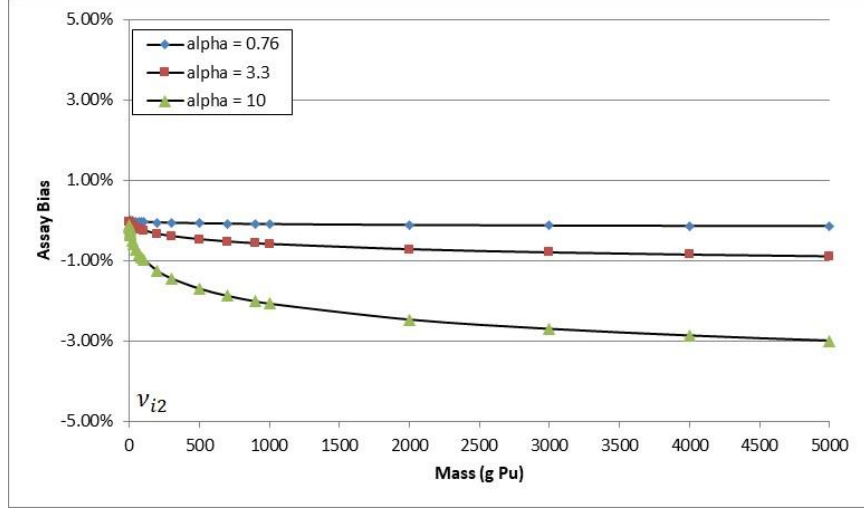


Figure 18. Impact of a 1% positive bias in the value of ν_{i2} on the mass assay result.

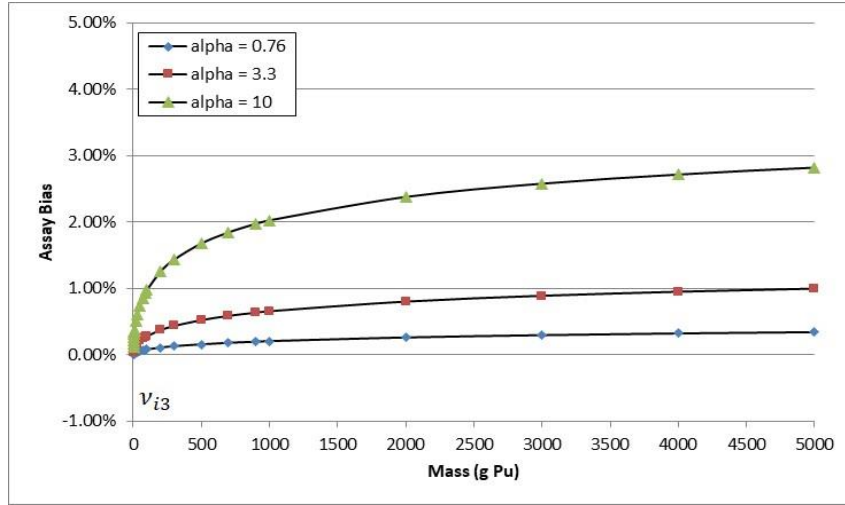


Figure 19. Impact of a 1% positive bias in the value of ν_{i3} on the mass assay result.

Assuming the values of ν_{i1} , ν_{i2} , and ν_{i3} are fully correlated, the uncertainty contribution to the m_{240} mass value is

$$\sigma_{m_{240}, \nu_i} = \sqrt{\left(\frac{\delta m_{240}}{\delta \nu_{i1}}\right)^2 \cdot \sigma_{\nu_{i1}}^2 + \left(\frac{\delta m_{240}}{\delta \nu_{i2}}\right)^2 \cdot \sigma_{\nu_{i2}}^2 + \left(\frac{\delta m_{240}}{\delta \nu_{i3}}\right)^2 \cdot \sigma_{\nu_{i3}}^2 + 2 \cdot \left(\frac{\delta m_{240}}{\delta \nu_{i1}} \cdot \frac{\delta m_{240}}{\delta \nu_{i2}} \cdot \sigma_{\nu_{i1}} \cdot \sigma_{\nu_{i2}} + \frac{\delta m_{240}}{\delta \nu_{i1}} \cdot \frac{\delta m_{240}}{\delta \nu_{i3}} \cdot \sigma_{\nu_{i1}} \cdot \sigma_{\nu_{i3}} + \frac{\delta m_{240}}{\delta \nu_{i2}} \cdot \frac{\delta m_{240}}{\delta \nu_{i3}} \cdot \sigma_{\nu_{i2}} \cdot \sigma_{\nu_{i3}}\right)}$$

The estimated uncertainty due to the induced fission parameters is shown in Figure 20.

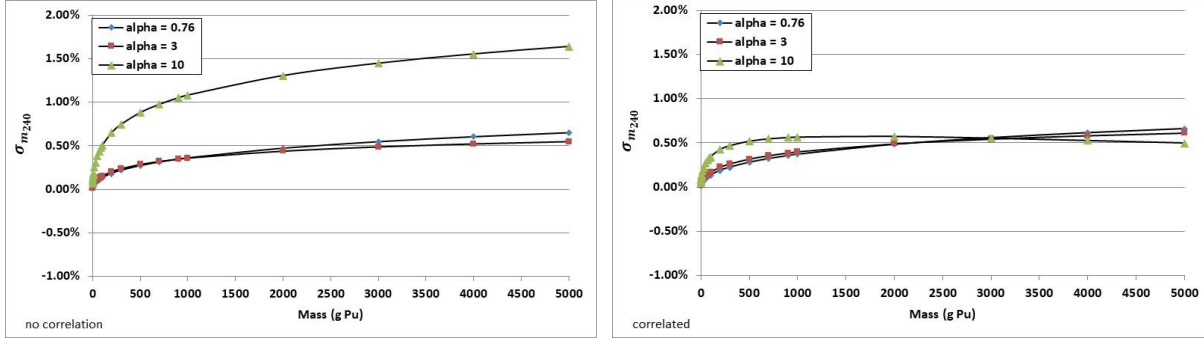


Figure 20. Uncertainty contribution from the induced fission moments assuming the values of ν_{i1} , ν_{i2} , and ν_{i3} are uncorrelated (left) and fully correlated (right).

3.5 FILL HEIGHT

Changes in fill height are almost always associated with a change in mass and multiplication; however, in this section we only consider the spatial dependence of the assay cavity detection efficiency on the assay result. The volume average neutron detection efficiency changes with the fill height of the container, as shown in Figure 21. If the container average efficiency differs from the stated detection efficiency, the fill height introduces a bias into the assay result. If the fill height is not constant for all items, a random uncertainty will be introduced.

To examine the fill height dependence, it is necessary to know how the system was calibrated. Calibrations based on a point source or volumetric containers will result in a different reference neutron detection efficiency and reference height. For the following example it is assumed that the detection efficiency was determined using a non-multiplying point source of ^{240}Pu located in the center of the assay cavity.

To estimate the uncertainty contribution due to the container fill height, the fill height is estimated from the assay total Pu mass result based on the assumed material-type characteristics. For instance, an item containing MOX powder may have a typical density of 2.5 g/cc but could be anywhere in the range of 2 to 4 g/cc. And for this example, the U:Pu ratio is 2::1 and the chemical forms of the constituents are UO_2 and PuO_2 only. For this example, 720 g Pu that is contained in a 10 cm ID container would have an expected fill height of 12.3 cm but could be as low as 7.7 or as high as 15.4 cm.

The bias due to the fill height is determined from the difference in the volume average efficiency for the 12.3 cm fill height relative to the point source efficiency. The volume average efficiency for the container is determined by integrating the expression for $\epsilon(r, z)$ over the material volume. In this example, the volume average efficiency relative to the point source efficiency is 0.995, suggesting that the efficiency used in the PME analysis would be 0.5% too large. Using the expression above for $\frac{\delta m_{240}}{\delta \epsilon}$,

$$\sigma_{m_{240}, FH} = \frac{\delta m_{240}}{\delta \epsilon} \cdot \Delta \epsilon,$$

and for this example, we would expect an average 0.7% negative bias in the assay result for alpha=0.76 (Figure 11). A plot of the mass assay bias as a function of fill height is shown in Figure 22.

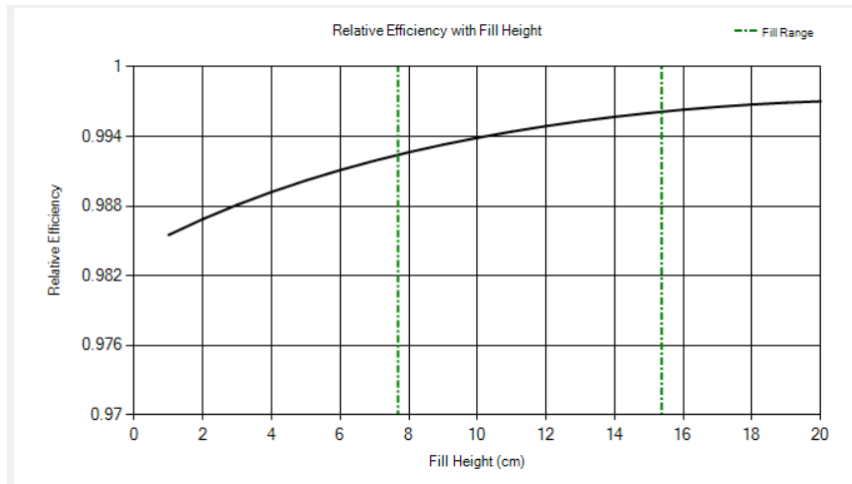


Figure 21. Calculated fill height impact on the average neutron detection efficiency for a typical multiplicity measurement.

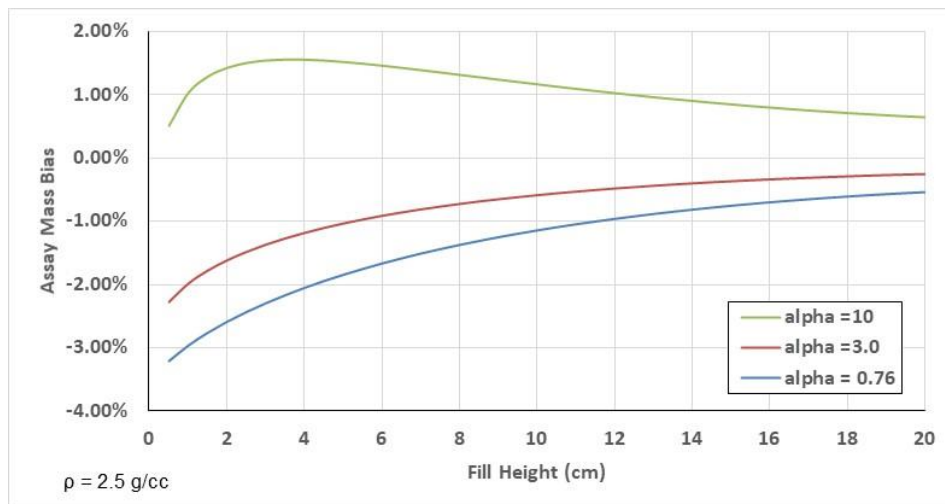


Figure 22. Expected bias in the mass assay result due to the container fill height for a 10 cm ID container located 5 cm above the assay cavity floor of a PSMC.

The random uncertainty component is estimated from the range of possible fill heights determined from the assay mass result and the expected density range of the material type. A probability distribution must be selected for the fill height distribution (e.g., normal, equal, or linear). We have arbitrarily chosen to use a normal distribution for the fill height and set the $\pm 3\sigma$ limits as h_{\min} and h_{\max} so that $\sigma_h = (h_{\max} - h_{\min})/6$. The resulting mass distribution also follows a near normal distribution, as shown in Figure 23. For comparison, the mass distribution for a hypothetical long PSMC with an 80 cm tall assay cavity is shown in Figure 24.

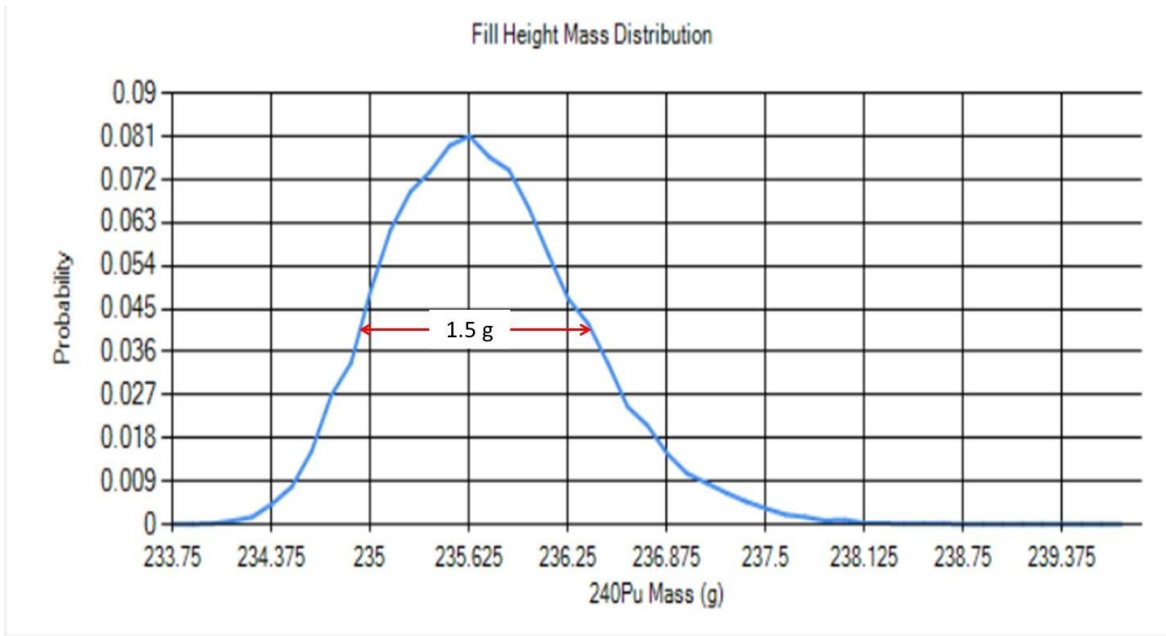


Figure 23. Estimated m_{240} assay result probability distribution due to fill height variation based on a random distribution of fill heights (based on 20,000 random fill heights) for measurements with a PSMC.

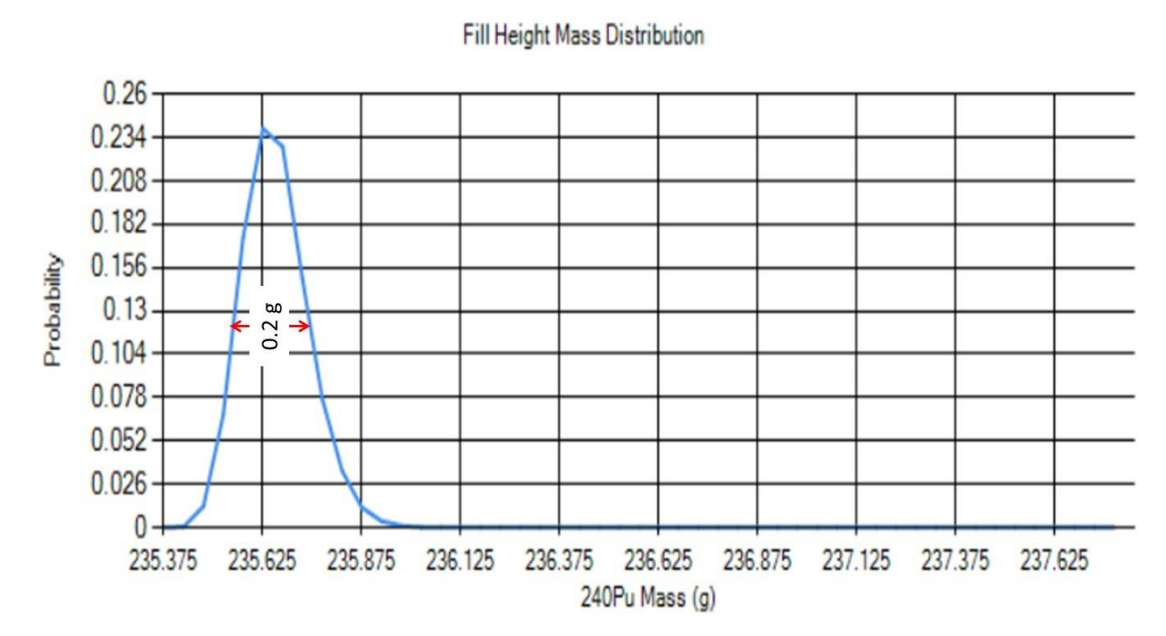


Figure 24. Estimated m_{240} assay result probability distribution due to fill height variation based on a random distribution of fill heights for a PSMC with a 80 cm tall assay cavity.

3.6 RADIAL OFFSET

In practice the container will not be loaded into the assay cavity perfectly on the axial centerline. This radial offset will result in both systematic and random error contributions. As with the fill height contribution, the volume average efficiency is determined using the expression for $\epsilon(r, z)$ integrated over the material volume relative to the response from a properly centered container. An example of the relative volume average efficiency as a function of the radial offset is shown in Figure 25, and the

resulting mass probability distribution is shown in Figure 26 (a 10 cm ID container assay using the PSMC or ENMC assuming a 1 cm average offset and 1 cm relative deviation about the average). As can be seen in Figure 26, the distribution is not well represented by the normal distribution. However, for a well-designed multiplicity counter, the random uncertainty contribution will be less than 0.2% so that representation of the random component as a normal distribution will not have a significant impact on the total measurement uncertainty.

The relative bias introduced by the radial offset is determined by evaluating the mass using the volume average efficiency for the item at both the cavity center and at the offset position.

$$\Delta_{radial} = \frac{m(\iint \varepsilon(r - r_{eff}, z)) - m(\iint \varepsilon(r, z))}{m(\iint \varepsilon(r, z))}$$

The random component, σ_{radial} , is determined from the standard deviation of 20,000 random locations about the radial offset position.

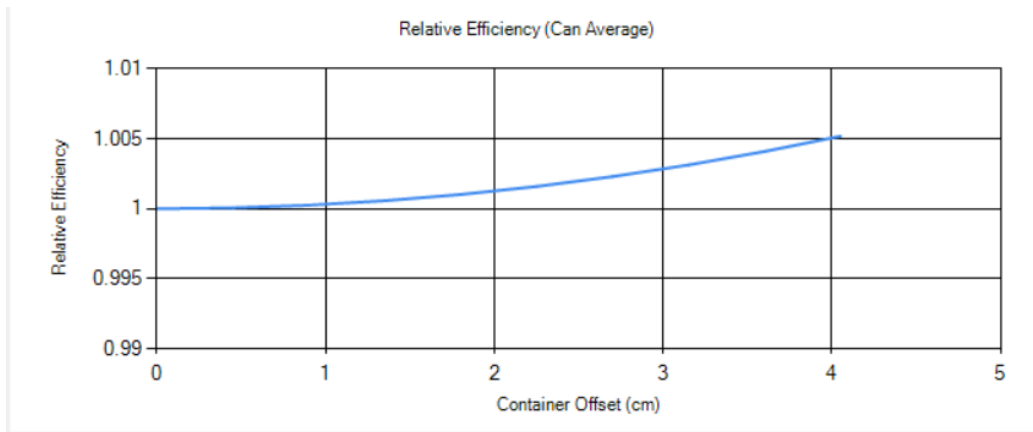


Figure 25. Change in volume average efficiency with radial offset (for a 10 cm OD can with 5 cm fill height).

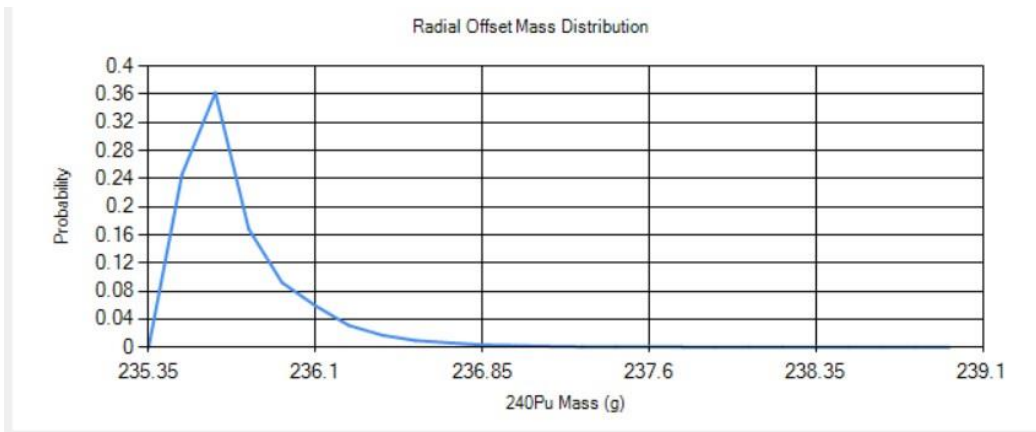


Figure 26. Probability distribution of reported assay results for a 10 cm OD container with a 1 cm typical radial offset and 1 cm deviation about that offset.

3.7 DENSITY EFFECTS

For a given material type (e.g., PuO₂ or MOX), as the density increases, the item's self-multiplication will increase, the average energy of the emitted neutrons and the induced fission moments will change, and the

moderating/absorbing properties of the material will increase, impacting the detection efficiency of the emitted neutrons. The PME only accommodates the change in multiplication; the other effects will result in measurement biases if proper calibrations and corrections are not applied.

The impact of density on the assay result has been examined via MCNP simulations of a series of PuO₂ and MOX materials assayed in the PSMC and ENMC counters. The sequence of simulated assays performed mimics the sequence of measurements that would be taken during the calibration of systems. The basic counter response is determined using a point source of ²⁴⁰Pu centered in the assay cavity. The simulated measurements resulted in the following parameters for a point located at the center of the assay cavity.

Table 9. Simulated neutron detector parameters for the PSMC and ENMC systems for a ²⁴⁰Pu point source.

	PSMC	ENMC
Efficiency	0.5336	0.6393
Doubles gate fraction	0.6558	0.6912
Triples gate fraction	0.4353	0.4870
Die-Away (μs)	49.9	22.3
Pre-Delay (μs)	4.5	1.5
Gate Width (μs)	64	32

If these parameters were to be used for the assay of containers of PuO₂ or MOX materials, significant biases would be incurred in the assay results, for example, a simulated assay of a series of PuO₂ items with increasing mass and fixed density ($\rho=2.5$ g/cc) and $\alpha=0.76$ and analyzed using the PME and parameters shown in Table 9. The simulated rates and mass analysis results for these items are provided in Table 10 and Table 11, and the resulting bias in the mass result is shown in Figure 27. Applying the point source calibration to the assay of full size containers can result in significant (~2.5%) relative errors.

Table 10. Simulated PSMC rates for the PuO₂ baseline items.

Item Properties					Simulated Rates					
Item	Pu mass (g)	m_{240} (g)	alpha	Input Multiplication	Singles		Doubles		Triples	
1	352.6	91.6	0.76	1.0509	89390	± 10	19383	± 8	4830	± 13
2	705.3	183.3	0.76	1.0775	183764	± 20	44278	± 18	13218	± 30
3	1057.9	274.9	0.76	1.0964	281189	± 31	72767	± 29	24335	± 50
4	1410.5	366.5	0.76	1.1110	380785	± 41	104003	± 40	37795	± 72
5	1763.2	458.2	0.76	1.1228	481970	± 52	137304	± 51	53129	± 96
6	2115.8	549.8	0.76	1.1326	584511	± 62	172375	± 63	70145	± 121
7	2468.5	641.5	0.76	1.1411	687989	± 73	209029	± 75	88914	± 147
8	2821.1	733.1	0.76	1.1484	792176	± 84	246617	± 87	108460	± 174
9	3173.7	824.7	0.76	1.1548	896819	± 94	285228	± 99	129381	± 202
10	3526.4	916.4	0.76	1.1605	1002091	± 105	324681	± 112	150875	± 230

Table 11. PME analysis results for the PuO₂ baseline items simulated rates using ²⁴⁰Pu point calibration.

Item Properties				Simulated Assay Results				
Item	m_{240} (g)	alpha	Expected Multiplication	Multiplication	Alpha	m_{240}	Bias	
1	92.5	0.76	1.0509	1.0424 ± 0.0003	0.7688 ± 0.0036	86.81 ± 0.10	-5.3%	
2	185.0	0.76	1.0775	1.0667 ± 0.0003	0.7656 ± 0.0037	174.11 ± 0.19	-5.0%	
3	277.5	0.76	1.0964	1.0840 ± 0.0003	0.7628 ± 0.0037	261.87 ± 0.29	-4.7%	
4	370.0	0.76	1.1110	1.0976 ± 0.0003	0.7620 ± 0.0037	349.60 ± 0.38	-4.6%	
5	462.5	0.76	1.1228	1.1085 ± 0.0003	0.7609 ± 0.0037	437.60 ± 0.47	-4.5%	
6	555.0	0.76	1.1326	1.1176 ± 0.0003	0.7600 ± 0.0037	525.85 ± 0.56	-4.4%	
7	647.5	0.76	1.1411	1.1260 ± 0.0003	0.7618 ± 0.0037	612.96 ± 0.65	-4.4%	
8	740.0	0.76	1.1484	1.1324 ± 0.0003	0.7593 ± 0.0037	702.05 ± 0.74	-4.2%	
9	832.5	0.76	1.1548	1.1386 ± 0.0003	0.7604 ± 0.0037	789.34 ± 0.82	-4.3%	
10	925.0	0.76	1.1605	1.1436 ± 0.0003	0.7569 ± 0.0036	879.40 ± 0.91	-4.0%	

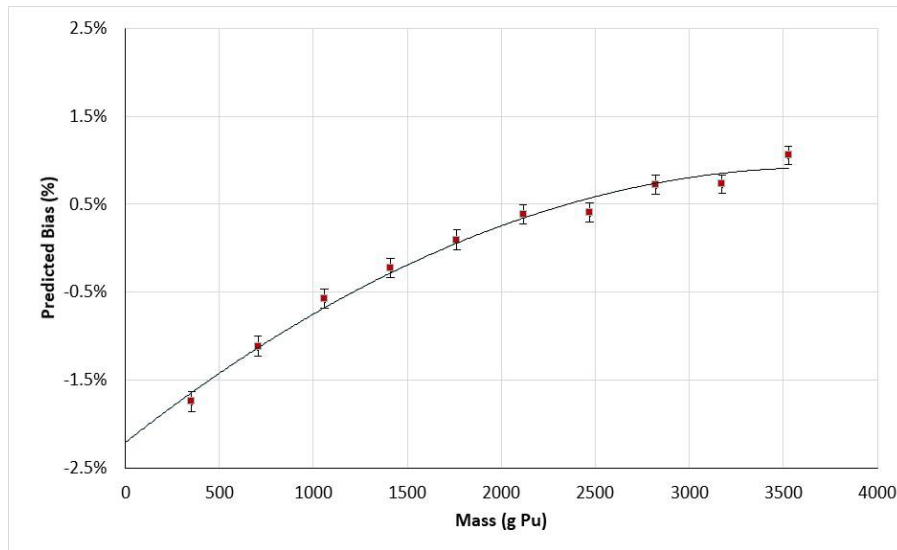


Figure 27. Mass assay bias resulting from the use of point source calibration parameters for volumetric items (PuO₂ at 2.5 g/cc).

If these same simulated assay results are used to “calibrate” the system (adjust the efficiency and gate fractions) in the same manner as calibration using representative standards, it is possible to eliminate the bias, as shown in Figure 28 for the PSMC and Figure 29 for the ENMC. The same series of containers (10 ID × 20 cm tall) and PuO₂ fill were performed for both counters. (The only difference is that the containers were located at the typical 5 cm above the cavity floor for the PSMC and 10 cm for the ENMC.) The adjusted detector parameters are provided in Table 12. Detector parameters for point source and volumetric calibrations ($\rho=2.5$ g/cc). These “successful” calibrations are possible because the efficiency and nuclear data dependences (to be discussed in a later section) are compensated for by use of incorrect gate fractions.

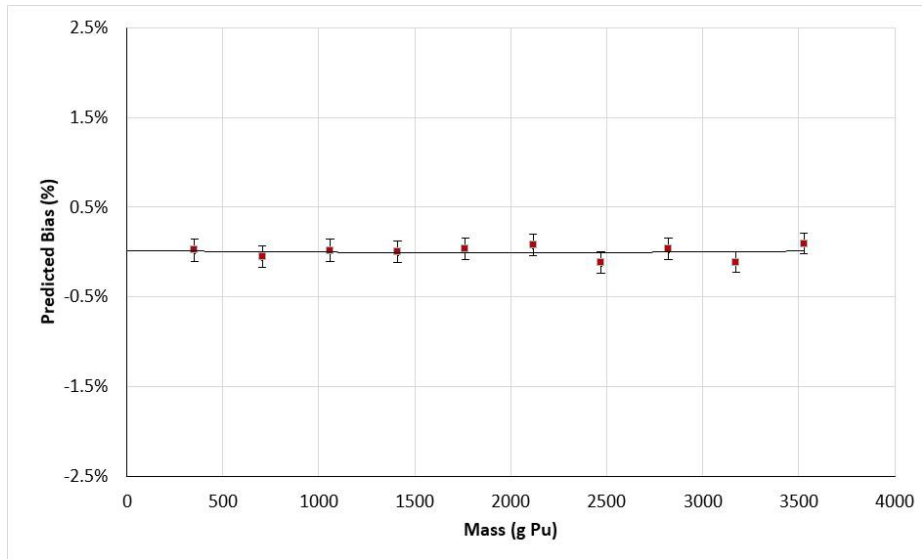


Figure 28. Mass assay bias using the PSMC following calibration based on the 2.5 g/cc PuO₂ containers.

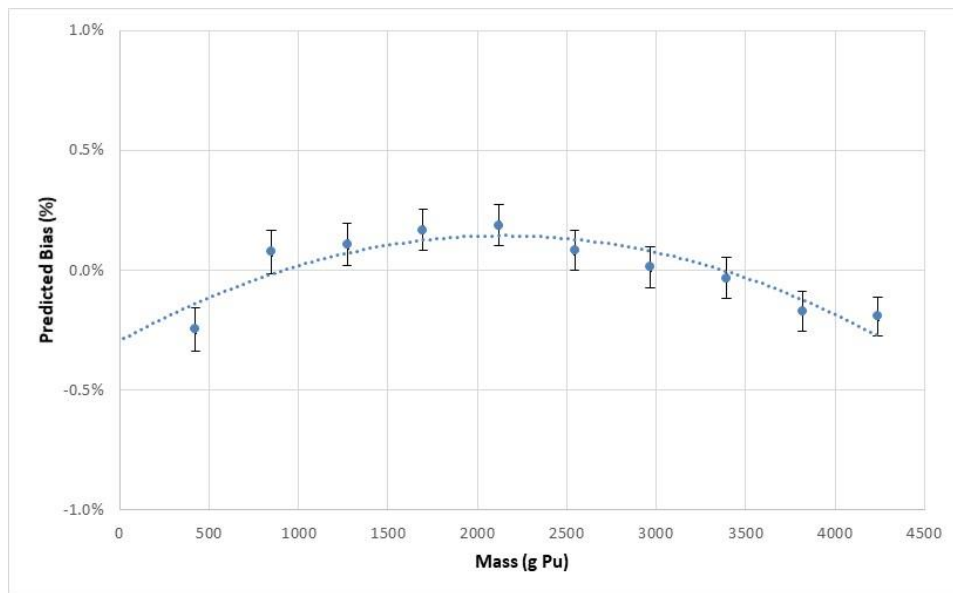


Figure 29. Mass assay bias using the ENMC following calibration based on the 2.5 g/cc PuO₂ containers.

Table 12. Detector parameters for point source and volumetric calibrations ($\rho=2.5$ g/cc).

Parameter	PSMC pt. src.	PSMC vol.	ENMC pt. src.	ENMC vol.
Efficiency	0.5336	0.5177	0.6218	0.6180
Doubles gate fraction	0.6558	0.6462	0.6912	0.6443
Triples gate fraction	0.4353	0.4066	0.4870	0.4123
Die-Away (μ s)	49.9	49.9	22.3	22.3
Pre-Delay (μ s)	4.5	4.5	1.5	1.5
Gate Width (μ s)	64	64	32	32

Applying the revised parameters to a more diverse set of materials (e.g., PuO₂ at various fill heights and densities) as shown in Figure 30 illustrates the primary limitation of the PME analysis. Although adjustment of the gate fractions could accommodate the deviations of the PuO₂ at fixed density, the standard PME analysis cannot accommodate the additional variables introduced by the changes in density. This will be shown more dramatically when discussing the impact of the (α, n) reactions on the measurements.

The bias in the assay mass result is both a function of Pu mass and density and can be estimated from the difference in density of the item under assay from the typical calibration item.

$$\Delta\rho = a_1 \cdot \left(\frac{m}{m_{ref} \cdot \rho} \right)^{a_2} \cdot (1 + a_3 \cdot e^{-a_4 \cdot \rho}) \cdot \delta\rho,$$

where $\delta\rho$ is the density differential, the parameters a_1 through a_4 are determined from measured or simulated data for a given container type and assay system, and m_{ref} is an arbitrary scaling factor used for convenience. For our example of a typical PSMC calibrated using 2.5 g/cc PuO₂ standards, the bias is given by

$$\Delta\rho = 0.017 \cdot \left(\frac{m}{1000 \cdot \rho} \right)^{\frac{3}{4}} \cdot (1 + 2.5 \cdot e^{-2.5 \cdot \rho}) \cdot \delta\rho.$$

Extending the simulated calibration to include a broader range of densities reduces the overall spread in mass results, but the bias as a function of mass becomes more complicated, as illustrated in Figure 31. In this case the overall bias could be generally represented by a cubic equation of the reported mass, but the deviations from estimated value would be as large as the estimated bias.

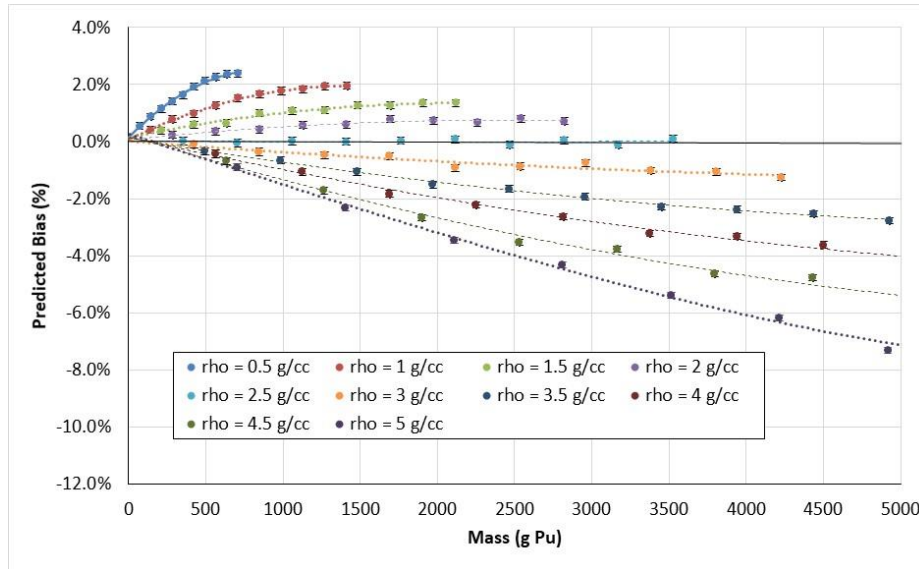


Figure 30. Mass assay bias as a function of Pu mass for several PuO₂ densities using the PSMC when calibrated using representative standards of a single density (2.5 g/cc).

The random uncertainty component due to variation in the expected density is determined from the potential range of the density relative to the expected value. We define the 1-sigma uncertainty in the density ratio, σ_{RUPu} , as (maximum ratio – minimum ratio)/6 and treat the uncertainty as if it follows a normal distribution.

$$\sigma_{\rho} = a_1 \cdot \left(\frac{m}{m_{ref} \cdot \rho} \right)^{a_2} \cdot (1 + a_3 \cdot e^{-a_4 \cdot \rho}) \cdot \frac{(\rho_{max} - \rho_{min})}{6}.$$

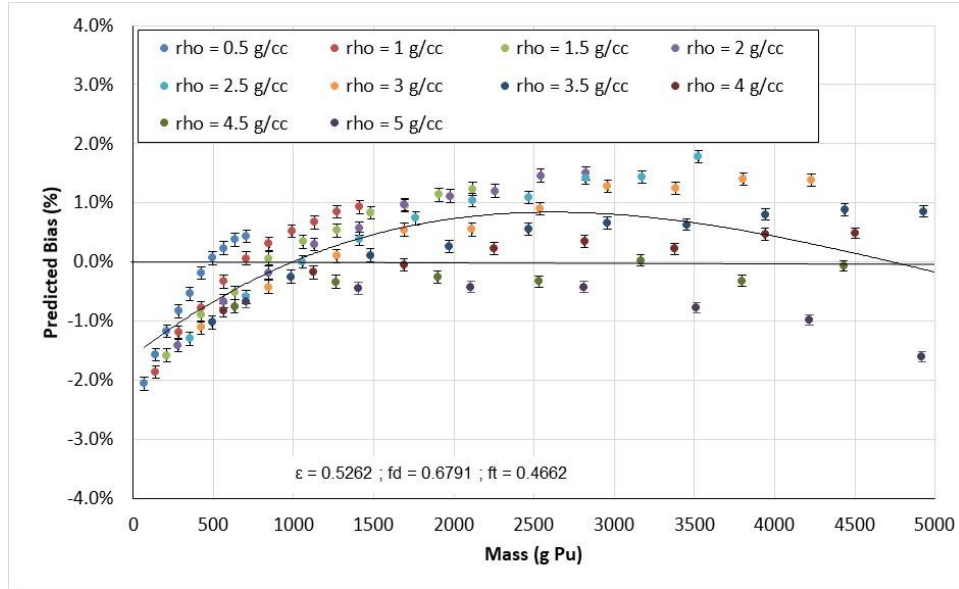


Figure 31. Mass assay bias as a function of Pu mass for several PuO₂ densities using the PSMC when calibrated using representative standards covering a broad range of PuO₂ densities.

The fill height effect on efficiency is readily apparent in the expected bias shown in Figure 31; however, it is also apparent that there are more factors impacting the measurement response. Two efficiency effects have been identified to this point, fill height and moderation. The simulated measurements depicted in Figure 30 were reanalyzed after adjusting the neutron detection efficiency for each measurement $\varepsilon \rightarrow \varepsilon(H, \rho)$ to investigate the potential that the residual uncertainty contribution was specifically related to density. The trial efficiency function was given as follows:

$$\varepsilon(H, \rho) = (1 + a \cdot \rho + b \cdot \rho^2) \cdot \iint \varepsilon(r, h) \cdot dr \cdot dh,$$

where a and b are empirically determined coefficients and ρ is the density of PuO₂. For the simulations evaluated above, the values for the coefficients were determined to be $a = 0.0015$ and $b = -0.00026$. Combining the variable efficiency, $\varepsilon(H, \rho)$, with the point source gate fractions, the biases were reevaluated, as shown in Figure 32. The reevaluated biases are seen to be much larger using this representation of efficiency, and the peculiar flat response as a function density is an artifact of constraining the average value of alpha to be equal to the input value (0.76).

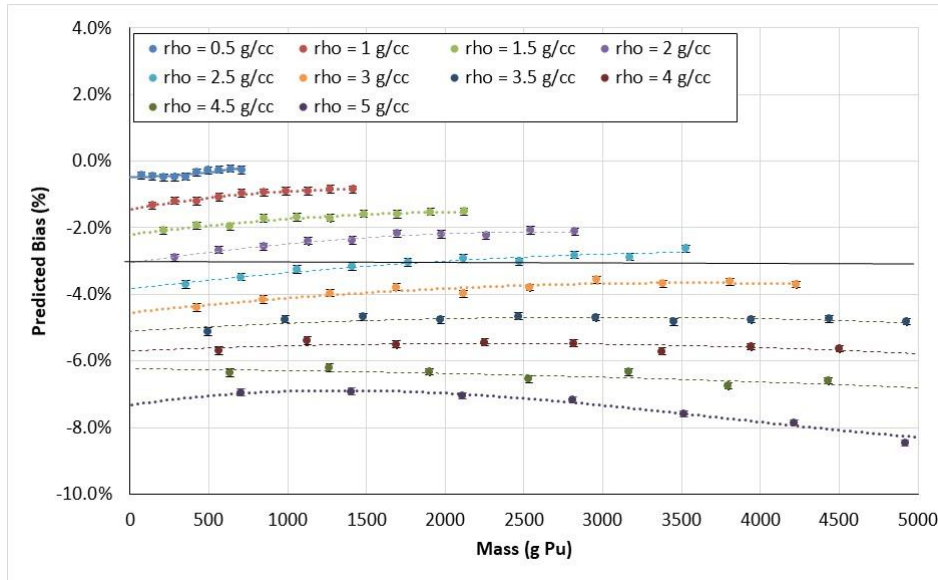


Figure 32. Mass assay bias as a function of Pu mass for several PuO₂ densities using fill height and density-dependent efficiency.

These remaining density-dependent biases indicate additional variables are impacting the analysis, which we attribute to the energy dependence of the induced fission rates and moments, and neutron detection efficiency. The induced fission rates and moments increase with increasing neutron energy, so the number of coincident neutrons emitted per induced fission depends on the source of the neutrons. The dependence of detection efficiency with energy means that the detection efficiency for the alpha-induced neutrons will be different following spontaneous or induced fission.

The biases seen in Figure 32 are the result of a number of factors.

- the energy dependence of the neutron detection efficiency (Figure 33)
- the energy dependence of the induced fission moments [32] [33] (e.g., the sensitivity of ν_{i1} to incident neutron energy is $\sim 5\%$ / MeV, so the difference in average neutron energy between ²⁴⁰Pu spontaneous fission neutron and (α , n) induced fission results in a $\sim 0.5\%$ change in the value of ν_{i1})
- the moderating effects of the material matrix [in this case oxygen (refer to Figure 34) introduces a maximum 0.3% relative effect on efficiency or 0.5 to 1% impact on the mass result]
- the moderation/absorption effects of the actinide content

While it is not recommended to try to use the seemingly predictable bias shown in Figure 32, it is possible to develop an uncertainty estimate from this response. First, it is necessary to make an assumption about how the counter was calibrated (e.g., using a single point source or a collection of representative standards of constant density).

Assuming a point source calibration to determine the neutron detection efficiency and gate fractions, the measured rates are analyzed first using the point source calibration value to provide a reference assay mass (m_{pt}). The rates are then reanalyzed using the revised efficiency based on the revised detection efficiency $\varepsilon(H, \rho)$ to provide a revised mass value (m_{rev}). The estimated bias due to density, Δ_ρ , is

$$\Delta\rho = m_{pt} - m_{rev} \cdot \left(1 + a_\rho \cdot (\rho_{item} - \rho_{ref})\right),$$

where ρ_{item} is the expected density for the item under assay and ρ_{ref} is the typical density of the standard items used to determine the sensitivity to density, a_ρ , as depicted in Figure 32.

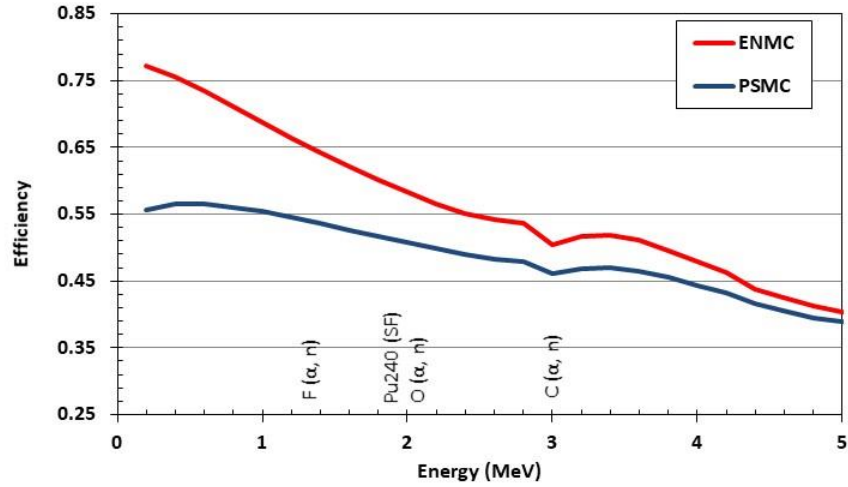


Figure 33. Simulated neutron detection efficiency as a function of neutron energy for the ENMC and PSMC systems.

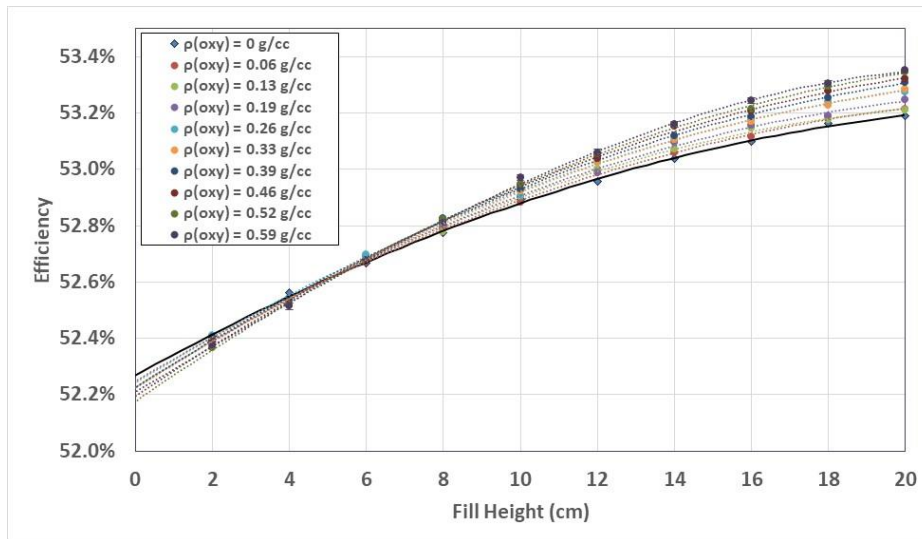


Figure 34. Simulated neutron detection efficiency as a function of increasing oxygen content for various fill heights in the PSMC. The 10 cm diameter canister contained 1 g Pu/cm fill height (0.0062 g/cc) while the oxygen content was increased incrementally from 0.06 to 0.6 g/cc.

3.7.1 Multiplication Bias Correction Factor

The ASTM C1500 standard [18] recommends that when assaying metallic items that, a multiplication-based bias correction be applied to the mass result of the form [6]

$$f_M = 1 + a \cdot (M - 1) + b \cdot (M - 1)^2,$$

where a and b are empirically determined constants or determined by Monte Carlo simulation. Although generally only used for dense materials, evaluation of the simulated bias results above suggests that such a correction is valuable even when the bulk density of the item is as low as 0.5 g/cc. The bias results displayed in Figure 30 have been replotted in Figure 35 as a function of the “assayed” (not the input) multiplication result with the fill height efficiency correction applied. A distinct dependence on multiplication is seen across the full range of masses and densities used for the simulations.

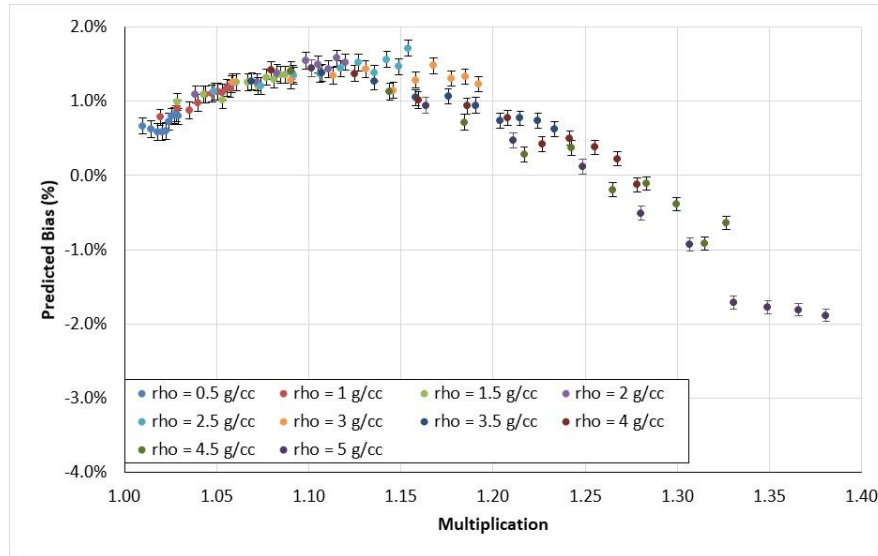


Figure 35. Mass assay bias as a function of Pu mass for several PuO₂ densities using fill height and density-dependent efficiency.

Fitting the simulated data yields $a = -0.15506$ and $b = 0.57276$ for this data set. By applying this correction factor to the simulated assay results (Figure 38), the resulting mass biases are less than 0.5% over a broad range of material types and mass is significantly reduced (Figure 36).

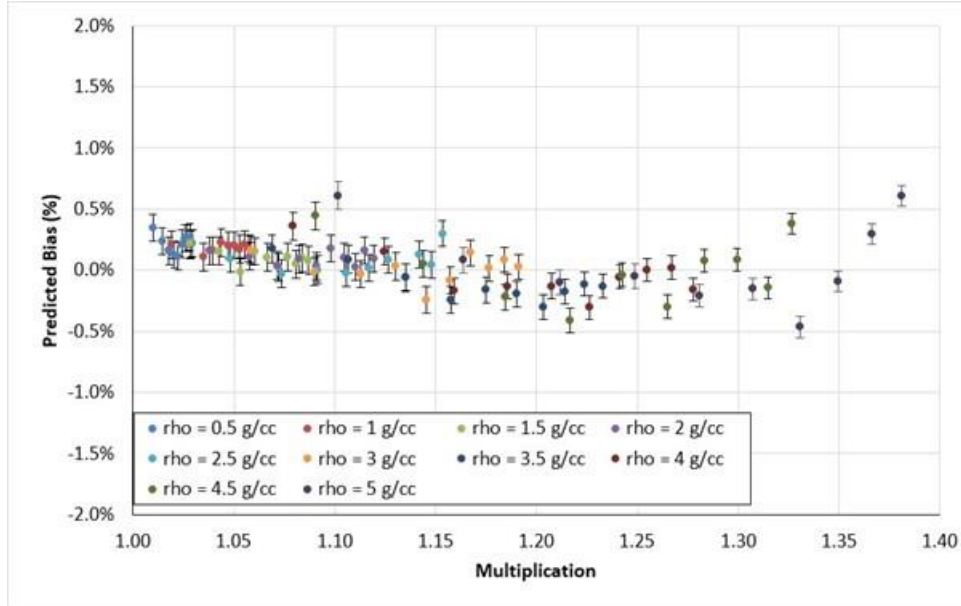


Figure 36. Mass assay bias as a function of Pu mass for several PuO₂ densities using fill height and density-dependent efficiency after application of the multiplication correction.

Because the multiplication correction is rarely applied, it suggests that analysis using the point source efficiency and gate fractions, combined with the fill height-dependent efficiency and multiplication correction, would provide a reasonable means to quantify the likely mass bias resulting from density variations. The bias contribution due to density variations, Δ_{ρ} , is given by

$$\Delta_{\rho} = f_M \cdot m(\varepsilon(h)) - m_{\varepsilon_0},$$

where h is the fill height,

$\varepsilon(h)$ is the volume average efficiency as a function of fill height, and

m_{ε_0} is the Pu mass determined using the cavity center detector parameters.

The fill height is estimated from the

$$h = m_{\varepsilon_0} / (f_w \cdot \rho),$$

where f_w is the Pu weight fraction of the Pu-bearing material and

ρ is the density of the Pu-bearing material.

3.7.2 Estimation of Bias Using the Ring Ratio

The ring ratio is typically defined as the ratio of counts in the inner to outer neutron detection ring, providing an indication of the average energy of the detected neutrons. Given that many of the biases associated with multiplicity analysis are thought to be dependent on neutron energy, it is worthwhile to examine the dependence of the above biases as a function of ring ratio. The bias results shown in Figure 31 (calibration based on full collection of 100 combinations of density and mass) have been replotted as a function of ring ratio in Figure 37. The dependence on the ring ratio and by association the neutron energy of the simulated bias is seen to be complex but with no obvious correlation between ring ratio and the density-dependent bias.

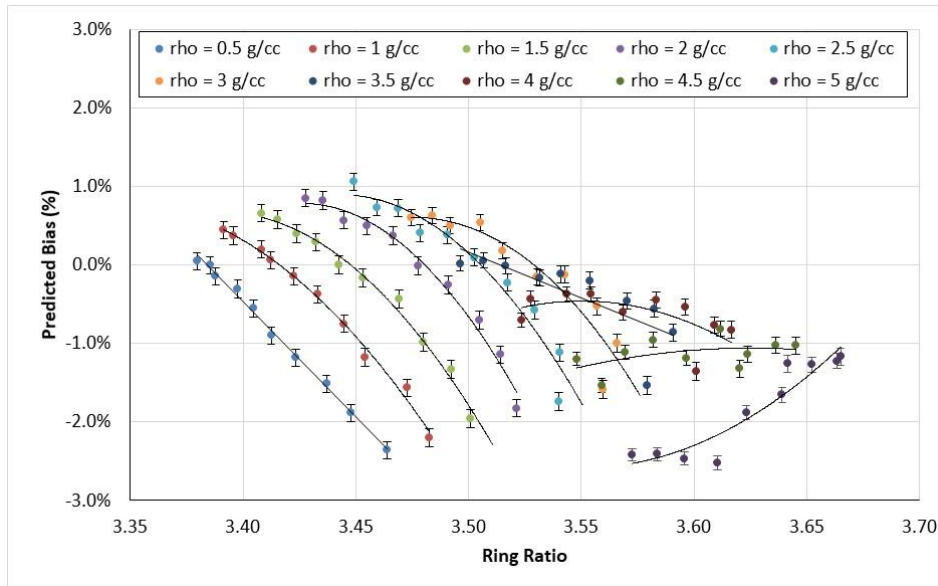


Figure 37. Mass assay bias as a function of ring ratio for several PuO₂ densities using fill height and density-dependent efficiency.

3.8 UPu Ratio

The analysis of MOX product-grade materials extends the previous discussion with the inclusion of uranium. The presence of uranium complicates the analysis by the introduction of a fissionable material (i.e., uranium) with different induced fission moments and energy dependence.

The impact of varying UPu ratios on the assay mass result is examined by first assuming that the multiplicity counter was calibrated using representative PuO₂ standards of constant density and relative ²⁴⁰Pu_{effective} ($\rho=3.0 \text{ g/cc}$, $^{240}\text{Pu}_{\text{eff}}/\text{g}=0.3144$). The simulated calibration results for these containers are provided in Table 13. Note these parameters are different from those for 2.5 g/cc material presented in Table 12 and the optimized gate fractions differ significantly from true values. Analysis of MOX materials with the same 3.0 g/cc density again results in significant biases, as shown in Figure 38.

Table 13. Simulated neutron detector parameters for the PSMC for a ²⁴⁰Pu point source and a volumetric calibration based on 3.0 g/cc PuO₂.

Parameter	Point Source	2 L containers
Efficiency	0.5336	0.5366
Doubles gate fraction	0.6558	0.6064
Triples gate fraction	0.4353	0.3664

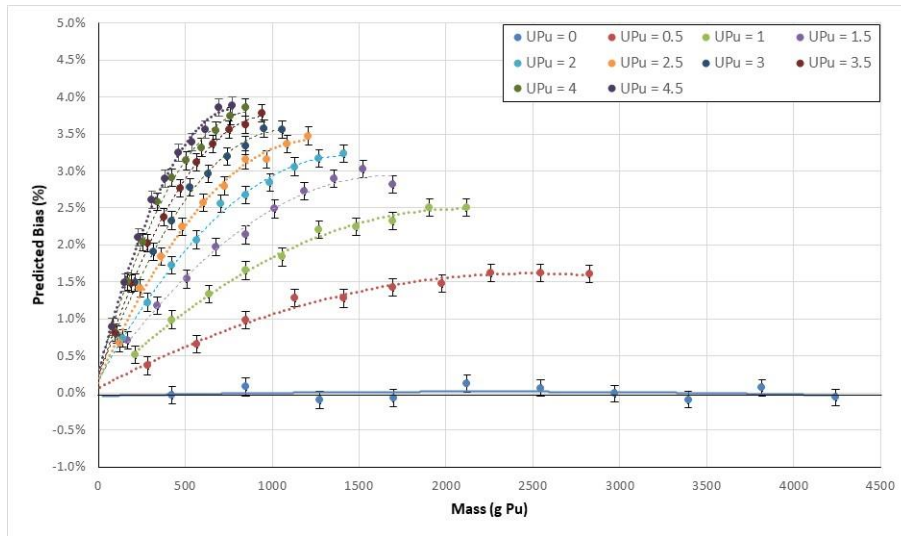


Figure 38. Simulated mass assay bias as a function of Pu mass and U/Pu ratio based on a traditional multiplicity counter mass calibration ($\rho=3.0$ g/cc, $^{240}\text{Pu}_{\text{eff}}/\text{g}=0.3144$) using the PSMC.

Additional optimizations based on chi-square minimizations of the simulated assay results and input values while varying the efficiencies and gate fractions (and constraining the collection average alpha result to the input value) do not afford an improved accuracy for an arbitrary item composition. In practice, such a broad range fit of the data only serves to shift the bias curves up or down as seen, for example, in Figure 39.

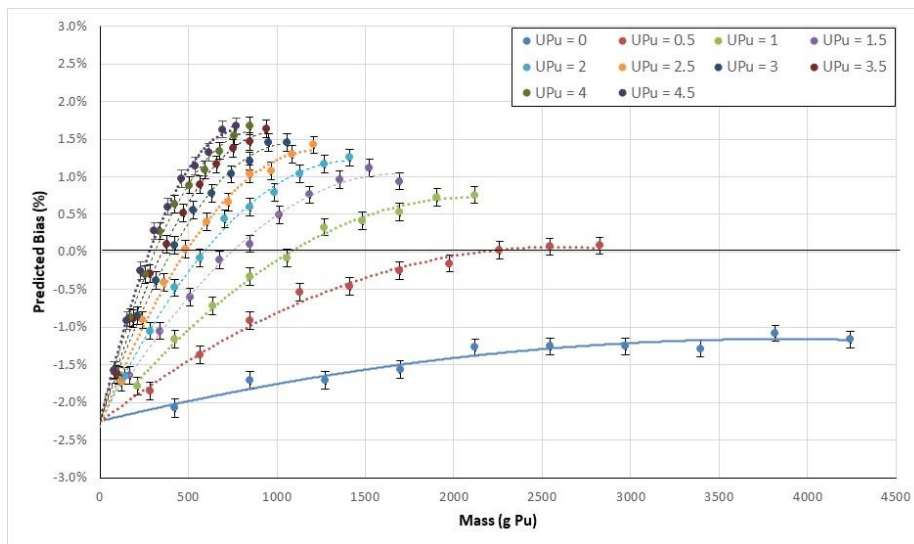


Figure 39. Simulated mass assay bias as a function of Pu mass and U/Pu ratio based on a traditional multiplicity counter mass calibration ($\rho=3.0$ g/cc, $^{240}\text{Pu}_{\text{eff}}/\text{g}=0.3144$, $\alpha=0.76$) over all masses and U/Pu ratios in the collection.

If instead we apply a calibration based on the point source parameters and implement, for the purposes of uncertainty evaluation, fill height and density-dependent efficiency correction, it is possible to estimate the impact of the increasing UO_2 content of the MOX items. Figure 40 presents the residual bias after application of the fill height and density-dependent calibration. Although the biases are smaller, they are still significant relative to most measurement targets. [To illustrate that this effect is not specific to the

PSMC, the series of simulated items were also performed for measurements using an ENMC (Figure 41). As expected, the predicted behaviors of the two systems are very similar.] Again, additional optimizations of the efficiency and gate fractions do not improve the overall fit results. Finally, plotting the bias as a function fill height (Figure 42) indicates that the bias cannot be expressed as a simple function of fill height.

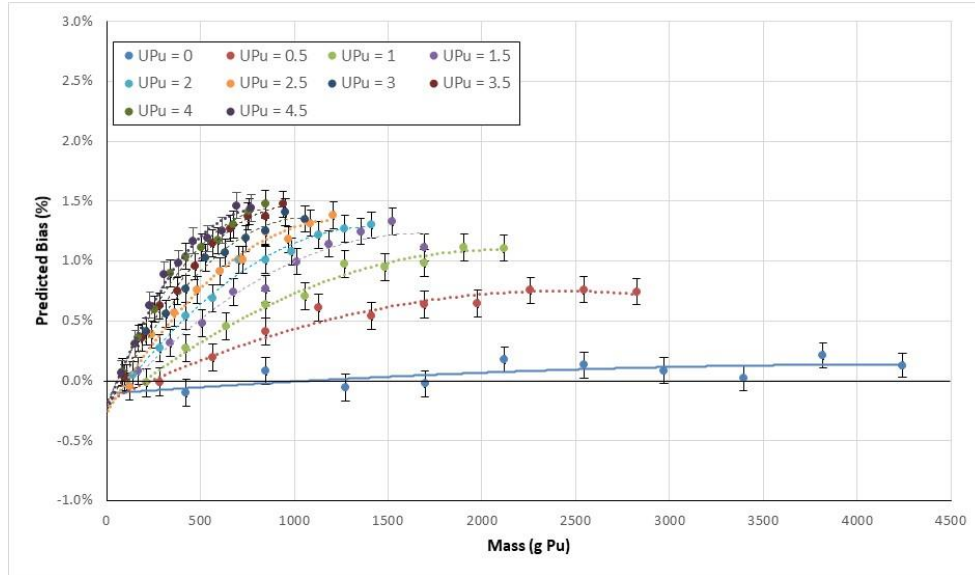


Figure 40. Simulated mass assay bias as a function of Pu mass and U/Pu ratio using fill height and density-dependent efficiency ($\rho=3.0$ g/cc, $^{240}\text{Pu}_{\text{eff}}/g=0.3144$) using the PSMC.

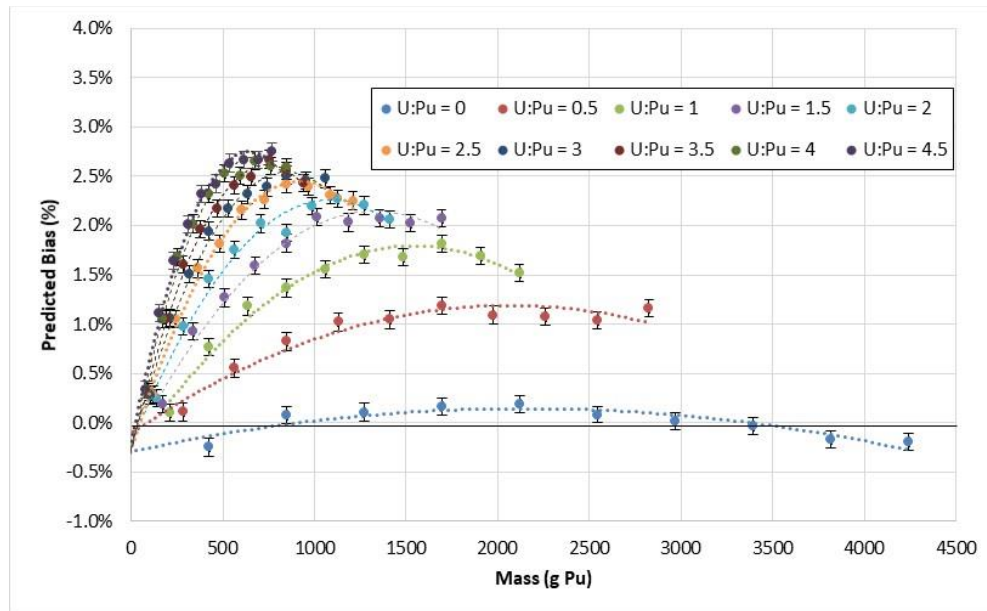


Figure 41. Simulated mass assay bias as a function of Pu mass and U/Pu ratio using fill height and density-dependent efficiency ($\rho=3.0$ g/cc, $^{240}\text{Pu}_{\text{eff}}/g=0.3144$) using the ENMC.

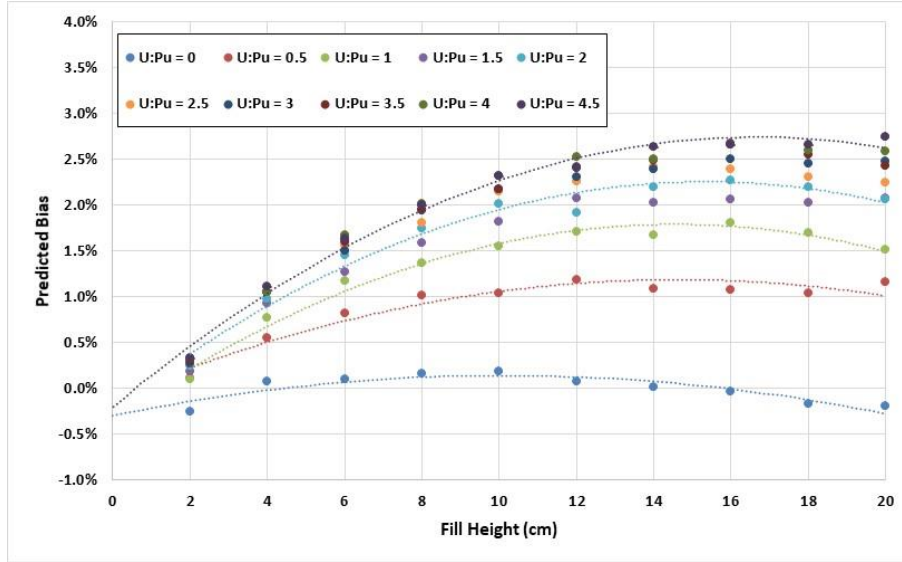


Figure 42. Simulated mass assay bias as a function of fill height and UPu ratio using fill height and density-dependent efficiency ($\rho=3.0$ g/cc, $^{240}\text{Pu}_{\text{eff}}/\text{g}=0.3144$) using the ENMC.

The remaining biases shown in Figure 40 and Figure 41 can be adequately described by a simple quadratic function of the item's UPu ratio and mass.

$$\Delta_{UPu} = \left[a_1 + a_2 \cdot m/m_{ref} + a_3 \cdot (m/m_{ref})^3 \right] \cdot \left(\frac{\Delta R_{UPu}}{a_4} \right)^{3/4},$$

where ΔR_{UPu} is the difference of the expected UPu ratio from the typical calibration item, and m is the total Pu mass of the item. For the examples here based on the simulated PSMC measurement, the following values provide an adequate representation of the expected bias due to the UPu ratio.

$$a_1 = 0.000176$$

$$a_2 = 0.00666$$

$$a_3 = -3.55\text{E-}4$$

$$a_4 = 1$$

m_{ref} is a scaling factor (set to 1000 in this example)

Figure 43 presents a comparison of the expected bias using the above expression with the data presented in Figure 41. (A semi-log scale was used to better separate the various UPu ratio curves at the lower masses.)

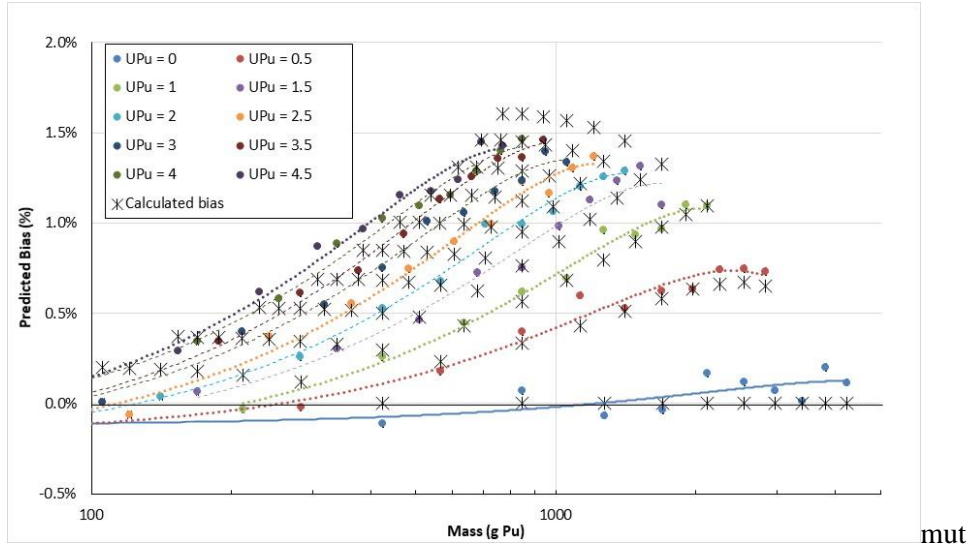


Figure 43. Comparison of the simulated and empirical bias estimates for assay of MOX material of varying fill height and UPu ratio efficiency ($\rho=3.0$ g/cc, $^{240}\text{Pu}_{\text{eff}}/\text{g}=0.3144$) using a PSMC.

The random uncertainty component due to variation in the expected UPu ratio is determined from the potential range of the ratio relative to the expected value. We define the 1-sigma uncertainty in the UPu ratio as (maximum ratio – minimum ratio)/6 and treat the uncertainty as if it follows a normal distribution.

$$\sigma_{UPu} = \left| \left[a_1 + a_2 \cdot m/m_{ref} + a_3 \cdot (m/m_{ref})^3 \right] \cdot \left(\frac{(UPu_{max} - UPu)^{4/3} - (UPu_{min} - UPu)^{4/3}}{6 \cdot a_4^{4/3}} \right) \right|$$

3.9 (ALPHA, n) UNCERTAINTY CONTRIBUTION

While we tend to think of “alpha” as a single factor in multiplicity analysis, the value of alpha is determined by a number of factors and depending upon the source of the (α , n) neutrons will have a different impact on the assay result.

The impact of the (α , n) neutron contribution to the uncertainty arises from a number of factors.

- The low-Z nuclide composition and concentration relative to the actinides,
- The isotopic distribution of the alpha-emitting nuclides within the item,
- the energy dependence of the neutron detection efficiency (Figure 33),
- the energy dependence of the induced fission moments [32] [33]
(e.g., the sensitivity of ν_{i1} to incident neutron energy is $\sim 5\%$ / MeV, so the difference in average neutron energy between ^{240}Pu spontaneous fission neutron and (α , n) induced fission results in a $\sim 0.5\%$ change in the effective value of ν_{i1}).

The impact of increasing alpha emission rate (e.g., increasing the ^{241}Am relative abundance) without changing the type of target was examined first. A series of 10 containers of increasing fill height of PuO_2 at constant density were simulated while incrementally increasing the (α ,n) rate. Analyzing the resulting

simulated rates using the center cavity point source efficiency and gate fractions yields the bias curves shown in Figure 44, yielding increasingly large biases as the value of alpha increases.

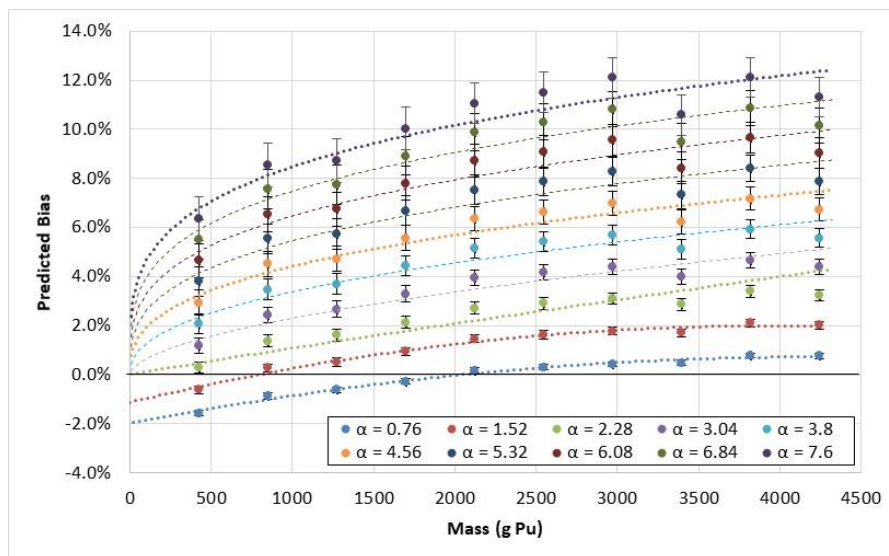


Figure 44. Mass assay bias as a function of Pu mass for increasing alpha value ($\rho=3.0$ g/cc, $^{240}\text{Pu}_{\text{eff}}/\text{g}=0.3141$), using the point source calibration.

If instead a volumetric calibration, based on calibration using representative standards (considering only 3 g/cc PuO_2 items with similar $^{240}\text{Pu}_{\text{effective}}$), is applied to the simulated data, a very different set of bias curves is obtained. In this case the resulting biases follow a linear response as a function of mass where the slope is dependent on the value of alpha, as shown in Figure 45. The resulting bias is seen to be highly dependent on the method of calibration, and it must be remembered that the linear responses in Figure 45 are dependent on the measured items each having the same characteristics as the “calibration” items. Although the objective of this report is to isolate each of the error contributors, it is worth noting at this time that even minor deviations from the calibration items have a significant impact on the assay result. For example, by applying the same calibration parameters to a collection of containers with lower density and $^{240}\text{Pu}_{\text{eff}}$, the bias curves change significantly, as shown in Figure 46. The overall swing in the expected bias values is in agreement with the density effects discussed in Section 3.7 (refer to Figure 30).

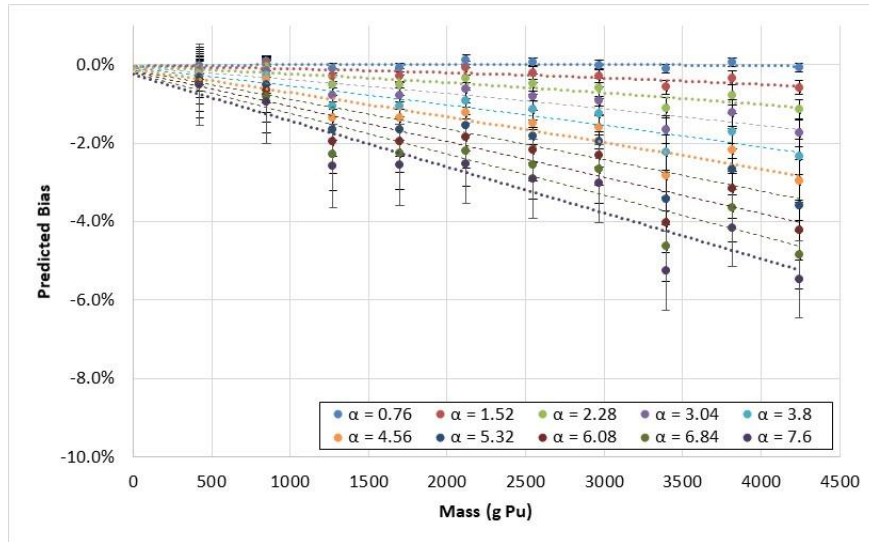


Figure 45. Mass assay bias as a function of Pu mass for increasing alpha value ($\rho=3.0$ g/cc, $^{240}\text{Pu}_{\text{eff}}/\text{g} = 0.3141$), using the volumetric calibration for containers of similar density and $^{240}\text{Pu}_{\text{eff}}/\text{g}$.

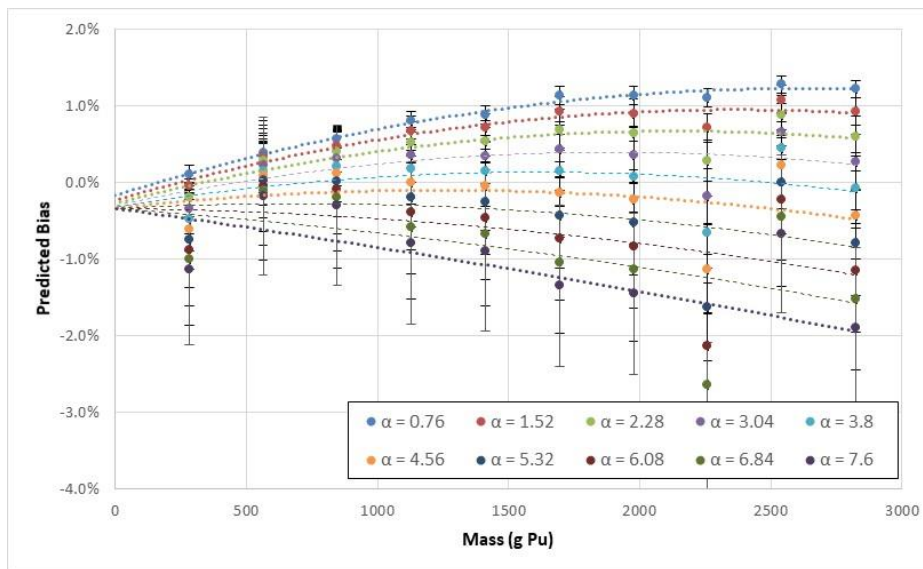


Figure 46. Mass assay bias as a function of Pu mass for increasing alpha value ($\rho=2.0$ g/cc, $^{240}\text{Pu}_{\text{eff}}/\text{g} = 0.2569$), using the volumetric calibration for containers of $\rho=3.0$ g/cc, $^{240}\text{Pu}_{\text{eff}}/\text{g} = 0.3141$.

For completeness, the special case where all materials under consideration are of the same material type and density has also been considered. The limited variables allow calibration yielding much lower biases, as shown in Figure 47. The maximum expected relative bias for this special case is less than 2%; however, such a constrained material type is considered an unlikely occurrence.

The detector parameters for the different optimizations presented in this section are provided in Table 14, illustrating the sensitivity of the analysis to the proper calibration method.

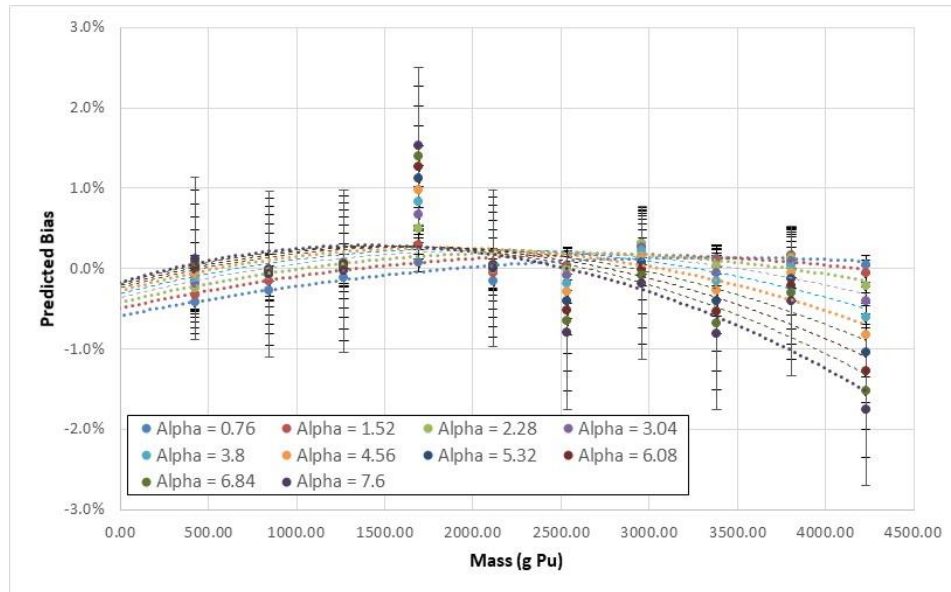


Figure 47. Simulated mass assay bias as a function of Pu mass for increasing alpha value ($\rho=3.0$ g/cc, $^{240}\text{Pu}_{\text{eff}}/\text{g}=0.3141$), using the volumetric calibration optimized for this material type.

Table 14. Simulated PSMC detector parameters for point source and volumetric calibrations ($\rho=3.0$ g/cc) used in Figure 44 through Figure 47.

Parameter	PSMC ^{240}Pu pt. src.	PSMC vol. ($\alpha=0.76$ only)	PSMC vol. ($\alpha=0.76$ to 7.6)
Efficiency	0.5336	0.5196	0.5276
Doubles gate fraction	0.6558	0.6523	0.6390
Triples gate fraction	0.4353	0.4187	0.4065
Die-Away (μs)	49.9	49.9	22.3
Pre-Delay (μs)	4.5	4.5	4.5
Gate Width (μs)	64	64	64

3.9.1 Impact of (α, n) due to Low-Z Impurities

The impact on the assay result due to several common low-Z impurities was examined by modifying the (α, n) neutron energy distribution. In addition to oxygen, B, Be, C, and F were considered. The (α, n) neutron energy distributions were obtained using Sources 4C [34], which adds another measure of uncertainty to the TMU estimates as these may differ from the true energy distributions (e.g. as given in Ref. [35]). Figure 48 shows the biases resulting from the introduction of these elements to product-grade PuO_2 sufficient to double the value of alpha relative to the clean oxide for Pu masses ranging from 430 to 4300 g. The most notable feature of the plot is that fluorine impurity results in a negative bias due to its lower average (α, n) neutron energy in comparison with that produced by oxygen.

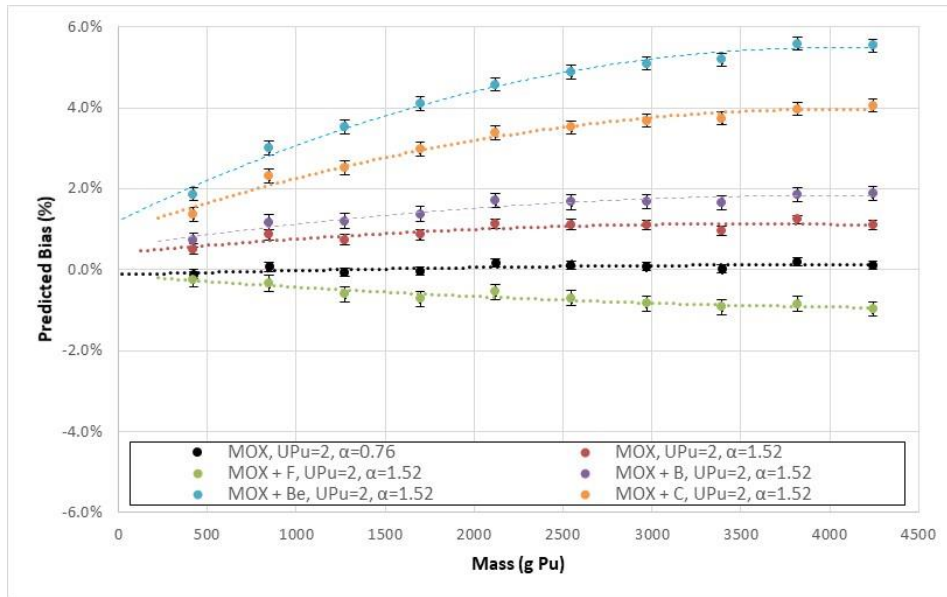


Figure 48. Mass assay bias as a function of Pu mass for constant alpha value ($\alpha=1.52$, $\rho=2.5$ g/cc, $^{240}\text{Pu}_{\text{eff}}/\text{g}=0.2479$) from various impurities.

The simulated ring ratios were also examined for these runs to determine if the ring ratio provides a suitable technique for correction for the impact of these impurities. An example is given in Figure 49 for the sequence of simulated containers plotted in Figure 48. While the trend toward higher ring ratios with lower average neutron energy is apparent in the figure, it is also apparent that the ring ratios can provide only limited information on the chemical makeup of the item. For example, it would not be possible to distinguish between Be and C impurities, and for these higher energy neutron emitters, it would not be possible to estimate a bias using the ring ratio.

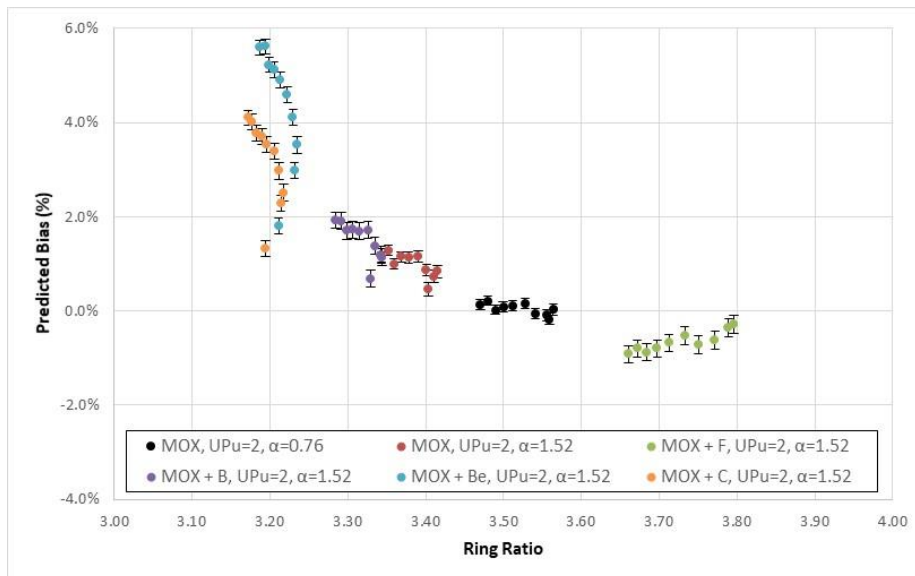


Figure 49. Mass assay bias as a function of ring ratio for constant alpha value ($\alpha=1.52$, $\rho=2.5$ g/cc, $^{240}\text{Pu}_{\text{eff}}/\text{g}=0.2479$) from various impurities.

For each of the low-Z elements examined, the impact of greater impurity levels and higher alpha values was examined. The expected biases for PuO₂ containing several hundred ppm and greater of fluorine is shown in Figure 50. The corresponding plots for boron and carbon are provided in Figure 51 and Figure 52, respectively.

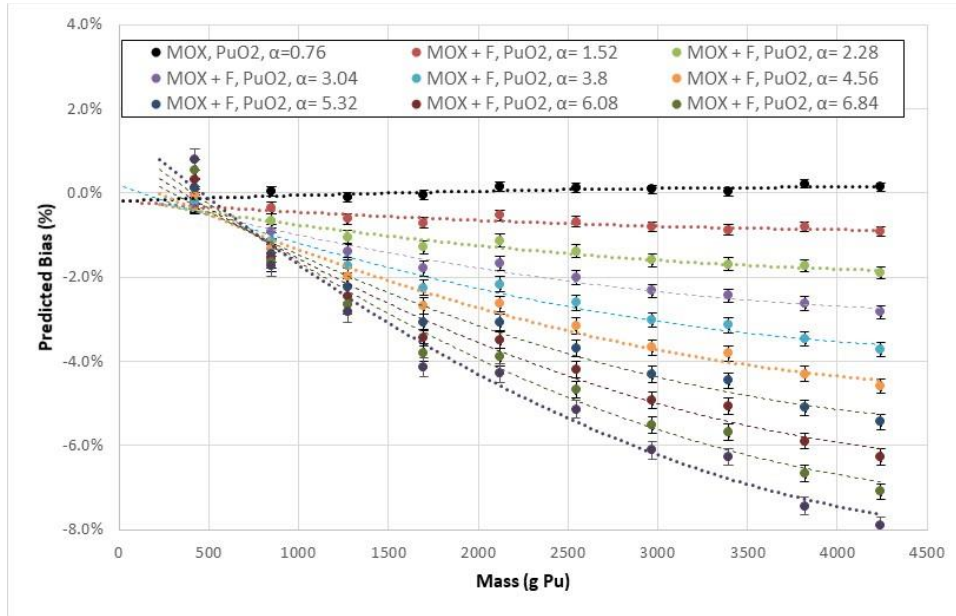


Figure 50. Assay bias as a function of mass for PuO₂ ($\rho=3.0$ g/cc, $^{240}\text{Pu}_{\text{eff}}/\text{g}=0.3144$) containing fluorine impurities (ranging from 800 to 8000 ppm).

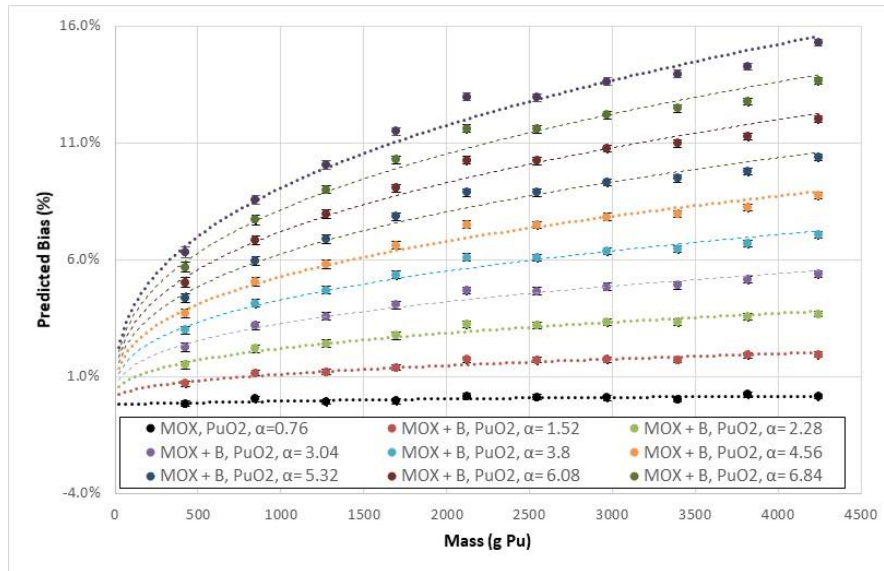


Figure 51. Assay bias as a function of mass for PuO₂ ($\rho=3.0$ g/cc, $^{240}\text{Pu}_{\text{eff}}/\text{g}=0.3144$) containing boron impurities (ranging from 400 to 4000 ppm).

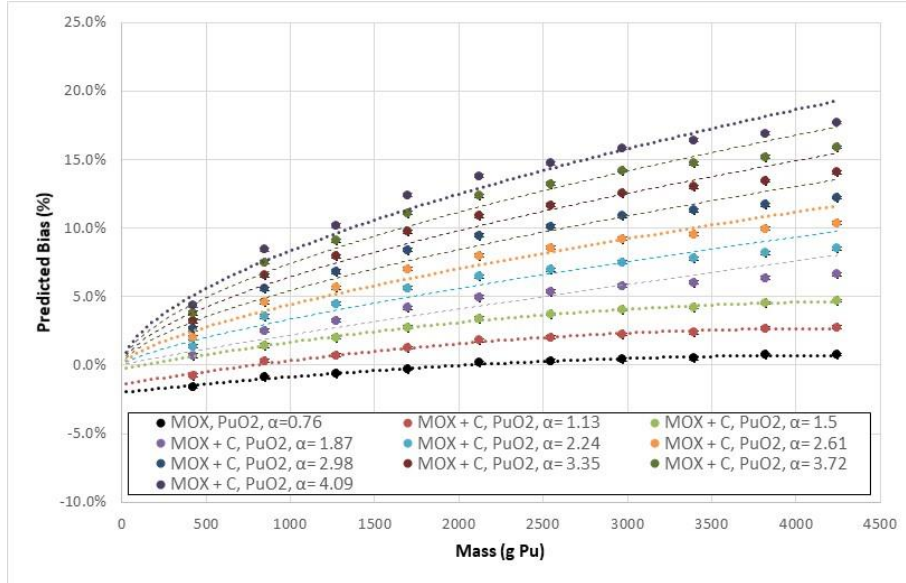


Figure 52. Assay bias as a function of mass for PuO₂ ($\rho=3.0$ g/cc, $^{240}\text{Pu}_{\text{eff}}/\text{g}=0.3144$) containing carbon as an impurity (ranging from ~5 to 50% by weight).

3.9.2 Estimation of the Bias due to (α , n) Events

From these simulations it appears the ring ratio and assay mass bias are not sufficiently well correlated to use the ring ratio as an estimator of the bias based on the simple point model equations (that is not to say that the ring ratio is not useful for analysis using any of the point model extensions). However, the ring ratio, if available, may be used as an indicator of the type of low-Z impurity [36], which determines where the bias with increasing alpha will be positive or negative. If the ring ratio is greater than the reference ring ratio for the calibration materials (lower average energy), the bias will be negative (assay underreports), and if the ratio is smaller (greater average energy), the bias will be positive. Without the ring ratio data, knowledge of the chemical impurity must be known in order to estimate the measurement bias. In general if the multiplicity counter is calibrated using a point source of ^{240}Pu in the center of the assay cavity, impurities due to lithium or fluorine will result in a negative bias due to the lower average energy of their (α , n) neutron events, while most other low-Z elements will give rise to a positive bias. Generally, the opposite will be true if the system is calibrated using a volumetric container with low alpha standards.

For the relationship between the expected bias and the alpha value for the item, the relative bias can be approximated by the following expression:

$$\Delta_{\alpha} = a + b \cdot \left(\frac{m}{m_{\text{ref}}} \right)^c \cdot \alpha.$$

The values of the a , b , and c parameters have been determined for the typical containers assayed in the PSMC for five light elements and are presented in Table 15. To illustrate the degree to which the predicted values reproduce, the simulated values are illustrated in Figure 53 for the boron impurities' simulations presented in Figure 51.

Table 15. Bias parameters for several common low-Z (α , n) emitters.

	Boron	Beryllium	Carbon	Oxygen	Fluorine
a	-0.0192	-0.0689	-0.0390	0.0033	0.0192
b	0.0029	0.0050	0.0085	0.0028	-0.0001
c	0.2961	0.4020	0.2804	0.2156	0.6201
m_{ref}	1.0000	1.0000	1.0000	1.0000	1.0000

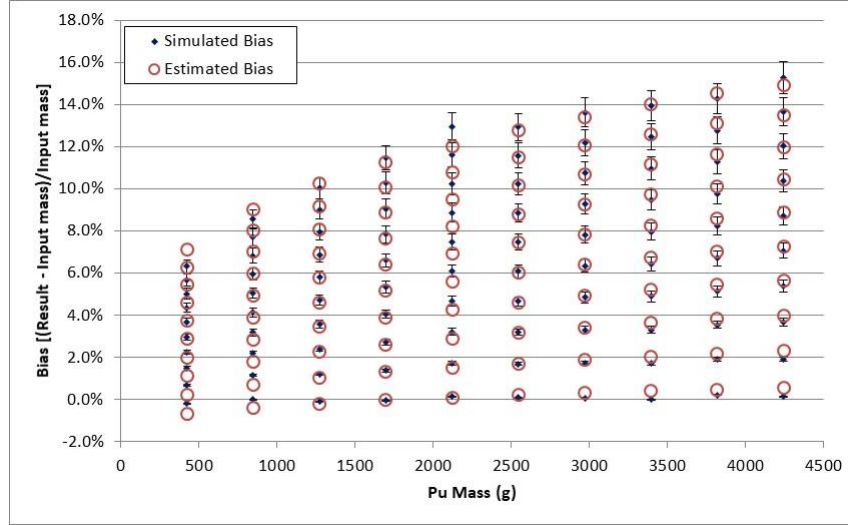


Figure 53. Comparison of the simulated and estimated biases for assay of PuO_2 containing significant boron impurities.

The relative random uncertainty component due to (α , n) is determined from the following.

$$\sigma_{\alpha} = \sqrt{\left(b \cdot \left(\frac{m}{m_{ref}}\right)^c \cdot \sigma_{\alpha}\right)^2 + \left(\frac{c \cdot b}{m_{ref}} \cdot m^{c-1} \cdot \alpha \cdot \frac{\delta m}{\delta \alpha} \cdot \sigma_{\alpha}\right)^2} \cong b \cdot \left(\frac{m}{m_{ref}}\right)^c \cdot \sigma_{\alpha}$$

$$\sigma_{\alpha} = b \cdot \left(\frac{m}{m_{ref}}\right)^c \cdot \sigma_{\alpha} \cdot \sqrt{1 + \left(\frac{c \cdot \alpha}{m} \cdot \frac{\delta m}{\delta \alpha}\right)^2} \cong b \cdot \left(\frac{m}{m_{ref}}\right)^c \cdot \sigma_{\alpha} .$$

3.10 BURNUP UNCERTAINTY CONTRIBUTION

The burnup contribution represents yet another error contribution resulting from the Pu isotopic composition of the item. Moving from low-burnup to high-burnup material, the fraction of ^{239}Pu and ^{241}Pu decreases as the $^{240}Pu_{effective}$ value increases, so the " $^{239}Pu_{effective}$ " value is also changing. Weapons-grade materials will have a lower source term but higher multiplication per unit mass than fuel-grade materials. The impact is proportional to the value of alpha. In a practical sense, calibration using one grade of Pu can introduce a bias in the assay of other grades of Pu. As an example, the relative bias resulting from changing $^{240}Pu_{effective}$ is shown in Figure 54. For this comparison, the material type was PuO_2 , with density 2.5 g/cc and $\alpha=0.76$. Additional simulations showed that the bias increases proportionally with the value alpha.

The burnup bias contribution is generally small and can be represented as a linear function of the difference between the calibration and item $^{240}\text{Pu}_{\text{effective}}$ values. The relative bias due to burnup differences is given by

$$\Delta_{BU} = a_1 + a_2 \cdot ({}^{240}\text{Pu}_{\text{eff,item}} - {}^{240}\text{Pu}_{\text{eff,cal}}) \cdot \alpha,$$

where a_1 and a_2 are determined from simulations or measurements. For the PSMC simulations, $a_1 = 0$ and $a_2 = 0.016$.

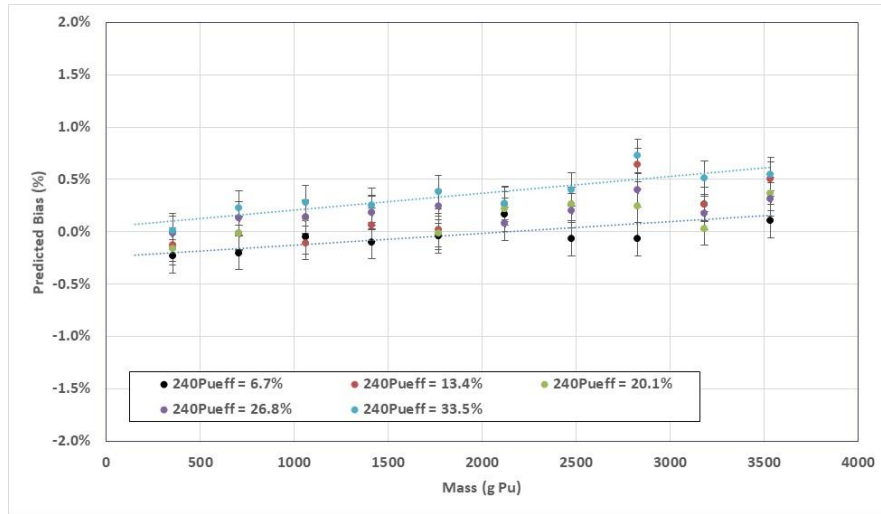


Figure 54. Bias as a function of Pu mass for several $^{240}\text{Pu}_{\text{effective}}$ values (PuO_2 , $\rho=2.5$ g/cc, $\alpha=0.76$).

Because the uncertainty in the ^{240}Pu effective value is relatively small ($\sim 1\%$), and the bias due to burnup is already small, the random contribution from the burnup component is essentially zero and negligible, and has been ignored.

3.11 MODERATOR UNCERTAINTY CONTRIBUTION

For this study we have considered only water contents up to 2 wt%, which is the equivalent of adding about 30 cc of water to 500 cc of MOX. For this series of simulations, a series of 10 containers (10 cm ID) each containing either PuO_2 or MOX with fill heights of 2 to 20 cm in 2 cm increments was used. For each series of containers, five water contents were examined from 0 to 2 wt% in 0.5 wt% increments. For these simulations, two materials were considered— PuO_2 and MOX with a UPu ratio = 2, $^{240}\text{Pu}_{\text{effective}} = 0.3144$, and bulk density of 3 g/cc.

At these levels for PuO_2 and MOX at UPu=2:1, the bias is small and consistent relative to the dry case across a broad mass range. The bias results for the two material types are provided in Figure 55 for the PuO_2 and Figure 56 for the MOX materials. The MOX results have not been corrected for the UPu bias discussed in Section 3.8, so the general arc as a function of mass is expected; the moderating effect of the water produces the spread between the curves.

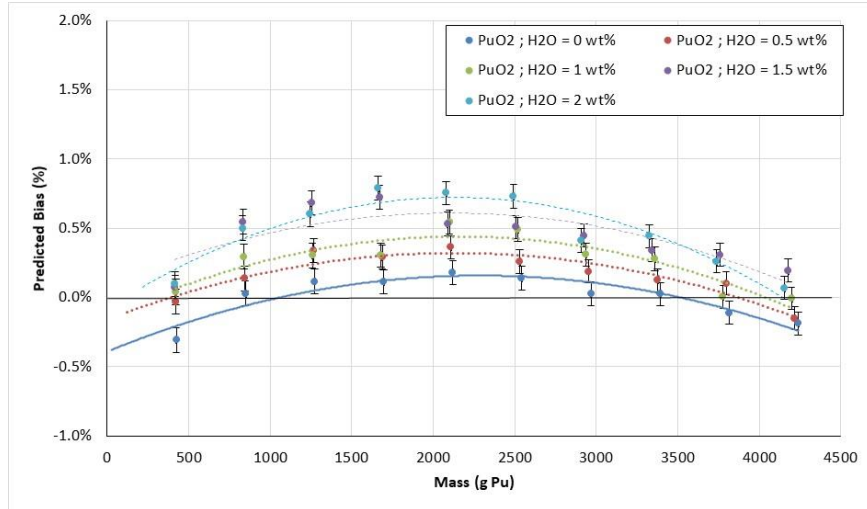


Figure 55. Simulated bias resulting from the assay of “damp” PuO₂ using the ENMC for increasing content of H₂O.

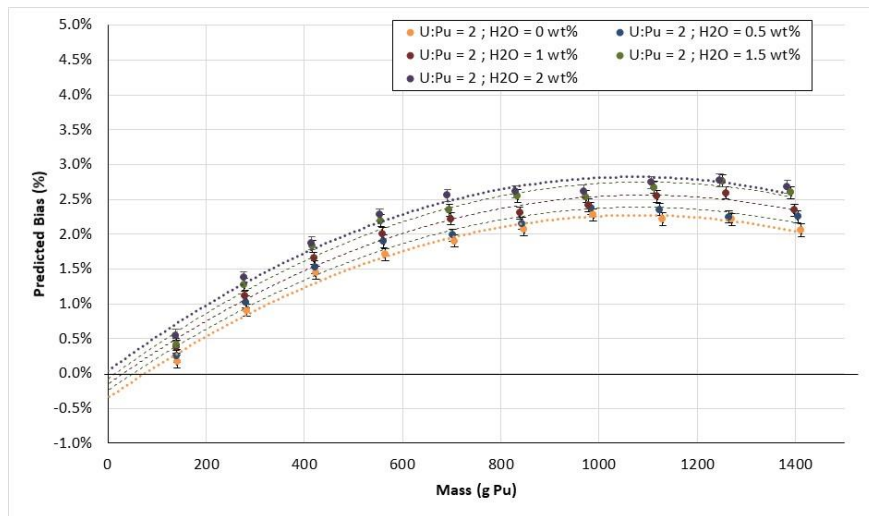


Figure 56. Simulated bias resulting from the assay of “damp” MOX using the ENMC for increasing content of H₂O.

The moderator can impact the assay result by lowering the average neutron energy and detection efficiency and by increasing the self-multiplication. The impact on the neutron detection efficiency is shown in Figure 57 and on the multiplication in Figure 58. The changes in the simulated multiplication (distinguished from the analysis multiplication result) are on the same order as the statistical error of the MCNP run, so from the MCNP simulations we can see that for these test cases the impact on the measurement results is almost entirely due to changes in the efficiency with increasing moderator content.

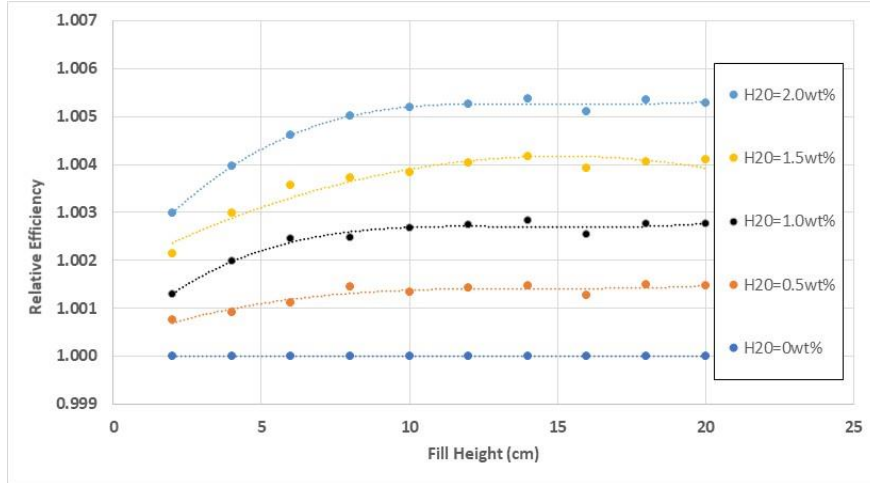


Figure 57. Volume average detection efficiency relative to dry oxide as a function of fill height for each of the simulated moisture loadings for both PuO₂ and MOX items.

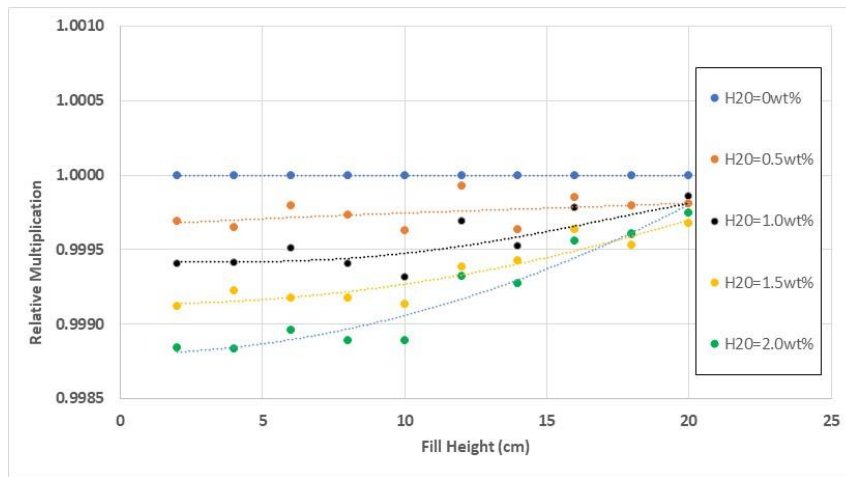


Figure 58. Multiplication relative to dry oxide as a function of fill height for each of the simulated moisture loadings for the PuO₂ containers.

The relative moderator bias, Δ_{mod} , introduced by the presence of moderating materials, expressed in terms of water equivalent, is represented as a quadratic in terms of the difference from the moderator content of the calibration standards.

$$\Delta_{mod} = a_1 + a_2 \cdot (w_{item} - w_{cal}) + a_3 \cdot (w_{item} - w_{cal})^2,$$

where w_{item} is the equivalent weight percentage of water in the item,
 w_{cal} is the equivalent weight percentage of water in the calibration items (typically = 0), and
 a_1 , a_2 , and a_3 are empirically determined by either measurement or simulation.

For the simulated data set we find that the moderator bias is well represented by

$$\Delta_{mod} = -0.30 \cdot w_{item}.$$

To illustrate the suitability of the moderator bias, the bias is applied as a correction factor to the data presented in Figure 55 and the revised plot provided in Figure 59. Similarly, Figure 60 shows the

moderator bias corrected results from Figure 56. While not perfect, the expression for Δ_{mod} provides a reasonable estimate of the bias. Measurements had previously been performed using a PSMC, where 1 wt% water had been deliberately added to three containers of MOX [3]. The relative bias for these items compared with dry oxides of similar mass resulted in an average bias of 0.3% agreeing with the simulated bias.

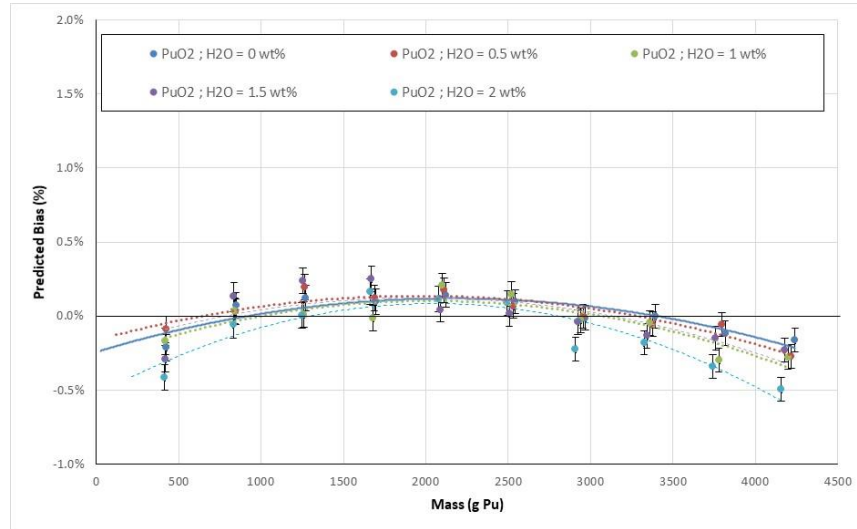


Figure 59. Simulated bias resulting from the assay of “damp” PuO₂ using the ENMC for increasing content of H₂O.

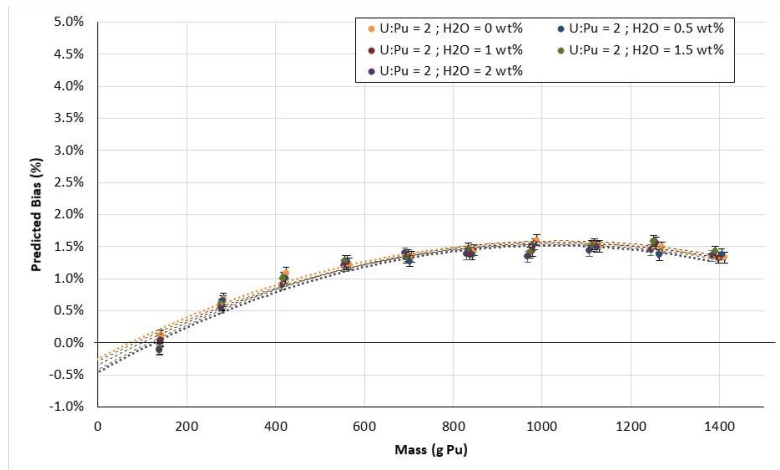


Figure 60. Simulated bias resulting from the assay of “damp” MOX material using the ENMC for increasing content of H₂O.

The random uncertainty component due to the presence of a moderator is determined from the potential range of the moderator content relative to the expected value. We define the 1-sigma uncertainty in the moderator content as (maximum content – minimum content)/6 and treat the uncertainty as if it follows a normal distribution.

$$\sigma_{mod} = (a_2 + 2 \cdot a_3 \cdot (w_{item} - w_{cal})) \cdot \sigma_{w_{item}} \cdot$$

The expression for Δ_{mod} above requires prior knowledge of the moderator content to determine the magnitude of the bias. Because the moderator effect is primarily an impact to the neutron detection

efficiency, it seems logical to try to apply the ring ratio data (again, if available) to provide a measure of the moderator bias. A plot of the relative neutron detection efficiency as a function of the ring ratio is provided in Figure 61. While there is a general trending with the efficiency, it is difficult to extract a useful bias function from the ring ratio measurement, this becomes even more challenging with the addition of low-Z materials to the Pu-bearing material. As with the (α , n) bias, the ring ratio serves more as an indicator of the presence of an interference than as a reliable tool (in other than special limited circumstances) for use in developing a correction.

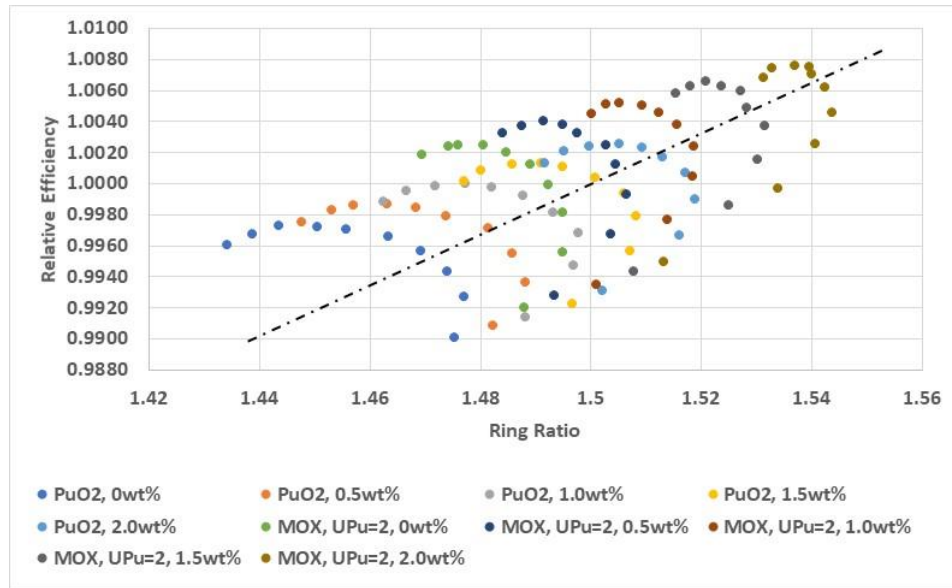


Figure 61. Simulated bias resulting from the assay of “damp” MOX material using the ENMC for increasing content of H₂O.

4. TOTAL MEASUREMENT UNCERTAINTY

We have identified the following error contributors, some of which are random, systematic, or have elements of each. For example, the systematic component of the radial component is the bias introduced by the average distance of non-centered containers away from the cavity centerline, while the random component derives from the assay-to-assay variation about the average distance. A summary of the significant error contributors is provided in Table 16.

Table 16. Uncertainty contributors to the multiplicity TMU.

Uncertainty Contributor	Random	Systematic	Requires
Counting Statistics	x		
Detector Parameters		x	Calibration results
²⁴⁰ Pu _{effective} Conversion		x	nuclear data/uncertainties
Fission Moments		x	nuclear data/uncertainties
Radial Offset	x	x	operating history
Fill Height	x	x	material declaration
Density	x	x	material declaration
(α , n)	x	x	material declaration
Burnup	x	x	material declaration
UPu Ratio		x	material declaration
Moderation	x	x	material declaration

The traditional neutron multiplicity uncertainty analysis incorporates only uncertainties related to the Pu isotopics distribution and due to counting statistics. As an example, the mass and uncertainty results from a 722 g MOX item assayed using a PSMC are provided in Figure 62. A breakdown of the collection of uncertainty contributions listed in the table above is presented in Figure 63 showing that the systematic contributors have a greater contribution to the TMU than the random components (note that counting statistics do not encompass all random error sources and so is not an accurate representation of measurement precision).

	Value	Uncertainty	
		Partial Correlation	Full correlation
Multiplication	1.0753	± 0.0016	0.0012
Alpha	0.817	± 0.018	0.011
Mass (g Pu240 eff)	235.561	± 2.857	1.773
Mass (g Pu)	709.486	± 8.641	5.395

Figure 62. Example of uncertainties reported for traditional multiplicity assay results. Note that most analysis software currently in use reports the uncertainties with fully correlated covariance terms, which in this case underreports the uncertainties.

The systematic fill height, density, UPu ratio, alpha, burnup, and moderator uncertainties have been expressed relative to an expected baseline condition (e.g., typical UPu ratio). However, there is also a variation in the parameters relative to the typical value. These variations introduce random variation in the reported assay result and so must be included in the random uncertainty determination. The total random uncertainty for m_{240} is given by

$$\sigma_{random} = \sqrt{\sigma_{statistical}^2 + \sigma_{radial}^2 + \sigma_{FH}^2 + \sigma_{\rho}^2 + \sigma_{UPu}^2 + \sigma_{\alpha}^2 + \sigma_{mod}^2}$$

To provide an estimate of the TMU, we have adopted the customary approach that the systematic contributions are added in quadrature, as presented in Figure 64.

$$\Delta_{systematic} = \sqrt{\Delta_{det}^2 + \Delta_{m_{eff}}^2 + \Delta_{v_s}^2 + \Delta_{v_i}^2 + \Delta_{radial}^2 + \Delta_{FH}^2 + \Delta_{\rho}^2 + \Delta_{UPu}^2 + \Delta_{\alpha}^2 + \Delta_{BU}^2 + \Delta_{mod}^2}$$

However, these systematic uncertainties represent uncorrected biases and the true impact on the assay result may be larger or smaller than indicated by this traditional approach. Alternatively, we might simply sum the systematic uncertainties. Contributors such as fill height and moderator content generally result in underreporting the mass value, while contributions from other contributors are dependent on the method of calibration and difference in material type between the item and calibration standards. For the analysis of the 722 g Pu item, the systematic error when calculated as the square root of the sum of the squares is 13.8 g (2%), while the simple summation result is 21.8 g (3%). The true contribution is likely to lie in between these two values.

The contributions from the material-specific components (density, UPu ratio, etc.) were determined in isolation from each of the other contributors; that is, reference cases spanning a range Pu masses were developed for the evaluation of each contributor and the impact of the error contributor quantified relative to the reference case. Multiple reference cases were examined for each contributor in order to establish its contribution uniquely. Examination of the expressions for the various biases in Sections 3.7 through 3.11 indicates that the biases are expected to be covariant to some extent; however, within the limitations of this study it was not possible to quantify these covariances.

Uncertainty Component	grams Pu240 effective:	grams Pu	sigma-m/m
Counting Statistics	2.857	8.607	1.213%
Detector Characterization:	1.961	5.907	0.832%
Pu240 Effective Conversion:	N/A	5.989	0.844%
Fission Moments:	2.17	6.538	0.921%
Radial Offset (Random):	0.257	0.776	0.1%
Radial Offset (Systematic):	0.31	0.934	0.13%
Fill Height (random):	0.604	1.821	0.256%
Fill Height (systematic):	-3.169	-9.545	-1.346%
Density (random)	1.474	4.441	0.626%
Density (systematic)	0.782	2.356	0.332%
(Alpha. n) random:	0.051	0.155	0.021%
(Alpha. n) bias:	0.154	0.466	0.065%
Burn_up (random):	0	0	0%
Burn_up (systematic):	0.006	0.018	0.002%
UPu Ratio (random):	0.07	0.211	0.029%
UPu Ratio (systematic):	1.87	5.634	0.794%
Moderator (random):	0	0	0%
Moderator (systematic):	0	0	0%

Figure 63. Example of additional uncertainty contributions to the multiplicity analysis for 722 g dry MOX powder assay using a PSMC.

	Result	Random	Systematic	Total	Declared	Difference
Multiplication	1.0753	± 0.0016				
Alpha	0.817	± 0.018				
Mass (g Pu240 eff)	235.561	± 3.227	4.778	5.766	239.424	
Mass (g Pu)	709.486	± 9.72	15.589	18.371	721.79	-12.304 g
Relative Uncertainty		1.37%	2.19%	2.58%		diff = -1.71%

Figure 64. Example of assay mass result total measurement uncertainty.

5. CONCLUSIONS

We have developed a Total Measurement Uncertainty model for Neutron Coincidence Multiplicity analysis of PuO₂ and MOX materials commonly assayed using the thermal neutron multiplicity counter. We have evaluated the uncertainty contributions arising from nuclear data, detector properties, the

detector characterization process, Pu composition and mass, and material form. Where feasible, the uncertainty contributor has been examined in context of the PME; otherwise, empirical response functions have been developed, primarily through simulations, to quantify the random or systematic error introduced.

Despite the association of multiplicity analysis with the notion of a calibration-free method, the multiplicity counting system must be calibrated using representative standards in order to derive the greatest potential accuracy from the measurement. If the material type is constrained to a very narrow band of chemical and isotopic composition and density, then an empirical calibration using representative standards to adjust the neutron detection efficiency and gate fractions results in a multiplicity analysis where the uncertainty is dominated by the measurement precision and declaration values of the calibration standards.

A TMU Estimator tool has been developed to assist in the evaluation of the multiplicity assay TMU. The tool is a Windows-based application and incorporates each of the uncertainty components discussed in this report. This tool will be made available as an open source code. An explanation of the code's usage is provided in Appendix A.

5.1 FUTURE WORK

This TMU analysis is limited by the constraints of the traditional point model. Although several extensions to the point model exist, they are not widely in use and the performance of the extensions is not well documented (i.e., the international standards such as ASTM do not encompass the extensions). Extension of this analysis to incorporate the more complex variants of the point model will provide greater flexibility in its application as well as more accurate uncertainty estimates. For example, the dual energy model potentially addresses the impact of impurities on the assay result. These impurities not only introduce large biases into the assay result but also there is a corresponding impact on the accuracy of the TMU estimate.

The uncertainty estimates developed for this study, suggest that additional bias corrections (e.g., fill height) could be applied to the multiplicity analysis if sufficient prior knowledge about the item under assay is available. Implementation of such bias correction factors could in principle result in improved accuracy for items not well represented by the calibration materials.

6. REFERENCES

- [1] D. Pelowitz, "MCNP6 User's Manual, LA-CP-13-00634, Rev. 0," Los Alamos National Laboratory, Los Alamos, NM, 2013.
- [2] H. Menlove, J. Baca, M. Krick, K. Kroncke and D. Langner, "Plutonium Scrap Multiplicity Counter - Operation Manual, LA-12479-M," Los Alamos National Laboratory, Los Alamos, NM, 1993.
- [3] K. Nakjima, S. Ishikawa, D. Davidson, R. McElroy and H. Menlove, "Operator Experience Measuring MOX Scrap at PNC Using the Plutonium Scrap Multiplicity Counter," in *ESARDA, 19th Annual Symposium on Safeguards and Nuclear Material Management, France, May 12-16, 1997*, Montpellier, France, 1997.
- [4] J. Stewart, H. Menlove, D. Mayo, W. Geist, L. Carrillo and G. Herrera, "The Epithermal Neutron Multiplicity Counter Design and Performance Manual: More Rapid Plutonium and Uranium Inventory Verifications by Factors of 5–20, LA-13743-M," Los Alamos National Laboratory, Los Alamos, NM, 2000.

- [5] R. D. McElroy, Jr. and S. Croft, "Comparison of List Mode Data Acquisition and Shift Register Multiplicity Measurements Using the Large Epi-Thermal Neutron Multiplicity Counter (LEMC)," *Journal of Radioanalytical and Nuclear Chemistry*, vol. 276, no. 3, pp. 725-730, 2008.
- [6] M. Krick, W. Harker, W. Geist and J. Longo, "INCC Software User's Manual, report LA-UR-10-6227," Los Alamos National Laboratory, Los Alamos, NM, March 29, 2009.
- [7] N. Ennslin et.al., "Application Guide to Neutron Multiplicity Counting, LA-13422-M,," Los Alamos National Laboratory,, Los Alamos, NM, 1998.
- [8] P. Santi and W. Geist, "Energy Dependent Bias in the Weighted Point Model, LA-UR-05-4287," Los Alamos National Laboratory, Los Alamos, NM, 2005.
- [9] D. Hauck and V. Henzl, "Spatial Multiplication Model as an Alternative to the Point Model in Neutron Multiplicity Counting, LA-UR-14-21991," Los Alamos National Laboratory, Los Alamos, NM, 2014.
- [10] J. Burward-Hoy, W. Geist, M. Krick and D. Mayo, "Achieving accurate neutron-multiplicity analysis of metals and oxides with weighted point model equations, LA-UR-04-4357," Los Alamos National Laboratory, Los Alamos, NM, 2004.
- [11] W. Geist et.al., "Reduction of Bias in Neutron Multiplicity Assay Using a Weighted Point Model, LA-UR-04-1149,," in *7th International Conference on Facility Operations-Safeguards Interface, February 29-March 5, 2004.*, Charleston, SC, 2004.
- [12] M. Krick, W. Geist and D. Mayo, "Weighted Point Model for the Thermal Neutron Multiplicity Assay of High-Mass Plutonium Samples, Los Alamos National Laboratory, LA-14157," Los Alamos National Laboratory, Los Alamos, NM, 2005.
- [13] S. Croft, E. Alvarez, . P. Chard, R. McElroy and S. Philips, "An Alternative Perspective on the Weighted Point Model for Passive Neutron Multiplicity Counting," in *Proceedings of the Institute of Nuclear Materials Management, 48th Annual Meeting*, Tucson, AZ, 2007.
- [14] M. Krick, D. Langner and J. Stewart, "Energy-Dependent Bias in Plutonium Verification Measurements Using Thermal Neutron Multiplicity Counters, LA-UR-97-3427," Los Alamos National Laboratory, Los Alamos, NM, 1997.
- [15] N. Ennslin, W. C. Harker, M. S. Krick, D. Langner, M. Pickrell and J. Stewart, "Application Guide to Neutron Multiplicity Counting,," Los Alamos National Laboratory report LA-13422-M, Los Alamos, NM, 1998.
- [16] R. McElroy Jr., S. Croft and S. Cleveland, "Direct Multiplication Measurement as an Alternative to Neutron Multiplicity Analysis, ORNL/TM-2015/130," Oak Ridge National Laboratory, Oak Ridge, TN, 2015.
- [17] R. D. McElroy, Jr. and S. Croft, "Preliminary Performance Results for a Direct Multiplication Measurement for Use in Neutron Multiplicity Analysis," in *International Nuclear Materials Management 55th Annual Meeting*, Atlanta, Ga, 2014.
- [18] A. C1500-08(2017), "Standard Test Method for Nondestructive Assay of Plutonium by Passive Neutron Multiplicity Counting," ASTM International, West Conshohocken, PA, 2017.
- [19] J. Hendricks et.al., "MCNPX Version 2.5, LA-UR-02-7086," Los Alamos National Laboratory, Los Alamos, NM, 2002.
- [20] R. McElroy, Jr. and S. Croft, "Total Measurement Uncertainty in Neutron Coincidence Multiplicity Analysis," in *Proceedings of the 60th Annual Meeting of the Institute of Nuclear Materials Management*, Palm Desert, CA, 2019.
- [21] R. Harry, "PIDIE, Plutonium Isotopic Determination Inter-Comparison Exercise," in *31st Annual Meeting of the Institute of Nuclear Materials Management, July 15-18, 1990*, Los Angeles, CA, 1990.

- [22] N. Dytlewski, M. Krick and N. Ensslin, "Measurement variances in thermal neutron coincidence counting," *Nucl Instrum and Meths in PR A327(1993)469-479.*
- [23] S. Croft, M. Swinhoe and V. Henzl, "Á Priori Precision Estimation for Neutron Triples Counting," in *The Second International Conference on Advancements in Nuclear Instrumentation, Measurement Methods and their Applications – ANIMMA, 6-9 June, 2011, the ICC, Ghent, Belgium.*, Ghent, Belgium, 2011.
- [24] Canberra Industries, "NDA 2000 Technical Reference Manuall V3.2," Canberra Industries, Meriden, CT, 2003.
- [25] N. Dytlewski, , "Dead-time corrections for multiplicity counters,," *Nucl. Instr. Meth*, vol. A305, pp. 492-494, 1991.
- [26] R. McElroy, Jr., S. Croft and S. Philips, "A New Method for the Determination of the Neutron Multiplicity Counter Dead Time Parameter," in *Proceedings of the 47th Annual Meeting of the Institute of Nuclear Materials Management*, Nashville, Tennessee, 2006.
- [27] E. Browne and R. Firestone, Table of Radioactive Isotopes, New York: John Wiley and Sons, 1986.
- [28] S. Croft, A. Nicholson, D. Henzlova and D. Favalli, "Representing the uncertainty structure of the factorial moments of ^{252}Cf and ^{238}Pu ," in *Advances in Nuclear Nonproliferation Technology & Policy Conference: Bridging the Gaps in Nuclear Nonproliferation*, Sante Fe, NM, 2016.
- [29] D. Reilly, "Los Alamos National Laboratory report LA-UR-90-732," Los Alamos National Laboratory, Los Alamos, NM, 1990.
- [30] I. Gauld, S. Croft, M. Pigni, A. Nicholson and M. Williams, "Systematic Approach to Nuclear Data Uncertainty Quantification for Nuclear Security Applications," in *Advances in Nuclear Nonproliferation Technology & Policy Conference: Bridging the Gaps in Nuclear Nonproliferation*, Sante Fe, NM, 2016.
- [31] M. Swihhoe, C. Mattoon, S. Croft, I. Gauld, A. Nicholson and V. Mozin, "Nuclear Data Uncertainty Quantification – a Practical Example for Nuclear Measurements," in *Advances in Nuclear Nonproliferation Technology & Policy Conference: Bridging the Gaps in Nuclear Nonproliferation*, Sante Fe, NM, 2016.
- [32] M. Zucker and N. Holden, "Energy Dependence of the Neutron Multiplicity Pn in Fast Neutron Induced Fission of ^{235}U and ^{239}Pu , BNL-38491," in *American Nuclear Society Annual Meeting 15 Jun 1986*, Reno, NV, 1986.
- [33] J. Lestone, "Energy and Isotope Dependence of Neutron Multiplicity Distributions, LA-UR-05-0288," Los Alamos National Laboratory, Los Alamos, NM, 2005.
- [34] E. F. Shores, "SOURCES 4C: A Code for Calculating (α , n), Spontaneous Fission, LA-UR-02-1839," Los Alamos National Laboratory, Los Alamos, NM, April 2002.
- [35] G. Jacobs and H. Liskien, "Energy spectra of neutrons produced by α -particles in thick targets of light elements," *Ann. Nucl. Energy*, vol. 10, no. 10, pp. 541-552, 1983.
- [36] D. Langner, M. Krick and D. Miller, "The Use of Ring Ratios to Detect Sample Differences in Passive Coincidence Counting," in *Proceedings of the 33rd Annual Meeting of the Institute of Nuclear Materials Management*, Orlando, FL, 1992.
- [37] W. Beyer, CRC Standard Mathematical Tables, 24th edition, Cleveland, Ohio: CRC Press, 1976.

APPENDIX A. MULTIPLICITY TMU ESTIMATOR

Multiplicity TMU Estimator

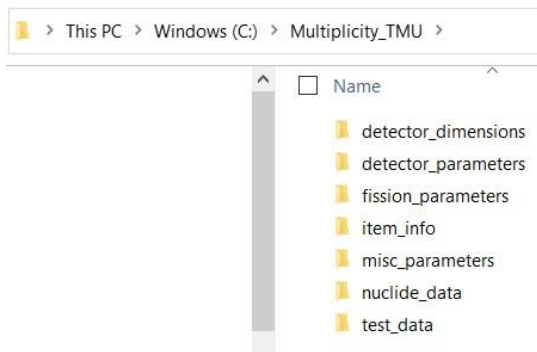
The TMU estimator is developed using Microsoft's Visual Studio / Visual Basic. The intent is that the user will be able to read in existing multiplicity counting data files and analyze them using the present common use Point Model Equations. Based on supplemental calibration and item information, the contributions to total measurement uncertainty (TMU) are quantified and then combined to provide a TMU estimate for the assay. The TMU estimator is intended as an aide to evaluation of measurement performance and as a means to identify the more significant sources of uncertainty impacting the assay result; however, at this time it has not been fully vetted.

The parameters included in the default files were developed for the PSMC and ENMC counting systems. The parameters can be applied to other systems, but the greater the design differences are, the less applicable the empirically determined bias estimates will be, and it is recommended that the parameters be reevaluated for the new counting system.

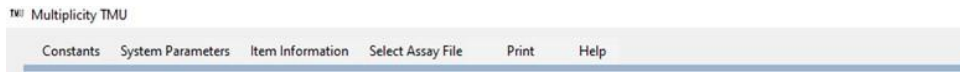
All nuclear data, calibration, and detector parameters used in the analysis are stored in text files using a CSV format. These parameters may be changed to suit the particular assay scenario. The detector parameter file may be used to replace the parameters stored in the assay file or to introduce the detector uncertainty terms not normally available in the assay result file. The isotopic data file allows modification of the isotopic data and uncertainties found in the assay result.

File Locations

The software requires that certain directories exist on the computer's C: drive. The software looks for certain default files in these directories (as will be described in the following sections). The required folders are shown in the following screenshot.



Main Menu Bar



The main menu bar provides five main selections.

- Constants
The constants menu item allows review/entry of

- Fission Moments
 - The values of ν_{s1} , ν_{s2} , ν_{s3} , ν_{i1} , ν_{i2} , ν_{i3} , and ϕ
 - The uncertainties and covariances can also be entered.
- Nuclide Data
 - Nuclide half-lives, spontaneous fission yields, (α , n) yields, and $^{240}\text{Pu}_{\text{equivalent}}$ conversion factors.
- System Parameters
 - The menu allows review/entry of system-specific parameters:
 - Calibration Parameters
 - Four categories of calibration parameters are entered through the Calibration Parameters screen.
 - Basic Detector Parameters (efficiency, gate width, gate fractions, dead-time)
 - Item-relevant calibration information (type, container information, UPu ratio, density, alpha, and moderator content) used to baseline bias calculations
 - Multiplication Correction Factor
 - A sub-menu to enter Dual Energy Multiplicity Parameters (for future use)
 - Detector Physical Parameters
 - This menu allows review/entry of parameters that physically describe the multiplicity counting system
 - Empirical TMU Parameters
 - This menu allows review/entry of parameters describing the empirically determined biases.
 - Typical Multiplication
 - Burnup Bias Estimate
 - UPu Bias Estimate
 - (α , n) Bias Estimate
 - Moderator Bias
 - Density Effect
 - Container Effect
 - Misc. Parameters
 - This menu allows review/entry of parameters used to set the
 - Statistical Filters
 - Iterations for Dithered Histograms
 - Number of random positions used to determine fill heights/radial offset biases
 - Item Information
 - This menu allows review/entry of parameters that describe the item under assay.
 - Isotopic Declaration
 - Container/Contents Description
 - Selection of the primary (α , n) impurity
 - Select Assay File
 - Allow selection of the INCC file to be analyzed
 - (At present the TMU tool only reads CAL, RTS and VER data (text) files.)
 - Print
 - Prints a series of screenshots of the home screen
 - At present, print capabilities for the app are rudimentary.
 - Help
 - Future Use

Constants



The Constants Menu navigates to the *Fission Moments* and *Nuclide Data* entry screens.

Fission Moments Data Entry Screen



The spontaneous and induced fission moments are entered in this screen.

Note: the covariance array must be completed even if all off-diagonal entries are zero.

The screenshot shows the 'Fission Moments' data entry screen. It features a table with columns for 'Fission Parameter', 'Value', 'Uncertainty', and a covariance matrix. Below the table are buttons for 'Select Constants File', 'Save as New File', and 'Accept'. The file path shown is 'c:\multiplicity_tmu\fission_parameters\current_fission_parameters.csv'.

Fission Parameter	Value	Uncertainty								
nu_s1	2.154	± 0.005	2.5E-05	0.000131	0.000421	0	0	0	0	0
nu_s2	3.789	± 0.013	0.000131	0.000169	0.000768	0	0	0	0	0
nu_s3	5.21	± 0.067	0.000421	0.000768	0.004489	0	0	0	0	0
nu_i1	3.1635	± 0.068	0	0	0	0.004624	0	0	0	0
nu_i2	8.305	± 0.0407	0	0	0	0	0.001656	0	0	0
nu_i3	17.782	± 0.151	0	0	0	0	0	0.022801	0	0
Φ	473.5	± 3.9	0	0	0	0	0	0	0	15.21

The data is saved in CSV file format.

The active fission moments data file is always named.

current_fission_parameters.csv

The active fission moments data file must be placed in the directory.

C:\multiplicity_tmu\fission_parameters

Additional fission moment data files may be created and saved using this form.

The new files may be saved to / read from any directory.

Pressing the *Accept* button copies the currently displayed parameters to the

current_fission_parameters.csv for use in the TMU analysis.

Nuclide Data Entry Screen



Nuclide half-lives, spontaneous fission yields, ^{240}Pu effective conversion factors, and the PuO_2 , PuF_4 (α, n) yields are entered in this screen.

The 'Nuclide Data' window displays a table with columns for Isotope, Half-life (y), Spont. Fission Yield (n/s/g), PuO_2 (α, n) Yield, PuF_4 (α, n) Yield, and Pu-240 Equivalent. Each cell contains a numerical value and a small error bar. Below the table, there is a button labeled 'Alpha, n conversion Values' which is currently disabled. At the bottom, there are three buttons: 'Select New File', 'Save as New File', and 'Accept'. The 'Select New File' button is active, and a text box next to it shows the file path: 'c:\multiplicity_tmu\nuclide_data\nuclide_decay_data.csv'.

Isotope	Half-life (y)	Spont. Fission Yield (n/s/g)	PuO_2 (α, n) Yield	PuF_4 (α, n) Yield	Pu-240 Equivalent
Pu238	87.74 ± 0.09	2590 ± 185	13400 ± 134	2200000 ± 100000	2.566 ± 0.235
Pu239	24100 ± 30	0.0218 ± 0.00109	38.1 ± 0.381	5600 ± 100	0 ± 0
Pu240	6560 ± 7	1020 ± 51	141 ± 1.41	21000 ± 1000	1 ± 0
Pu241	14.35 ± 0.2	0.05 ± 0.0025	1.3 ± 0.013	170 ± 10	0 ± 0
Pu242	376000 ± 2000	1720 ± 75	2 ± 0.02	270 ± 10	1.702 ± 0.036
Pu244	8260000 ± 900000	1779.44 ± 200	0.8494 ± 0.008494	1.72 ± 0.1	1.7446 ± 0.1745
Am241	433.6 ± 0.5	1.18 ± 0.059	2690 ± 26.9	25260.162 ± 1000	0.0017 ± 0.0001
Cf252	2.645 ± 0.008	234000000 ± 2350000000	600000 ± 12000	0 ± 0	1 ± 0

The data is saved in CSV file format.

The active nuclide decay data file is always named.
nuclide_decay_data.csv

The active nuclide decay data file must be placed in the directory.
C:\multiplicity_tmu\nuclide_data

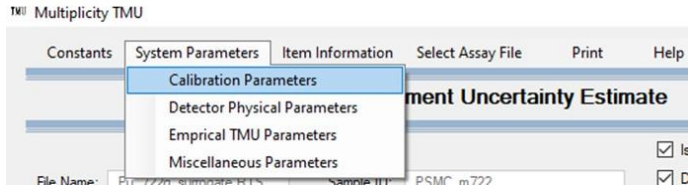
Additional nuclide decay data files may be created and saved using this form.

The new files may be saved to / read from any directory.

Pressing the *Accept* button copies the currently displayed parameters to the *nuclide_decay_data.csv* for use in the TMU analysis.

Note that the “*Alpha, n conversion Values*” button is not active.

Calibration Parameters



Calibration parameters for the “calibration-free” multiplicity analysis are entered here. The parameters entered include basic detection, dead-time correction, and multiplication correction factor in addition to basic information related to the mass calibration.

The 'Calibration Parameters' dialog box displays a covariance matrix and various input fields for calibration and multiplication correction parameters.

Detection Parameter	Value	Uncertainty	1	2	3	4	5	6	7	8	9	10
Efficiency	0.543	± 0.00322402	1.04E-05	0	0	0	0	0	0	0	0	0
Die-Away (us)	49.9	± 0.87	0	0.7569	0	0	0	0	0	0	0	0
Gate Width (us)	64	± 0	0	0	0	0	0	0	0	0	0	0
f_d	0.6117	± 0.00044815E	0	0	0	2.01E-07	0	0	0	0	0	0
f_l	0.3896	± 0.00079626E	0	0	0	0	6.37E-07	0	0	0	0	0
Dead-time												
a (us)	0.3093	± 0.003093	0	0	0	0	0	9.57E-06	0	0	0	0
b (us ²)	0.0998	± 0.00099774E	0	0	0	0	0	9.95E-07	0	0	0	0
c (ns)	85	± 0.90945990E	0	0	0	0	0	0	0.827117	0	0	0
d (ns) *	85.85	± 3.27406595E	0	0	0	0	0	0	0	10.7195	0	0
τ	104	± 0.45	0	0	0	0	0	0	0	0	0	0.2025

* Parameters are dependent on deadtime model.

c:\multiplicity_tmu\detector_parameters\det_parameters.csv

Calibration Parameters

- Point Source, Cavity Center
- Distributed Typical Fill Height (cm) 5
- Cal Standard Container Wall Thickness (cm) 0.1
- Cal Standard Container Wall Material Stainless Steel
- Cal Standard U:Pu Ratio 0
- Cal Standard density (g/cc) 3
- Cal Standard ²⁴⁰Pu effective/g> 0.33
- Cal Standard Alpha 0.76
- Cal Standard Moderator Content (H2O wt%) 0

Multiplication Correction

CF = 1+a(M-1)+b(M-1)²

a: -0.15506 ± 0.0015

b: 0.57276 ± 0.0057

covar(a,b): 0

Apply Correction

- Checking the *Point Source, Cavity Center* box calculates biases relative to a point source calibration.
- Checking the *Distributed* box calculates biases relative to a volumetric mass calibration.
- *Typical Fill Height*: The average or typical standards fill height during the calibration.
- *Cal Standard Container Wall Thickness*: The wall thickness of the typical standard container used during calibration.

- *Cal Standard Container Wall Material:* Material of the containers used during calibration. A bias is calculated for stainless steel containers.
- *Cal Standard UPu Ratio:* The average UPu ratio of the representative standards used to calibrate the system (UPu=0 → PuO₂).
- *Cal Standard density:* The average or typical bulk density of the representative standards used to calibrate the system.
- *Cal Standard ²⁴⁰Pu_{effective}:* The average or typical ²⁴⁰Pu_{effective} value of the representative standards used to calibrate the system.
- *Cal Standard alpha:* The average or typical alpha value of the representative standards used to calibrate the system.
- *Cal Standard Moderator Content:* The average or moderator content of the representative standards used to calibrate the system. Enter in terms of equivalent H₂O wt% of the standards.

The *Multiplication Correction Factor* is applied to the computed m_{240} equivalent mass value and the total Pu mass value.

- *Apply Correction checkbox:* If checked, the multiplication correction will be applied.

The data is saved in CSV file format.

The active detector parameter file is always named.

det_parameters.csv

The detector parameter file must be placed in the directory.

C:\multiplicity_tmu\detector_parameters

Additional detector parameter files may be created and saved using this form.

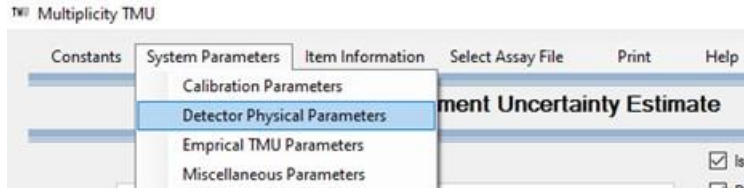
The new files may be saved to / read from any directory.

Pressing the *Accept* button copies the currently displayed parameters to the *det_parameters.csv* for use in the TMU analysis.

Note: The covariance array must be completed; the diagonal variance entries are NOT automatically populated.

Note: that the “*Dual Energy Multiplicity Analysis*” button is active; however, the Dual Energy analysis has not been implemented.

Detector Physical Parameters



These parameters physically describe the assay system; many of these parameters are not presently used but are intended for future use. At present the TMU analysis makes use of the following.

- *Cavity Type*: Only cylindrical cavities are currently supported.
- *Cavity Height*: Distance between the top of the bottom end plug and the bottom of the top end plug (cm).
- *Cavity Width or Dia.*: The assay cavity ID or shorter horizontal dimension for a rectangular cavity (cm).
- *Cavity Length*: The assay longer horizontal dimension for a rectangular cavity (cm).
- *Cd liner thickness*: The thickness of the inner Cd liner (cm).
- *Tube ID*: Inner diameter of the ^3He tubes (cm).
- *Tube Active Length*: Active length of the vertical ^3He tubes (cm).
- *Number of Rows*: Number of rows or rings of ^3He tubes about the assay cavity.
- *Item Stand Height*: Distance from the bottom of the item to the assay cavity floor.
- *Row Radius and Tube Numbers*: Tube pattern for the ^3He tubes.

Counter:

File Name:

Cavity Type	<input type="text" value="Cylindrical"/>	
Cavity Height (cm)	<input type="text" value="40"/>	
Cavity Width or Dia. (cm)	<input type="text" value="19"/>	
Cavity Length (cm)	<input type="text" value="19"/>	
Cd Liner thickness (cm)	<input type="text" value="0.1"/>	
Tube ID (cm)	<input type="text" value="2.54"/>	
Tube Active Length (cm)	<input type="text" value="71.12"/>	
Number of rows	<input type="text" value="4"/>	
	Radius (cm)	Tubes (#)
Row 1	<input type="text" value="13.1"/>	<input type="text" value="19"/>
Row 2	<input type="text" value="17.27"/>	<input type="text" value="25"/>
Row 3	<input type="text" value="21"/>	<input type="text" value="18"/>
Row 4	<input type="text" value="24.72"/>	<input type="text" value="18"/>
Row 5	<input type="text" value="0"/>	<input type="text" value="0"/>
Item Stand Height (cm)	<input type="text" value="5"/>	

Note: The radius of the outer most ring of tubes is needed for the volumetric efficiency calculation.

The data is saved in CSV file format.

The active detector parameter file is always named
current_det_dimensions.csv

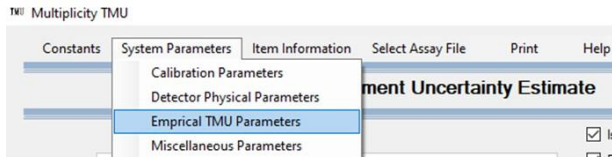
The detector parameter file must be placed in the directory
C:\multiplicity_tmu\detector_dimensions

Additional detector parameter files may be created and saved using this form.

The new files may be saved to / read from any directory.

Pressing the “Make Current Item” updates the *current_det_dimensions.csv* file.

Empirical TMU Parameters Entry Screen



The empirical parameter data entry screen allows review/entry of the parameters for the estimation of uncertainty contributors. Parameters are entered for

- Typical Multiplication Estimate
- Burnup Bias Estimate
- UPu Bias Estimate
- (α , n) Bias Estimate
- Moderator Bias Parameters
- Density Effect Bias Parameters
- Container (Wall Thickness) Effect

The information is stored in a CSV file; note that there is only one file for the empirical parameters, the file name and its location are C:\Multiplicity_TMU\misc_parameters\TMU_empirical_parameters.csv. After editing the file, the changes may be saved by pressing the “Save” button.

Each of the following represents a portion of the empirical parameters screen.

Typical Multiplication

The typical multiplication is an estimate of the typical multiplication as a function of total Pu mass for a given material density, burnup, and UPu ratio. It is used only to provide an estimated measurement precision for comparison against the observed precision for the item under assay. The form of the expression adds a power function and polynomial to allow for flexibility in representing the estimated multiplication value.

Typical Multiplication Parameters
for estimated precision curves

$$M = 1 + k_1 \cdot \left(\frac{m_{Pu}}{k_2}\right)^{k_3} + k_4 + k_5 \cdot m_{Pu} + k_6 \cdot m_{Pu}^2 + k_7 \cdot m_{Pu}^3$$

k(1) <input style="width: 80%;" type="text" value="0.003"/>	k(4) <input style="width: 80%;" type="text" value="0"/>
k(2) <input style="width: 80%;" type="text" value="1"/>	k(5) <input style="width: 80%;" type="text" value="0"/>
k(3) <input style="width: 80%;" type="text" value="0.49"/>	k(6) <input style="width: 80%;" type="text" value="0"/>
	k(7) <input style="width: 80%;" type="text" value="0"/>

Burnup Bias Estimate

The bias introduced by the difference of the typical $^{240}\text{Pu}_{\text{effective}}$ value between the item under assay and the calibration standards. This difference can introduce a small bias that increases with the value of alpha. The offset parameter a_1 should generally be set to 0.

Burn-up Bias Estimate Parameters
Impact of deviation from 240Pu_{eff} of calibration standards

$$\Delta_{BU} = a_1 + a_2 \cdot \left({}^{240}\text{Pu}_{eff,item} - {}^{240}\text{Pu}_{eff,cal} \right) \cdot \alpha$$

Dev_240_par(1)
 Dev_240_par(2)

UPu Bias Estimate Parameters

The UPu bias is a function of total Pu mass and the difference of the UPu ratio of the item under assay and the calibration items. The reference mass, m_{ref} , is an arbitrary a scale factor. Note that changing the scale factor requires a corresponding change in the values of UPu_par(2) and UPu_par(3).

UPu Bias Estimate Parameters
Impact of deviation from 240Pu_{eff} of calibration standards

$$\Delta_{UPu} = \left[a_1 + a_2 \cdot \frac{m_{Pu}}{m_{ref}} + a_3 \cdot \left(\frac{m_{Pu}}{m_{ref}} \right)^2 \right] \cdot \left(\frac{R_{UPu} - R_{Ref}}{\alpha_4} \right)^{3/4}$$

UPu_par(1)
 UPu_par(2)
 UPu_par(3)
 UPu_par(4)
 mref

(alpha, n) Bias Estimate

Bias parameters are entered for each of the five low-Z elements (B, Be, C, O, and F). The impurity to evaluate is selected in the Item Information Screen.

(alpha, n) Estimate Parameters
Impact of deviation from alpha value of calibration standards

$$\Delta_{\alpha} = a + b \cdot \left(\frac{m}{m_{ref}} \right)^c \cdot \alpha$$

	Boron	Beryllium	Carbon	Oxygen	Fluorine
alpha_par(1)	<input type="text" value="-0.0192"/>	<input type="text" value="-0.0689"/>	<input type="text" value="-0.039"/>	<input type="text" value="0.0033"/>	<input type="text" value="0.0192"/>
alpha_par(2)	<input type="text" value="0.0029"/>	<input type="text" value="0.005"/>	<input type="text" value="0.0085"/>	<input type="text" value="0.0028"/>	<input type="text" value="-0.0001"/>
alpha_par(3)	<input type="text" value="0.2961"/>	<input type="text" value="0.402"/>	<input type="text" value="0.2804"/>	<input type="text" value="0.2156"/>	<input type="text" value="0.6201"/>

Moderator Bias Parameters

The moderator bias is applicable only for relatively small water equivalent impurities (H₂O wt% <5). At water loading greater than 5 wt%, the bias folds back on itself, resulting in a negative rather than positive biases.

Moderator Parameters
Impact of deviation from moderator content of calibration standards

$$\Delta_{mod} = a_1 + a_2 \cdot (w_{item} - w_{cal}) + a_3 \cdot (w_{item} - w_{cal})^2$$

mod_par(1)

mod_par(2)

mod_par(3)

Matrix Density Effect

The bias due to density is a function of total Pu mass and the difference of the density of the item under assay and the calibration items. The reference mass, m_{ref} , is an arbitrary scale factor. Note that changing the scale factor requires a corresponding change in the values of a_1 .

Density Effect Parameters
Impact of deviation from material density of calibration standards

$$\Delta m_{240,\rho} = a_1 \left(\frac{m}{m_{ref} \cdot \rho_{typ}} \right)^{a_2} \cdot (1 + a_3 \cdot e^{-a_4 \rho}) \cdot (\rho_{typ} - \rho_{ref})$$

rho_par(1)

rho_par(2)

rho_par(3)

rho_par(4)

m_ref

Container Wall Effect

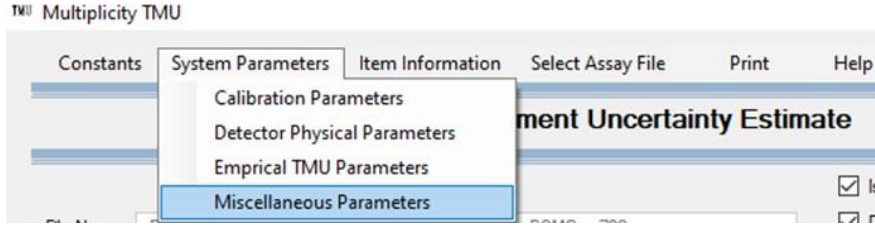
The container wall effect is an empirical modification of the efficiency applied in the solution of the PME based on the difference between the wall thickness of the item under assay and the wall thickness of the calibration standards. In the case of a stainless steel container, the walls tend to moderate the detected neutrons, resulting in an overestimate of the count rates. To compensate, the neutron detection efficiency is modified.

Container Effect Parameters
Impact of deviation from material and thickness of container wall from those of the calibration standards.

$$\varepsilon = \varepsilon_0 \cdot (1 + a_1 \cdot (t_{item} - t_{cal}))$$

wall_par(1)

Miscellaneous Parameters

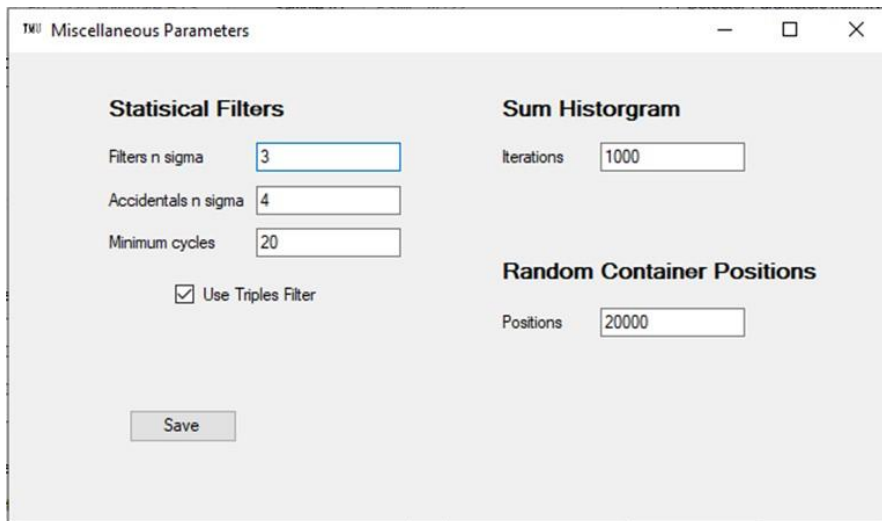


The miscellaneous parameters screen, accessed from the System Parameters menu, includes the traditional neutron coincidence counting filter settings used to reject cycles determined to be outliers. To apply the filters, a minimum number of cycles must have been acquired. The “filters n sigma” value represents the number of standard deviations away from the mean; a cycle rate must be in order to reject the cycle.

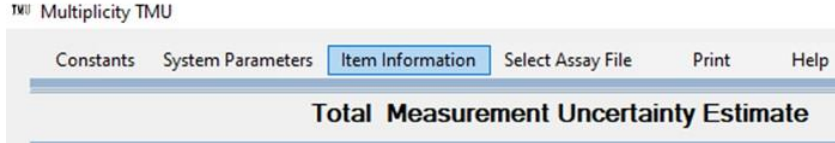
The iterations entry under Sum Histogram indicates the number of times the summed histogram is modified (jittered or dithered) in order to produce standard deviation and estimated covariance for the assay if no cycle-by-cycle data is present.

The number of random container positions is the number of random radial offsets at which the container is placed in order to generate the radial offset mass distribution. The same value is used to set the number of random fill heights used to create the fill height mass distribution.

The information is stored in a CSV file. Note that there is only one file for the empirical parameters. The file name and its location are C:\Multiplicity_TMU\misc_parameters\TMU_general_parameters.csv. After editing the file, the changes may be saved by pressing the “Save” button.



Item Information Screen



The item information screen allows for a variety of information about the item under assay to be input.

Isotopics: The isotopic declaration will only be used if the user unchecks the Use INCC Isotopics button on the main analysis screen. The user may wish to use this entry to provide the isotopics data for the assay if none were present in the assay result file, or to revise the abundance or uncertainty entries. The relative abundances are entered as weight fractions. Date format is MM/DD/YYYY.

Californium-252 is expected to dominate any measurement in which it is present. Entering in ^{252}Cf will switch the output screens to display the masses in terms of ^{252}Cf . If ^{252}Cf is present, remember to use the appropriate fission parameters.

Container Information: The container dimensions, ID and height, are entered in cm. The container wall thickness and material are used to the container wall thickness correction.

Fill Height range entries are inactive – fill heights are estimated from the density range and assay mass result.

Material Characteristics: These parameters are used to estimate the biases introduced as the material type begins to differ from the characteristics of the standards items used during calibration.

Main Screen

The main screen is divided into functional sections.

- Count Rate Summary
- Isotopics Decay Correction and Preliminary Assay Analysis
- Uncertainty Component Overview
- Total Measurement Uncertainty Summary

Count Rate Summary

The count rates from the assay result file (i.e., RTS, VER, or CAL) determined with the parameters set at time of assay are presented for reference. To allow investigation of the the impact of various parameters on the measurement result, the detector parameters and statistical filters may be overridden and the rates reevaluated.

- Unchecking the *Isotopics from INCC File* box substitutes the isotopics values from the Item Information Screen.
- Unchecking the *Detector Parameters from INCC File* box substitutes the efficiency, gate fractions fractions from the Detector Parameters screen.
- Unckecking the *INCC Deadtime Correction* box calculates the dead-time using the Dytlewski dead-time method (ensure the dead-time parameters c , d , and τ are properly configured before using).

The revised rates based on the updated parameters are provided in the *Average Rates from Histograms* box. The rates covariance matrices are provided for both the INCC report and the revised rates. The uncertainties and covariances are calculated from the cycle-by-cycle rates. For comparison the rates determined from the summed histogram are also provided. The summed histogram uncertainties are determined from the analytical expression discussed in Section 3.1.

The uncertainties have also been evaluated using a dithering technique where the summed histogram is perturbed in order to evaluate the bin-to-bin cross correlations in the histograms. The rates uncertainties from the dithering approach should be equivalent to the calculated uncertainty value reported for the summed histograms.

The ring ratio from the INCC report is also provided (ratio of scaler 1 to scaler 2).

Total Measurement Uncertainty Estimate

File Name: Pu_T22q_sumgate.RTS Sample ID: PSMC_m722

Isotopes from INCC File
 Detector Parameters from INCC File
 INCC Deadtime Correction

Refresh

Count Rates

Rates Reported by INCC

Singles: 254944.856 ± 8.417

Doubles: 57221.774 ± 88.725

Triples: 17070.356 ± 204.826

Rates Covariance Matrix (from cycle by cycle data)

70.8618	467.6906	901.4367
467.6906	7872.281	-4727.7148
901.4367	-4727.7148	41953.7905

Good Cycles: 4 / 4

Total Count Time: 4000

Average Rates from Histograms

Singles: 253619.47 ± 8.345

Doubles: 56191.062 ± 86.74

Triples: 17166.814 ± 205.022

Rates Covariance Matrix (from cycle by cycle data)

69.6551	446.6206	895.679
446.6206	7523.9825	-4822.2845
895.679	-4822.2845	42034.0921

Good Cycles: 4 / 4

Total Count Time: 4000

QC Check n-sigma: 3

Rates Calculated from INCC Summed Histogram

Singles: 253619.468 ± 10.351

Doubles: 56190.958 ± 68.516

Triples: 17165.689 ± 182.836

Ping Ratio: 0 ± NaN

Rates from Revised Summed Histogram

Singles: 253646.441 ± 10.351

Doubles: 56191.058 ± 68.516

Triples: 17165.81 ± 182.836

Rates Standard Deviation (dithered histograms)

10.102	72.419	184.322
--------	--------	---------

Rates Covariance Matrix (dithered histogram)

102.053	-96.035	-41.875
-96.035	5244.636	1924.433
-41.875	1924.433	33974.92

Iterations: 1000

Isotopics Data and Initial Results

If the *Isotopics from INCC File* box is checked, the isotopic abundances from the INCC file will be displayed. If the *Isotopics from INCC File* box is not checked, the isotopic abundances from the current item file will be displayed. The isotopic abundances are displayed in terms of weight fraction and the Pu isotopic abundances, excluding Am, will always sum to 1. The initial values, the abundances at time of declaration, are decay corrected to the assay date.

The $^{240}\text{Pu}_{\text{effective}}$ value in terms of ($\text{g } ^{240}\text{Pu} / \text{g Pu}$) is calculated from the decay-corrected abundances and the weighting factors entered from the *Nuclide Data* screen. The expected alpha value, determined assuming the material is in the form of PuO_2 , and the material adjusted alpha value are presented for comparison with the assayed value of alpha.

The assay results for the INCC file rates and the revised rates are displayed.

These reported uncertainties represent only the contribution due to the counting statistics and isotopics declaration and are equivalent to those provided by the traditional multiplicity analysis codes.

Isotopic Composition from INCC file
Pu_722g_surrogate.RTS

Initial Values

Pu-238 0.0103 ± 1E-05

Pu-239 0.6357 ± 0.000637

Pu-240 0.2406 ± 0.000241

Pu-241 0.0745 ± 7.5E-05

Pu-242 0.0379 ± 3.8E-05

Pu-244 0 ± 0

Pu Declaration Date 4/19/1995

Am-241 0.0104 ± 1E-05

Am Declaration Date 4/19/1995

Cf-252 0 ± 0

Cf Declaration Date 6/1/1985

Corrected to Assay Date

Pu-238 0.0103 ± 1E-05

Pu-239 0.63664 ± 0.0009

Pu-240 0.24095 ± 0.00034

Pu-241 0.07413 ± 0.0001

Pu-242 0.03795 ± 5E-05

Pu-244 0 ± 0

Am-241 0.01088 ± 7E-05

Cf-252 0 ± 0

Measurement Date 6/6/1995

Effective Mass 0.33201 ± 0.0028 g Pu240 / g Pu

Expected Alpha Value 0.96666 ± 0.02268

Material Type MOX

Material Adjusted Alpha 0.96666 ± 0.02268

Assay Results (using data file rates)

	Value	Uncertainty	
		Partial Correlation	Full correlation
Multiplication	1.0745	0.0016	0.0012
Alpha	0.81	0.018	0.011
Mass (g Pu240 eff)	236.585	2.864	1.779
Mass (g Pu)	712.57	8.661	5.413

Assay Results (using re-evaluated rates)

	Value	Uncertainty	
		Partial Correlation	Full correlation
Multiplication	1.0779	0.0016	0.0013
Alpha	0.874	0.02	0.012
Mass (g Pu240 eff)	226.581	2.845	1.777
Mass (g Pu)	682.437	8.602	5.403

Contributors to the Total Measurement Uncertainty

The uncertainty contribution from each of the sources considered are presented in terms of m_{240} and total Pu mass as well as the relative uncertainty (i.e., σ_m/m) for each component. The uncertainties are divided into random and systematic components (systematic are identified by blue labels, random by black labels).

Next to each contributor is a “details” button. Pressing the button will bring up a new screen that provides additional information on the determination of the uncertainty component.

The detector parameters contribution is only displayed if *Detector Parameters from INCC File* box is unchecked. Unchecking the box causes the detector parameters with uncertainty estimates to be read from the detector parameters file (*c:\multiplicity_tmu\detector_parameters\det_parameters.csv*). This is because the INCC report files do not included uncertainties for the detector parameters.

The “*info*” button is provided as a means to display the parameters used during the analysis if the *Detector Parameters from INCC File* box is checked.

Uncertainty Component	grams Pu240 effective:	grams Pu	sigma-m/m	
Counting Statistics	<input type="text" value="2.845"/>	<input type="text" value="8.571"/>	<input type="text" value="1.255%"/>	<input type="button" value="details"/>
Detector Component Unavailable				<input type="button" value="details"/> <input type="button" value="info"/>
Pu240 Effective Conversion:	<input type="text" value="N/A"/>	<input type="text" value="5.761"/>	<input type="text" value="0.844%"/>	<input type="button" value="details"/>
Fission Moments:	<input type="text" value="2.097"/>	<input type="text" value="6.317"/>	<input type="text" value="0.925%"/>	<input type="button" value="details"/>
Radial Offset (Random):	<input type="text" value="0.243"/>	<input type="text" value="0.734"/>	<input type="text" value="0.1%"/>	<input type="button" value="Radial Offset details"/>
Radial Offset (Systematic):	<input type="text" value="0.292"/>	<input type="text" value="0.88"/>	<input type="text" value="0.12%"/>	
Fill Height (random):	<input type="text" value="0.604"/>	<input type="text" value="1.819"/>	<input type="text" value="0.266%"/>	<input type="button" value="Fill Height details"/>
Fill Height (systematic):	<input type="text" value="-2.01"/>	<input type="text" value="-6.053"/>	<input type="text" value="-0.887%"/>	
Density (random)	<input type="text" value="1.377"/>	<input type="text" value="4.149"/>	<input type="text" value="0.608%"/>	<input type="button" value="Empirical Bias Details"/>
Density (systematic)	<input type="text" value="0.73"/>	<input type="text" value="2.201"/>	<input type="text" value="0.322%"/>	
(Alpha, n) random:	<input type="text" value="0.317"/>	<input type="text" value="0.957"/>	<input type="text" value="0.14%"/>	
(Alpha, n) bias:	<input type="text" value="1.794"/>	<input type="text" value="5.403"/>	<input type="text" value="0.791%"/>	
Wall Effect (systematic):	<input type="text" value="0.296"/>	<input type="text" value="0.894"/>	<input type="text" value="0.131%"/>	
Burn_up (systematic):	<input type="text" value="0.006"/>	<input type="text" value="0.019"/>	<input type="text" value="0.002%"/>	
UPu Ratio (random):	<input type="text" value="0.032"/>	<input type="text" value="0.098"/>	<input type="text" value="0.014%"/>	
UPu Ratio (systematic):	<input type="text" value="1.736"/>	<input type="text" value="5.228"/>	<input type="text" value="0.766%"/>	
Moderator (random):	<input type="text" value="0"/>	<input type="text" value="0"/>	<input type="text" value="0%"/>	
Moderator (systematic):	<input type="text" value="0"/>	<input type="text" value="0"/>	<input type="text" value="0%"/>	

Total Measurement Uncertainty – Summary

The total measurement uncertainty summary sections roll up the uncertainty from each of the contributors. The random and systematic contributions are displayed separately, and a summed value (simply added in quadrature) is also provided.

The uncertainty contributions from each of the sources considered are presented in terms of m_{240} and total Pu mass, as well as the relative uncertainty (i.e., σ_m/m) for each component.

If a declared mass value was provided from either the input data file or the Item information file, absolute and relative differences are provided.

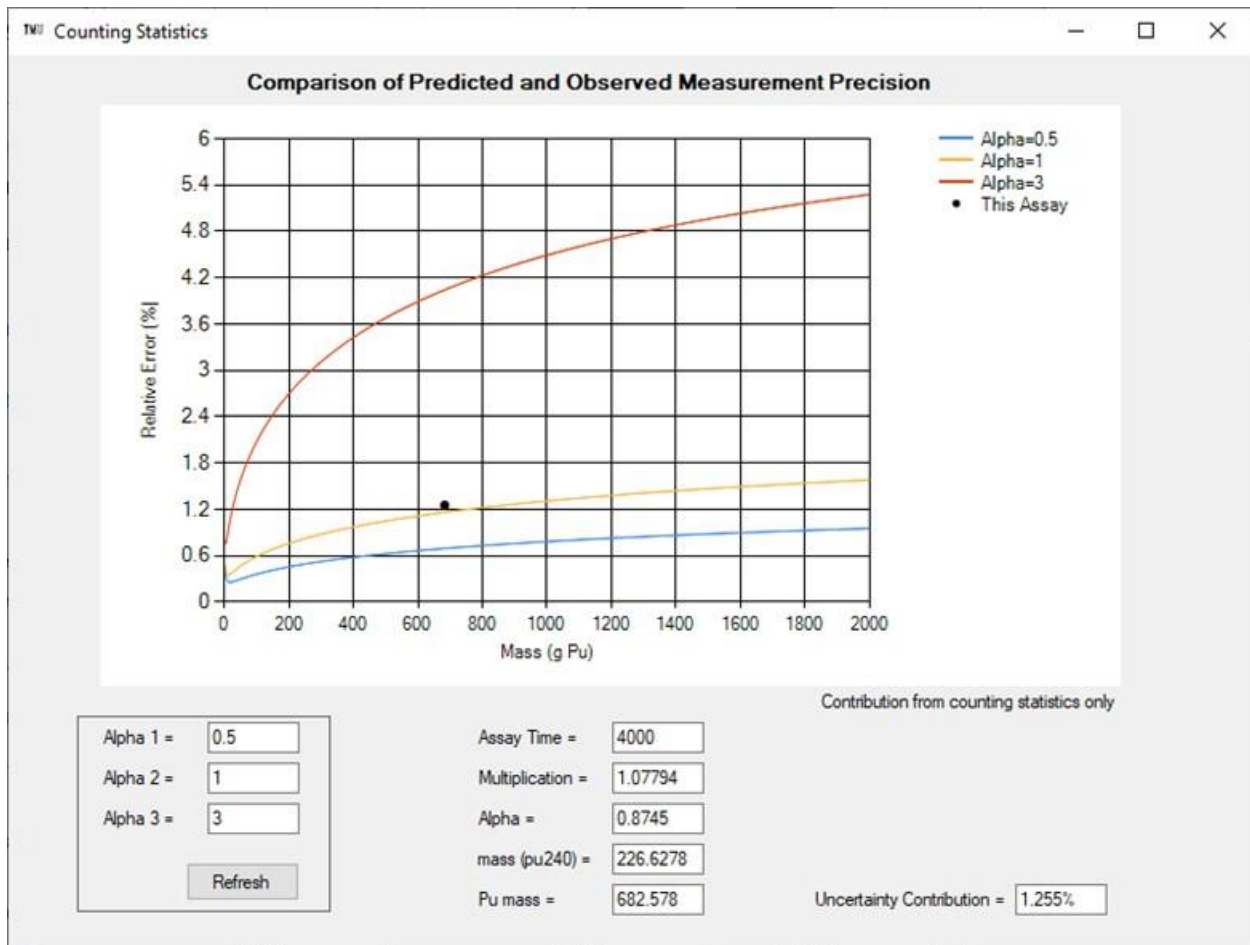
Total Measurement Uncertainty						
File Name:	Pu_722g_surrogate.RTS		Assay Date:	95.06.06 13:41:02		
Sample ID:	PSMC_m722		TMU Analysis Date:	10/19/2020		
	Result	Random	Systematic	Total	Declared	Difference
Multiplication	1.0779 ±	0.0016				
Alpha	0.874 ±	0.02				
Mass (g Pu240 eff)	226.581 ±	3.187	3.921	5.053	239.424	
Mass (g Pu)	682.437 ±	9.599	13.141	16.274	721.79	-39.353 g
Relative Uncertainty		1.4%	1.92%	2.38%		diff = -5.46%
End of Analysis						

Counting Statistics Detail

The counting statistics contribution is determined in accordance with the methods described in Section 3.1 of the report. The relative uncertainty is presented in comparison with the expected values determined using the typical multiplication values as a function of Pu mass for three values of alpha. The measured and expected values should be similar (within a factor of 1.3) for the same value of alpha if there are no unexpected interferences.

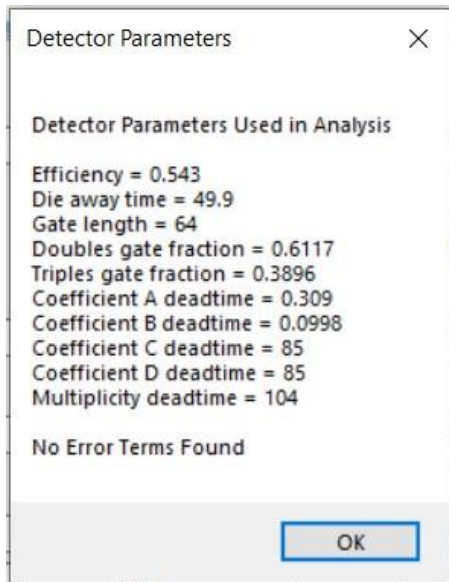
The alpha values for the curves may be overwritten to simplify comparison.

Press the refresh button after entering the desired values.



Detector Parameters – Information Pop-Up

Displays the detector parameters extracted from the input file.



Detector Parameters – Detail Page

Displays the input detector parameters and uncertainty contribution from each. The combined uncertainty includes the contribution from the covariance terms.

The uncertainty contributions from each of the sources considered are presented in terms of m_{240} and total Pu mass, as well as the relative uncertainty (i.e., σ_m/m) for each component.

Detector Uncertainty Contribution to TMU

Detector Parameters

Fission Parameter	Value	Uncertainty	1	2	3	4	5	6	7	8	9	10
Efficiency	0.543	± 0.00322402	1.04E-0	0	0	0	0	0	0	0	0	0
Die-Away (us)	49.9	± 0.87	0	0.7569	0	0	0	0	0	0	0	0
Gate Width (us)	64	± 0	0	0	0	0	0	0	0	0	0	0
f_d	0.6117	± 0.00044815	0	0	0	2.01E-0	0	0	0	0	0	0
f_t	0.3896	± 0.00079826	0	0	0	0	6.37E-0	0	0	0	0	0
Dead-time Parameters												
a (us)	0.3093	± 0.003093	0	0	0	0	0	9.57E-0	0	0	0	0
b (us^2)	0.0998	± 0.00099774	0	0	0	0	0	0	9.95E-0	0	0	0
c (ns)	85	± 0.90945990	0	0	0	0	0	0	0	0.8271	0	0
d (ns) *	85.85	± 3.27406595	0	0	0	0	0	0	0	0	10.719	0
τ	104	± 0.45	0	0	0	0	0	0	0	0	0	0.2025

* Parameter d<0 use Carberna Dead-time model

Detector Characterization Contribution to Uncertainty

	grams Pu240 effective:	grams Pu	sigma-m/m
Efficiency	1.761	5.306	0.77%
Die-Away (us)	0	0	0%
Gate Width (us)	0	0	0%
f_d	0.363	1.093	0.16%
f_t	0.435	1.313	0.19%
Dead-time Parameters			
a (us)	0.37	1.114	0.16%
b (us^2)	0.029	0.089	0.01%
c (ns)	0.048	0.144	0.02%
d (ns) *	0	0	0%
τ	0.374	1.126	0.16%
Combined	1.925	5.798	0.84%

²⁴⁰Pu_{effective} Conversion

This screen provides the mass uncertainty due to the uncertainty in the value of ²⁴⁰Pu_{effective}, including the impact of the nuclear data uncertainties. The uncertainty contribution to the value of ²⁴⁰Pu_{effective} is provided for each component (units in terms of g/g) for all components other than the roll-up value, which is presented as a relative uncertainty in terms of percent.

TW Pu240 effective conversion
— □ ×

Initial Values

Pu-238 ±

Pu-239 ±

Pu-240 ±

Pu-241 ±

Pu-242 ±

Pu-244 ±

Pu Declaration Date

Am-241 ±

Am Declaration Date

Cf-252 ±

Cf Declaration Date

Isotopes Corrected to Assay Date

Pu-238 ±

Pu-239 ±

Pu-240 ±

Pu-241 ±

Pu-242 ±

Pu-244 ±

Am-241 ±

Cf-252 ±

Measurement Date

Equivalent Pu240 effective (g/g)

Pu-238 ±

Pu-239 ±

Pu-240 ±

Pu-241 ±

Pu-242 ±

Pu-244 ±

Am-241 ±

Weighted Equivalent Pu240 effective (g/g)

±

±

±

±

±

±

±

Pu240 Effective / Pu

Uncertainty due to isotopes declaration

Uncertainty due to decay correction

Uncertainty due to fission yield

Combined Uncertainty

Relative Uncertainty

±

Fission Moment Contribution Detail

The screen provides a summary of the input nuclear data parameters and uncertainties used for the analysis.

The uncertainty contributions from each of the nuclear data values are considered and are presented in terms of m_{240} and total Pu mass, as well as the relative uncertainty (i.e., σ_m/m) for each component.

Fission Parameter	Value	±	Uncertainty							
nu_s1	2.154	±	0.005		2.5E-05	0.000131	0.000421	0	0	0
nu_s2	3.789	±	0.013		0.000131	0.000169	0.000768	0	0	0
nu_s3	5.21	±	0.067		0.000421	0.000768	0.004489	0	0	0
nu_11	3.1635	±	0.068		0	0	0	0.004624	0	0
nu_i2	8.305	±	0.0407		0	0	0	0	0.001656	0
nu_i3	17.782	±	0.151		0	0	0	0	0	0.022801
Φ	473.5	±	3.9		0	0	0	0	0	15.21

Assay Bias from Nuclear Data Uncertainties			
	grams Pu240 effective:	grams Pu	sigma-m/m
nu_s1	0	0	0%
nu_s2	-1.088	-3.275	-0.48%
nu_s3	1.16	3.495	0.51%
nu_11	-0.675	-2.032	-0.3%
nu_i2	-0.115	-0.345	-0.06%
nu_i3	0.38	1.146	0.16%
Φ	-1.867	-5.623	-0.83%

Contribution to Uncertainty		
Uncertainty	2.097	6.318
		0.925%

Axial Response Profile Detail

The axial response profile of the counter introduces an additional variation in detection efficiency as a function of container fill height. The screen provides a summary of the input parameters used in the analysis (detector physical properties and container properties) and the resulting uncertainties due to improper loading of the container. Plots of the calculated axial response profile and volume average efficiency as a function of container fill height are provided. The average, minimum, and maximum fill heights are determined from the reported mass value, the typical and bounding densities for the matrix material.

The green, vertical, dashed lines in the plot of relative density with fill height represent the minimum and maximum fill heights. The plot provides a visual indication of the impact on the detection efficiency relative to declared detection efficiency for the counter.

The mass distribution as a function of fill height is presented as the probability distribution of mass result as a function of reported mass based on a user-selectable number of random container loadings. The width of this distribution represents the random contribution to uncertainty, while the difference between the midpoint of the distribution and mass value determined using the declared efficiency for the counter represents the fill height bias.

Fill Height Contribution to the TMU

Print

Cavity Type:

 Cavity Height (cm):

 Cavity Width or Dia. (cm):

 Cavity Length (cm):

 Cd Liner thickness (cm):

 Tube ID (cm):

 Tube Active Length (cm):

 Number of rows:

Row	Radius (cm)	Tubes (#)
Row 1	<input type="text" value="13.1"/>	<input type="text" value="19"/>
Row 2	<input type="text" value="17.27"/>	<input type="text" value="25"/>
Row 3	<input type="text" value="21"/>	<input type="text" value="18"/>
Row 4	<input type="text" value="24.72"/>	<input type="text" value="18"/>
Row 5	<input type="text" value="0"/>	<input type="text" value="0"/>

Item Stand Height (cm):

 Container Inner Dia. (cm):

 Average Radial Offset (cm):

 Random Radial Offset (cm):

Estimated Fill Height. (cm):

 Estimated Minimum Fill Height. (cm):

 Estimated Maximum Fill Height. (cm):

Counter:

 Item Id:

 Systematic Bias:

 Relative Range: to

 Random Contribution:

(assuming normal distribution about the assumed fill.)

Note: Assayed mass distribution about average is not normal.

**Note: assumes volumetric calibration
Pt source efficiency calibration adds bias
(over reports due to underestimate efficiency)**

Additional Bias From Point Source Calibration:

Note: Fill height estimated from assay mass and density inputs

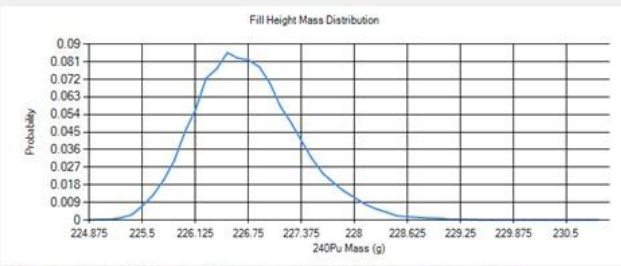
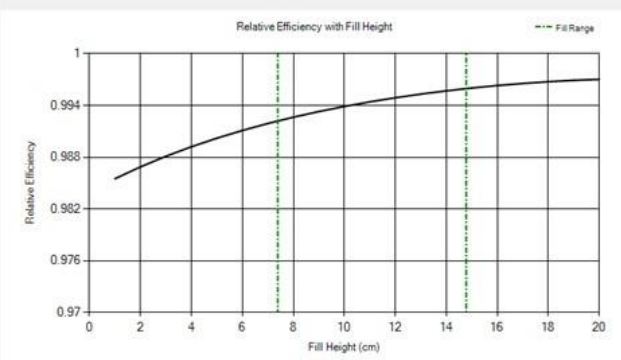
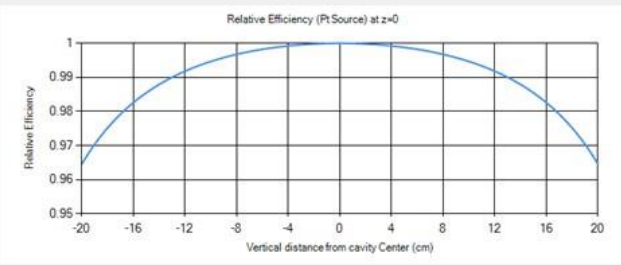
**Note: Outermost Tube diameter is used in current calculations
Inner tube diameters required for future enhancement**

Note: Tube number dependence is a future enhancement

Relative to Point Calibration

 Relative to Distributed Calibration

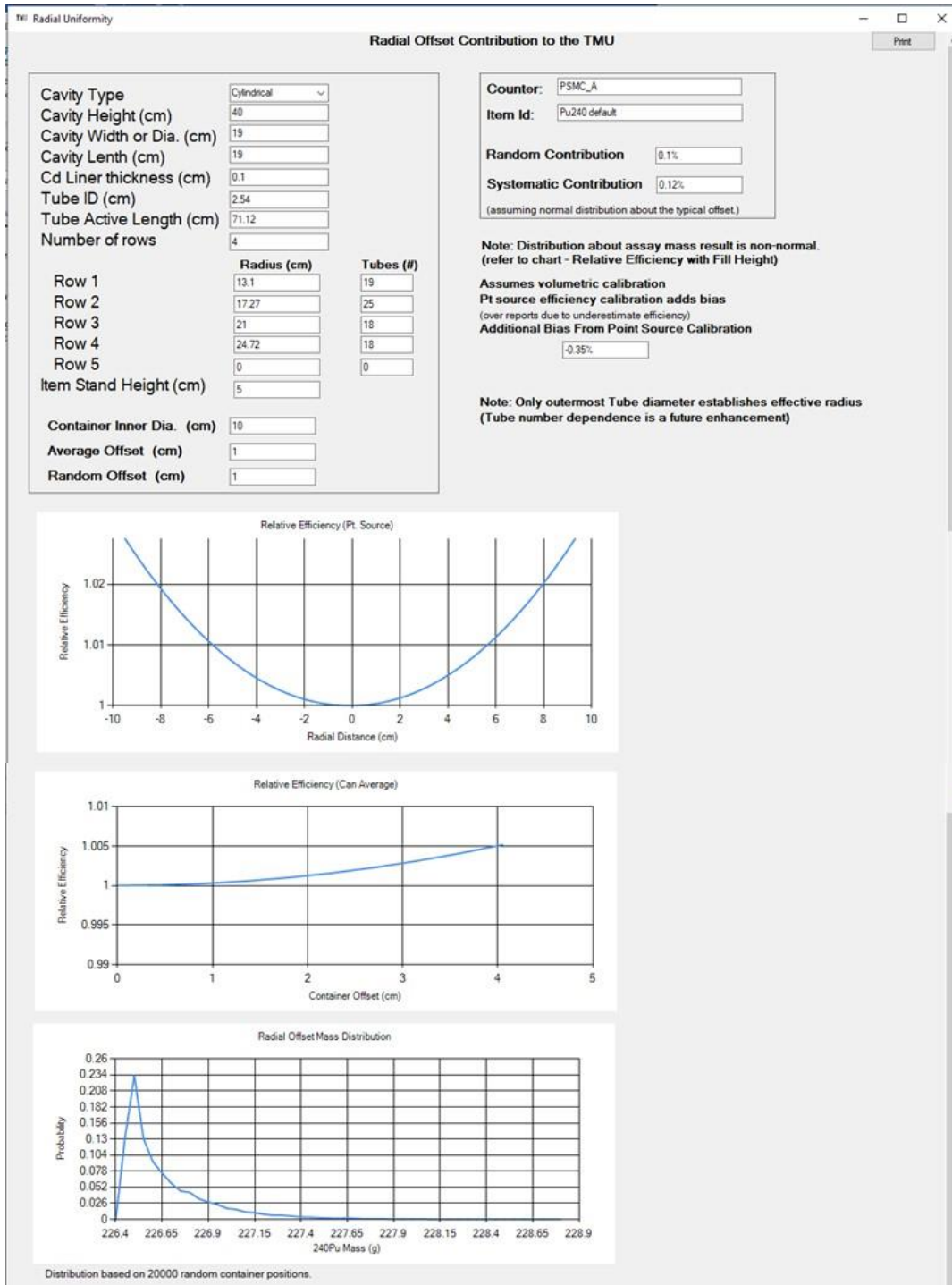
 Typical calibration fill height (cm):



Distribution based on 20000 random fill heights between the likely minimum and maximum fill heights.

Radial Offset Detail

The screen provides a summary of the input parameters used in the analysis (detector physical properties and container properties) and the resulting uncertainties due to improper loading of the container. Plots of the calculated radial response profile and volume average efficiency as a function of radial offset are provided. The radial offset mass distribution represents the probability distribution of mass result as a function of reported mass based on a user-selectable number of random container loadings.



Empirical Bias Details

Empirical Biases

Pu Isotopic (burn-Up) Bias

$$\Delta_{BU} = \alpha_1 + \alpha_2 \cdot ({}^{240}\text{Pu}_{eff,item} - {}^{240}\text{Pu}_{eff,cal}) \cdot \alpha$$

dev_240_par(1): Cal Standards typical 240Pueff (%):

dev_240_par(2): Item 240Pueff / g (%):

Estimated Bias:

UPu Ratio Bias

$$\Delta_{UPu} = \left[\alpha_1 + \alpha_2 \cdot \frac{m_{Pu}}{m_{ref}} + \alpha_3 \cdot \left(\frac{m_{Pu}}{m_{ref}} \right)^2 \right] \cdot \left(\frac{R_{UPu} - R_{Ref}}{\alpha_4} \right)^{1/4}$$

UPu_par(1): Typical UPu Ratio:

UPu_par(2): Minimum Expected UPu Ratio:

UPu_par(3): Maximum Expected UPu Ratio:

UPu_par(4): Assay Mass Result:

Ref:

Standards Typical UPu Ratio:

Estimated UPu Ratio Bias:

Random UPu Component:

(alpha, n) Bias

$$\Delta_a = a + b \cdot \left(\frac{m}{m_{ref}} \right)^c \cdot \alpha$$

alpha_par(1): Assay Alpha value: +/-

alpha_par(2): Standards Typical Alpha Value:

alpha_par(3):

Ring Ratio: +/-

Ref. Ring Ratio:

Estimated Alpha Value Bias:

Random Component:

Expected Bias Direction:

Expected Impurity

Boron

Beryllium

Carbon

Oxygen

Fluorine

Density Bias

$$\Delta m_{240,\rho} = a_1 \left(\frac{m}{m_{ref} \cdot \rho_{typ}} \right)^{a_2} \cdot (1 + a_3 \cdot e^{-a_4 \rho}) \cdot (\rho_{typ} - \rho_{ref})$$

rho_par(1):	<input type="text" value="0.017"/>	Reference Density (g/cc):	<input type="text" value="3"/>
rho_par(2):	<input type="text" value="0.75"/>	Typical Item Density (g/cc):	<input type="text" value="2.5"/>
rho_par(3):	<input type="text" value="2.5"/>	Minimum Expected Density (g/cc):	<input type="text" value="2"/>
rho_par(4):	<input type="text" value="2.5"/>	Maximum Expected Density (g/cc):	<input type="text" value="4"/>
m_ref:	<input type="text" value="1000"/>		
Estimated Bias:	<input type="text" value="-0.33%"/>		
Random Component:	<input type="text" value="0.6%"/>		

Alternate Density Bias

Multiplication	<input type="text" value="1.0779"/>
Mult Corr. Fact.	<input type="text" value="0.9913"/>
Assay Eff./Pt Eff	<input type="text" value="1.0068"/>
Estimated Bias	<input type="text" value="-0.97%"/>

Moderator Bias

$$\Delta_{mod} = a_1 + a_2 \cdot (w_{item} - w_{cal}) + a_3 \cdot (w_{item} - w_{cal})^2$$

mod_par(1):	<input type="text" value="0"/>	Typical Moderator Content:	<input type="text" value="0"/>
mod_par(2):	<input type="text" value="0.3"/>	Minimum Moderator Content:	<input type="text" value="0"/>
mod_par(3):	<input type="text" value="0"/>	Maximum Moderator Content:	<input type="text" value="0"/>
Standards Moderator Content (cal_mod):	<input type="text" value="0"/>		
Expected Moderator Bias:	<input type="text" value="0%"/>		
Random Component:	<input type="text" value="0%"/>		

Container Wall Effect Bias

$$\varepsilon = \varepsilon_0 \cdot (1 + a_1 \cdot (t_{item} - t_{cal}))$$

Item Wall Material:	<input type="text" value="Stainless Steel"/>	Item Wall Thickness (cm):	<input type="text" value="0.2"/>
Standards Wall Material:	<input type="text" value="Stainless Steel"/>	Standards Wall Thickness (cm) :	<input type="text" value="0.1"/>
wall_par(1):	<input type="text" value="-0.01"/>		
Wall Effect Bias:	<input type="text" value="0.13%"/>		